Gradient Theory:

Prediction of interfacial tension using the associated perturbed anisotropic chain theory

August 1995

Mark Wijtkamp

TU Delft
Technische Universiteit Delft

Faculteit der Scheikundige Technologie en der Materiaalkunde

Gradient Theory:

Prediction of interfacial tension using the associated perturbed anisotropic chain theory

Masters thesis of:

Mark Wijtkamp

August 1995

Supervisors:

Ir P.M.W. Cornelisse
Dr ir C.J. Peters
Prof. dr ir J. de Swaan Arons

Laboratory of Applied Thermodynamics and Phase Equilibria
Faculty of Chemical Technology and Material Science
Delft University of Technology

Abstract

The behaviour of interfaces in fluid systems is of fundamental and practical importance. Interfacial tensions in fluid mixtures are often required for the design of chemical process equipment. In oil reservoirs, the surface/interfacial tension is held responsible for the migration of hydrocarbons and, therefore, the recovery from these reservoirs.

A theory, which is of particular significance for computation of interfacial tensions is the gradient theory (GT), originally introduced by Rayleigh (1892) and van der Waals (1894). The required inputs of gradient theory are the Helmholtz free energy density of the homogeneous fluid and the so-called influence parameters, c_{ij} of the inhomogeneous system. This influence parameter is related to the direct correlation function of the homogeneous fluid. This result means that all the important inputs of gradient theory can be derived from the properties of the homogeneous fluid.

The relation for the Helmholtz free energy density was derived from the associated perturbed anisotropic chain theory (APACT). This theory was designed to treat mixtures that associate through hydrogen-bonding or through the interaction between dipolar or quadrupolar molecules.
One disadvantage of using APACT is that it overpredicts the critical pressure as well as the critical temperature for hydrogen-bonding, polar or non-polar fluids. This unfortunate effect also occurs in mixtures, as was shown for systems containing carbon-dioxide.

To test the model, the interfacial tensions of water, linear alcohols from methanol up to 1-decanol, n-butane, n-pentane, n-hexane, n-heptane, n-octane, n-decane, carbon-dioxide, benzene, and their mixtures were calculated. The interfacial tension of the pure compounds can be accurately described when the influence parameter, fitted to experimental interfacial tension data, is a linear function of temperature.
The ability to predict interfacial tension of mixtures was studied for systems, such as water/n-alkanes, n-alcohols/n-alkanes, n-alcohols/n-alcohols, water/n-alcohols, carbon-dioxide/n-alkanes, benzene/n-alcohols and benzene/n-hexane, water/methanol/1-propanol and carbon-dioxide/n-butane/n-decane.
It was shown that the gradient theory in cooperation with the APACT equation of state can predict interfacial tension of liquid-vapor and liquid-liquid interfaces, of the studied mixtures, reasonably well. Predictions can even be approved by using a binary interaction parameter, k_{ij} which corrects the attractive part of APACT.
In order to calculate interfacial tensions, the density profiles of all the components present in the mixture, must be obtained. A remarkable effect was observed in the obtained density profiles of 1-propanol/n-heptane. The increasing density, along the interfacial zone, of 1-propanol causes a decrease in the concentration of n-heptane. This effect was not unique for this system and occurs in almost every binary system with n-alcohols and an alkane or a n-alcohol as second component. A possible orientation of the alcohol molecules in the interface can cause this effect, resulting in a decrease of the n-heptane density.

Contents

1. Introduction

The interfacial tension of fluid systems is of fundamental and practical importance. Interfacial tensions of fluid mixtures are often required for a rational design of chemical process equipment, involving interphase heat and mass transfer. Processes in which interfaces play an important role are supercritical-fluid extraction, liquid-liquid extraction, distillation, humidification, and absorption of gases, to mention only a few. In oil reservoirs high pressure interfacial/surface tension is held responsible for the migration of hydrocarbons and gases, and, therefore for the succes of recovery from these hydrocarbon reservoirs (Chun and Wilkinson, 1994).

In the past decades the theoretical predictions of surface tension lagged behind predictions of phase behaviour of fluid mixtures. Over the past years there has been considerable advancement in the molecular theory of interfacial phenomena. A theory which is of particular significance for computation of surface/interfacial tensions and the fluid microstructure is the gradient theory (GT). This theory was originally introduced by Rayleigh (1892) and van der Waals (1894) and was rediscovered by Cahn and Hilliard (1958). Carey et al. (1978) made this theory easy to use for semiempirical prediction of interfacial tensions.
Although the assumptions, which where made at the derivation of the gradient theory, seems to limit its validity at near critical conditions of fluid phases, model calculations suggest that the theory can be applied accurately to systems which are far away from the critical point (Cornelisse, 1991 ; Cornelisse et al., 1993).

The required inputs of gradient theory consists of the Helmholtz free energy density f of the homogeneous fluid and the so-called influence parameter, c_{ij} of the inhomogeneous fluid. This influence parameter is rigorously related to the direct correlation function of a homogeneous fluid. The direct correlation function itself is related to the more familiar pair correlation function given by Ornstein and Zernike (1914). This result means that through gradient theory all the important inputs can be derived from the properties of the homogeneous fluid.

The purpose of this work is to predict interfacial tensions of liquid-vapour and liquid-liquid interfaces in binary and ternary systems, which properties deviate from ideal solution due to strong specific intermolecular interactions. These interactions involve hydrogen bonding or interactions between dipolar or quadrupolar molecules.
The pure components that were selected to test the calculations based on the APACT equation of state are: water, the linear alcohols from methanol up to 1-decanol, n-butane, n-pentane, n-hexane, n-heptane, n-octane, n-decane, carbon-dioxide and benzene.

The binary systems studied is this project were systems containing water/n-alkanes, n-alcohols/n-alkanes, water/n-alcohols, carbon dioxide/n-alkanes, and benzene/n-alcohols. The ternary systems are carbon dioxide/n-butane/n-decane and methanol/1-propanol-water.

The phase behaviour and the relation of the homogeneous Helmholtz free energy f are calculated using the associated perturbed anisotropic chain theory (APACT) equation of state (Ikonomou and Donohue, 1986). This equation of state was designed to treat pure fluids and mixtures that associate through hydrogen bonding or through the interaction between dipolar or quadrupolar molecules. It also takes into account differences in size and shape of the molecules.
In order to predict interfacial tensions of mixtures, an empirical relation for pure component influence parameter, c_{ii} as a function of temperature is derived from pure component interfacial tensions.

This report contains the following subjects. In chapter 2 an introduction in the theory of interfaces is given and secondly the gradient theory as well as the APACT equation of state are described. Chapter 3 will deal with the programming section, followed by chapter 4, which discusses the calculated results. Finally, conclusions and closing remarks are given in chapter 5.

2. Theory

2.1 Thermodynamics of inhomogeneous systems

The considerable powers provided by the thermodynamic laws can be used by building the theory of inhomogeneous systems around them. It was assumed that the entropy function exists for inhomogeneous systems in equilibrium and obeys the second law. This means that the internal states (i.e.,density and composition distributions) of an isolated system change, in any spontaneous process, in such a way that entropy increases to a maximum value at equilibrium. In other words, it is assumed that the entropy statement of the second law of thermodynamics is the same whether the system is homogeneous or inhomogeneous. This postulate is generally accepted in the thermodynamic treatment of interfaces.

If the entropy function S of a system exists, so does the Helmholtz free energy F, defined by F = U - TS. A different statement of the second law is that the internal states of a closed, isothermal system take on values that minimize the Helmholtz free energy at equilibrium. This minimum principle provides a convenient bases for investigation of the existence and stability of the microstructure of inhomogeneous fluids.

In a homogeneous system the thermodynamic state can be fully described by temperature T, volume V and overall composition N. Thermodynamic quantities can be expressed as a function of these three variables. However, in inhomogeneous fluids the density distributions $\rho(r)$ must be specified as well for the determination of these quantities.

Of particular significance are the chemical potentials $\mu_1,...,\mu_n$ in the theory of a inhomogeneous fluid. The chemical potentials of a homogeneous system can be calculated as a change in the Helmholtz free energy upon an addition of a molecule of species α. This is done while holding the temperature, volume and amounts of the other species constant. It doesn't matter where the molecule α is added in the fluid. However, since density in inhomogeneous systems vary with space, the change in Helmholtz free energy will depend on where the molecule α is added in the system. Addition of δN_α molecules to a small volume τ fixed at the point r_0 is given in Figure 2.1. Since $N_\alpha = \int_V \rho_\alpha(r)\, d^3r$, then δN_α must be $\delta N_\alpha = \int_V \delta\rho_\alpha\, d^3r$. When temperature, volume, and density distributions are kept constant then the chemical potential at r_0 can be computed from

$$\mu_\alpha = \lim_{\delta N_\alpha \to 0} \frac{F([\rho + \delta\rho_\alpha]) - F([\rho])}{\delta N_\alpha} = \lim_{\tau, \delta n_\alpha \to 0} \frac{F([\rho + \delta\rho_\alpha]) - F([\rho])}{\int_\tau \delta\rho_\alpha d^3r} \qquad (2.1)$$

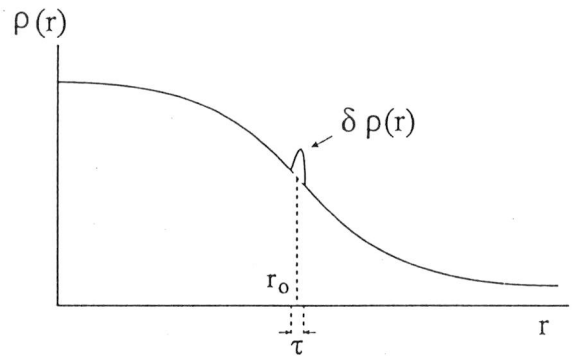

Figure 2.1. Change in density distribution upon adding of δN_α molecules to a small volume element τ on the position r_o.

The right-hand side of Eq. 2.1 denotes the functional derivative of F. The chemical potential measured at some position r_0 is expressed by

$$\mu_\alpha(r_o) = \left(\frac{\partial F}{\partial \rho_\alpha(r_o)} \right)_{T, V, \beta, \beta \neq \alpha} \tag{2.2}$$

In homogeneous bulk phases the condition for chemical equilibrium is that the chemical potential of each species is the same in both phases. If we assume that the chemical potential everywhere in a inhomogeneous system at equilibrium is constant, then Eq. 2.2 becomes an expression from which the density distributions at equilibrium can be extracted instead of an equation that calculates the chemical potential of a species α.
It was proved by Davis and Scriven (1982) that the chemical potential do indeed turn out be constant anywhere in a inhomogeneous fluid at equilibrium.

2.2 Pressure tensor and tension in an interface

The most commonly considered interface in a fluid is a horizontal interface between to isotropic fluid phases. Due to gravity, the lighter face will be on top and the heavier at the bottom. Aside from ordering the phases, the force of gravity has no effect on fluid properties over distances which are several times larger than the width of the interfacial zone. The equation of hydrostatics thus becomes $\nabla \mathbf{P} = 0$ in the vicinity of a planar interface and in the absence of an external field other than gravity. The pressure tensor **P** is given by

$$\mathbf{P} = \begin{pmatrix} P_{xx} & P_{xy} & P_{xz} \\ P_{yx} & P_{yy} & P_{yz} \\ P_{zx} & P_{zy} & P_{zz} \end{pmatrix} \tag{2.3}$$

Under planar conditions, the equation of hydrostatics becomes

$$\frac{dP_{xx}}{dx} = \frac{dP_{xy}}{dx} = \frac{dP_{xz}}{dx} = 0 \tag{2.4}$$

This implies that P_{xx}, P_{xy}, P_{xz} are constant in a planar system. Above or below an interface **P** is isotropic and equals $\mathbf{I} \cdot P_B$, where P_B is the bulk pressure at equilibrium and I is the unity matrix. Hydrostatic
equilibrium for a planar interface leads to

$$P_{xx} = P_B \text{ , and } P_{xy} = P_{xz} = 0 \tag{2.5}$$

It follows from symmetry of the pressure tensor for a planar interface at equilibrium that

$$P_{yx} = P_{zx} = 0 \tag{2.6}$$

Finally, the transverse isotropy of a flat interface implies

$$P_{yy} = P_{zz}, \quad P_{yz} = P_{zy} = 0 \tag{2.7}$$

From the equations above it can be concluded that a planar interface has only two distinct principal stresses, namely a normal one $P_N = P_{xx}$ and a transverse one $P_T = P_{zz}$. The pressure tensor thus becomes

$$\mathbf{P} = \begin{pmatrix} P_N & 0 & 0 \\ 0 & P_T & 0 \\ 0 & 0 & P_T \end{pmatrix} \tag{2.8}$$

Because $\mathbf{P} = P_B \cdot \mathbf{I}$ in the bulk phase, below or above the interfacial zone, it follows that $P_N = P_T$ when x is greater than the width l_w of the interfacial zone. From the three conditions stated above, hydrostatic equilibrium and planarity, symmetry, and transverse isotropy of the pressure tensor, it can be concluded that P_T only depends on the position in the interfacial zone. If a transducer of height L and width w is placed at the positions drawn in Figure 2.2, then the force detected by the transducer face will be

$$Force_I = -\int_{-L/2}^{L/2} P_T w \, dx \tag{2.9}$$

$$Force_B = -P_N w L = -\int_{-L/2}^{L/2} P_N w \, dx \tag{2.10}$$

where $Force_I$ denote the force on the interface and $Force_B$ the force on the bulk phase.

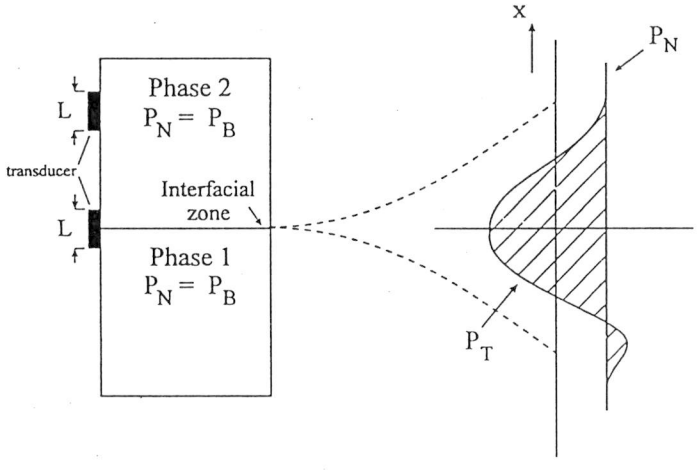

Figure 2.2. Two-phase system separated by a planar interface. Normal pressure, P_N, and transverse pressure, P_T profiles across the interfacial zone.

The difference between these two forces is the increase in the force exerted on the transducer caused by the tension of the interface. The tension is given by $(F_I - F_B)/w$, or

$$\gamma = \int_{-L/2}^{L/2} (P_N - P_T)\, dx \tag{2.11}$$

Since $P_N - P_T = 0$ outside the interfacial zone, the limits of the integral in Eq. 2.9 can be extended to ± infinity, so that

$$\gamma = \int_{-\infty}^{\infty} (P_N - P_T)\, dx \tag{2.12}$$

The fact that the tension of a stable interface is positive implies that P_T must be a function of x and that in the interfacial zone part of P_T is less than P_N. From the experimental fact that the widths of low pressure, high-tension interfaces are of the order of tens to hundreds of angstroms, it follows that the transverse pressure is negative over part of the interfacial zone. A possible profile of the transverse pressure across an interface is sketched in Fig. 2.2. It was shown that molecular models do indeed predict such P_T-profiles from molecular theory (Carey, Davis and Scriven, 1978).
In the interfacial zone, there can be regions of tension, where $P_T < P_N$ and regions of compression, where $P_T > P_N$. The only criterium for stability in an interface requires that the integral of $P_N - P_T$ is positive across the zone.

In the last part of this paragraph formulas are derived for the pressure tensor from the Helmholtz free energy density f(r). For this purpose it is convenient to use to following expression for the total Helmholtz free energy of a system:

$$F = \int_V f(r)\, d^3r \tag{2.13}$$

where f(r) is the Helmholtz free energy density.
If a planar one-component system is considered, as in Fig. 2.3, the change in Helmholtz free energy at constant temperature from an increment in volume, ΔV is

$$\begin{aligned} \Delta F &= \frac{\partial F}{\partial V}\Delta V + \frac{1}{2}\frac{\partial^2 F}{\partial V^2}(\Delta V)^2 + \ldots \\ &= -P_T\, \Delta V + O(\Delta V)^2 \end{aligned} \tag{2.14}$$

where $\Delta V = \Delta A(x_o)\Delta x_o$; Δx_o is the width of the piston in the x-direction.

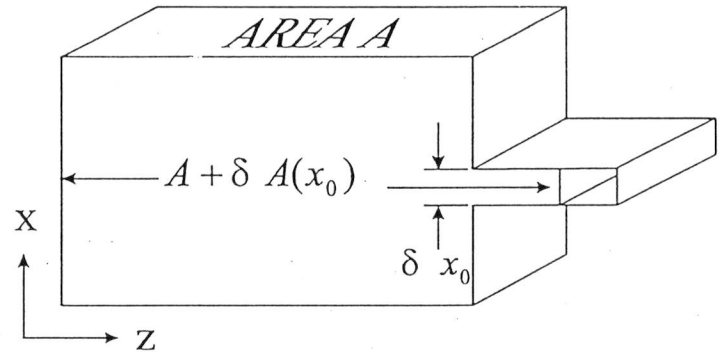

Figure 2.3. One-component planar system, with free-energy change

The transverse pressure at x_o can be calculated from

$$P_T = - \lim_{\Delta V \to 0} \frac{\Delta F}{\Delta V}$$

$$= - \lim_{\Delta V \to 0} \frac{\int_V [\, f([\rho + \Delta\rho]) - f([\rho]) \,] d^3r}{\Delta V} \qquad (2.15)$$

$$- \lim_{\Delta V \to 0} \frac{\int_{\Delta V} f([\rho]) d^3r}{\Delta V}$$

The second member of Eq. 2.15 reduces to $-f(x_o)$ when ΔV goes to zero. The first member is evaluated with the following expressions (N is the number of particles).

$$\Delta N = \frac{\partial N}{\partial V} \Delta V + \frac{1}{2} \frac{\partial^2 N}{\partial V^2} (\Delta V)^2 + \ldots \qquad (2.16)$$

$$= -\rho(x_o) \Delta V + \Theta(\Delta V)^2$$

because

$$N = \int_V \rho \, d^3r \qquad (2.17)$$

and

$$\delta N = \int_{\Delta V} \delta\rho \, d^3r \qquad (2.18)$$

The change in volume can therefore be expressed as

$$\int_{\Delta V} d\rho\, d^3r = -\rho(x_o)\Delta V + \Theta(\Delta V)^2$$

$$\Delta V \to 0 \Rightarrow \tag{2.19}$$

$$\Delta V = -\frac{1}{\rho(x_o)} \int_{\Delta V} d\rho\, d^3r$$

The ΔV in the first member of Eq. 2.15 can be replaced by Eq. 2.19. The resulting expression has the form of the functional derivative of F (Eq. 2.1), thus the chemical potential. The transverse pressure, as in Eq. 2.15, then becomes

$$P_T(x_o) = \rho(x_o)\mu(x_o) - f(x_o) \tag{2.20}$$

The multicomponent version of Eq. 2.20 is obtained by replacing $\rho\mu$ by $\Sigma\rho_\alpha\mu_\alpha$ to give

$$P_T(x) = \sum_{\alpha=1}^{N} \rho_\alpha(x)\,\mu_\alpha(x) - f(x) \tag{2.21}$$

The tension of a planar interface taken from Eq. 2.12 together with Eq. 2.21 gives

$$\gamma = \int_{-\infty}^{\infty} \left(P_N + f(x) - \sum_{\alpha=1}^{N} \rho_\alpha(x)\,\mu_\alpha \right) dx \tag{2.22}$$

The tension is computed directly from the Helmholtz free energy by replacing a small piston in Fig. 2.3 by a piston wide compared to the interfacial zone. The Helmholtz free energy change upon a isothermal change in area, ΔA of the piston is

$$\Delta F = -\left[\int_{-\Delta x_o/2}^{\Delta x_o/2} P_T(x)\, dx \right] \Delta A = -P_N \Delta V + \left[\int_{-\infty}^{\infty} (P_N - P_T)\, dx \right] \Delta A \tag{2.23}$$

$$= -P_N \Delta V + \gamma \Delta A$$

Equation 2.23 yields the well-known thermodynamic expression, namely

$$\gamma = \left(\frac{\partial F}{\partial A} \right)_{T,V,N} \tag{2.24}$$

2.3 Gradient theory

2.3.1 General treatment of a nonuniform system

It was suggested by Cahn and Hilliard (1958) that the Helmholtz free energy density per molecule, f, in a nonuniform region depend on the local composition and the composition of the immediate environment. They expressed f as the sum of two parts, which are functions of the local composition ρ and the local composition derivative. Further they assumed that the composition gradient is small compared to the reciprocal of the intermolecular distance and that the composition ρ and its derivatives are independent variables. Providing f is a continuous function of these variables, it can be expanded in a Taylor series about f_o, which is the free energy per molecule of the homogeneous fluid with composition ρ. The leading terms are:

$$f(\rho,\nabla\rho,\nabla^2\rho,...) = f_o(\rho) + \sum_i^3 L_i \frac{\partial\rho}{\partial x_i} + \sum_{ij}^3 k_{ij}^{(1)} \frac{\partial^2\rho}{\partial x_i\,\partial x_j} + \frac{1}{2}\sum_{ij}^3 k_{ij}^{(2)} \frac{\partial\rho}{\partial x_i}\frac{\partial\rho}{\partial x_j} + ... \qquad (2.25)$$

where the subscripts 1, 2 and 3 on the variable x_i denote the x, y and z components, respectively. The components L_i, $k_{ij}^{(1)}$ and $k_{ij}^{(2)}$ are given by:

$$L_i = \left[\frac{\partial f}{\partial\left(\frac{\partial\rho}{\partial x_i}\right)}\right]_0$$

$$k_{ij}^{(1)} = \left[\frac{\partial f}{\partial\left(\frac{\partial^2\rho}{\partial x_i\,\partial x_j}\right)}\right]_0 \qquad (2.26)$$

$$k_{ij}^{(2)} = \left[\frac{\partial^2 f}{\partial\left(\frac{\partial\rho}{\partial x_i}\right)\left(\frac{\partial\rho}{\partial x_j}\right)}\right]_0$$

Since it was assumed that the local free energy f is a function only of f_o and the composition derivatives, then f, a scalar function, must be invariant with respect to the direction of the gradient. This means that only the terms with even powers of the operator ∇ can appear. This statement leads to the following sets of equations:

$$L_i = 0$$

$$k_{ij}^{(1)} = \frac{1}{2}k_1 = \left[\frac{\partial f}{\partial \nabla^2 \rho}\right]_0 \quad for \quad i=j$$

$$k_{ij}^{(1)} = 0 \quad for \quad i \neq j \tag{2.27}$$

$$k_{ij}^{(2)} = \frac{1}{2}k_2 = \frac{1}{2}\left[\frac{\partial^2 f}{(\partial |\nabla \rho|)^2}\right]_0 \quad for \quad i=j$$

$$k_{ij}^{(2)} = 0 \quad for \quad i \neq j$$

Eq. 2.25 then reduces to:

$$f(\rho, \nabla^2 \rho) = f_o(\rho) + \frac{1}{2}k_1 \nabla^2 \rho + \frac{1}{2}k_2 (\nabla \rho)^2 + \ldots \tag{2.28}$$

To obtain the total free energy F from Eq. 2.13, Eq. 2.28 must be integrated over the volume V.

$$F = \int f \, d^3 r = \int \left[f_o(\rho) + k_1 \nabla^2 \rho + k_2 (\nabla \rho)^2\right] d^3 r \tag{2.29}$$

By applying the divergence theorem (Grootendorst and Meulenbeldm, 1987), to eliminate the term $\nabla^2\rho$ from Eq. 2.4, one obtains

$$F = \int \left[f_o(\rho) + c\,(\nabla \rho)^2 + \ldots \right] d^3 r \tag{2.30}$$

where

$$c = -\frac{dk_1}{d\rho} + k_2$$

$$= -\left[\frac{\partial^2 f}{\partial \rho \, \partial \nabla^2 \rho}\right]_0 + \left[\frac{\partial^2 f}{(\partial |\nabla \rho|)^2}\right]_0 \tag{2.31}$$

Eq. 2.30 expresses the helmholtz free energy of a small volume of nonuniform solution as the sum of two contributions, one being the helmholtz free energy that this volume would have in a homogeneous solution at local composition and the second a gradient energy which is a function of the non-local composition.
For systems with more than one component, the helmholtz free energy can be expressed in the form

$$F = \int \left[f_o(\rho) + \sum_{i,j}^{N} \frac{1}{2} c_{ij} \nabla \rho_i \cdot \nabla \rho_j \right] d^3 r \tag{2.32}$$

The chemical potential of species i, $\mu_i = \partial F / \partial \rho_i(r)$, obtained from Eq. 2.1 obeys a second order differential equation that can be rearranged to

$$\sum_{j}^{N} \nabla \cdot (c_{ij} \nabla \rho_j) - \frac{1}{2} \sum_{k,j}^{N} \frac{\partial c_{kj}}{\partial \rho_i} \nabla \rho_k \cdot \nabla \rho_j = \frac{\partial \omega}{\partial \rho_i} \tag{2.33}$$

where ω is the thermodynamic potential

$$\omega(\rho) = f_o(\rho) - \sum_{i}^{N} \rho_i \mu_i \tag{2.34}$$

Equation 2.33 is the equilibrium equation, which is a condition for minimum free energy of an inhomogeneous fluid. With (2.33) the determination of a given fluid microstructure becomes a nonlinear boundary value problem. The existence of a fluid microstructure is governed by ω (and therefore the Helmholtz free energy of the homogeneous fluid) and the influence parameters c_{ij}, which affect the stability and characteristic length scale of microstructures. The relation for the influence parameters is (Bongiorno et al., 1975, 1976 and Yang et al., 1976)

$$c_{ij} = \frac{kT}{6} \int s^2 C_0^{ij}(s;\rho) \, d^3 s \tag{2.35}$$

where C_O^{ij} is the two-body direct correlation function between component i and j in a homogeneous system. This result together with Eq. 2.33 shows that through gradient theory the equilibrium distributions of a classical inhomogeneous fluid is determined only by the homogeneous fluid properties, f_o and C_O^{ij}.
The two-body direct correlation function is related to the more familiar pair correlation function $g_O^{ij}(r;\rho)$, which is given by Ornstein and Zernike (1914):

$$g_0(r_{12}) - 1 = C_0(r_{12}) + \rho \int C_0(r_{13}) \left[g_0(r_{23}) - 1 \right] d^3 r_3 \tag{2.36}$$

If we consider a planar system, $\rho = \rho(x)$ then Eq. 2.33 can be multiplied by $d\rho_i/dx$, integrated, and summed over i to yield

$$\sum_{i,j}^{N} \frac{1}{2} c_{ij} \frac{d\rho_i}{dx} \frac{d\rho_j}{dx} = \omega(\rho) + K \tag{2.37}$$

where K is a constant of integration.

The boundary conditions for a planar interface are: $\rho_i(x = -\infty) = \rho^{(1)}$ and $\rho_i(x = \infty) = \rho^{(2)}$. From the thermodynamic conditions of phase equilibria, it follows that μ_i is the equilibrium chemical potential and that K equals the equilibrium pressure, p_o. With these conditions $f_o(\rho)$ from Eq. 2.32 can be eliminated to get

$$F = \sum_{i}^{N} N_i \mu_i - P_N V + A \int_{-\infty}^{\infty} \sum_{i,j}^{N} \frac{d\rho_i}{dx} \frac{d\rho_j}{dx} dx \tag{2.38}$$

from which the interfacial tension can be written as

$$\gamma = \sum_{i,j} \int_{-\infty}^{\infty} c_{ij} \frac{d\rho_i}{dx} \frac{d\rho_j}{dx} dx = 2 \int_{-\infty}^{\infty} \left[f_o(\rho\{x\}) - \sum_{i}^{N} \rho_i \mu_i + p_o \right] dx \tag{2.39}$$

It should be noted that the derivation of Eq. 2.39 does not yield the same expression for γ as obtained through deriving Eq. 2.22. The surface tension from Eq. 2.39 is twice as large compared to the tension from (2.22). This inadequacy lies in the fact that the assumptions used in deriving an expression for $P_T(x)$ are incomplete. Due to the difficulty of defining $P_T(x)$ (Rowlinson and Widom, 1988), Eq. 2.22 is still used to give an insight of how the transverse pressure is distributed in a fluid interface.

2.3.2 Applications to a planar interface

For a one-component fluid Eq. 2.37 can be solved directly to give

$$dx = \sqrt{\frac{c}{2}} \frac{d\rho}{\sqrt{\Delta\omega(n)}} \tag{2.40}$$

where $\Delta\omega(\rho) = \omega(\rho)-P_N$. With this Eq. 2.39 can be put into the profile-independent form

$$\gamma = \sqrt{2} \int_{\rho_g}^{\rho_l} \sqrt{c\,\Delta\omega(\rho)}\, d\rho \tag{2.41}$$

The $\Delta\omega(\rho)$ is represented is Figure 2.4.. It can be seen that $\Delta\omega(\rho)$ is the vertical distance between the curve of $f_o(\rho)$ and a straight line ($\rho\mu$) touching the f_o at the liquid and vapor densities. In a multicomponent system $\Delta\omega(\rho)$ is the vertical distance from the tangent plane parallel to $\Sigma_i\rho_i\mu_i$ in ρ_i space and touching the $f_o(\rho)$ surface at bulk phase points. Again $\Delta\omega(\rho)$ corresponds to the Helmholtz free energy density of the homogeneous fluid measured relative to the free energy of the two-phase system at the overall composition ρ. The $\Delta\omega(\rho)$ follows the composition path across the interface in the integral defining γ.
When the critical point is reached, $\Delta\omega$ flattens out rapidly between ρ_g and ρ_l. This means that the surface tension goes to zero when the critical point is approached.
Flattening of the Helmholtz free energy curve is probably the only mechanism of low tensions in one-component systems. Interfaces near the critical point become broad because $\Delta\omega(\rho) \rightarrow 0$ and $dx \propto \Delta\omega^{-1/2}\, d\rho$ according to Eq. 2.40.
It is convenient for a multicomponent fluid to introduce a path function $\wp$, which increases monotonically, according to $(d\wp)^2 \equiv \Sigma_{i,j} G_{ij}\, d\rho_i\, d\rho_j$ as the density ρ, across the interfacial zone, changes from bulk phase 1 (ρ_1) to bulk phase 2 (ρ_2). The coefficients of G_{ij} (positive definite matrix) can be chosen freely to assure the monotonicity of $\wp$. If, for example, component 1 increases monotonically across the interfacial zone then $\wp=\rho_1$ is acceptable. When none of the densities is monotonic or it is not known whether any is monotonic, then the arc length $(d\wp)^2 = \Sigma_i (d\rho_i)^2$ is a good choice for $\wp$. In any case, a suitable path function can be constructed. Using the chain rule of differentiation ($d\rho/dx = d\rho/d\wp\ d\wp/dx$), Eq. 2.37 can be rearranged to

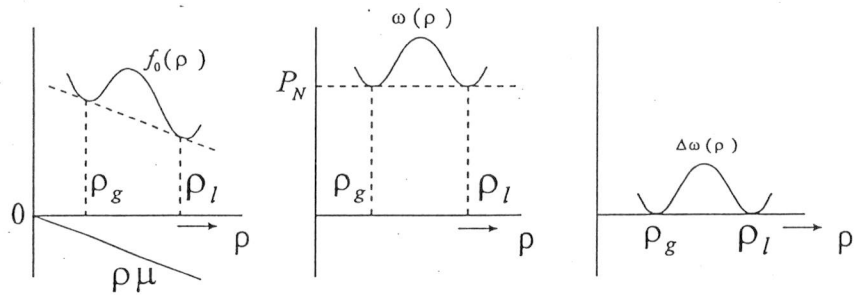

Figure 2.4 Helmholtz free energy $f_0(\rho)$ and thermodynamic potential difference $\Delta\omega(\rho)$ of a one-component inhomogeneous system.

$$d\wp = \sqrt{\frac{2\,\Delta\,\omega(\rho)}{\sum_{i,j} c_{ij}\frac{d\rho_i}{d\wp}\frac{d\rho_j}{d\wp}}}\,dx = \sqrt{\chi(\wp)}\,dx \tag{2.42}$$

From this it follows from Eq. 2.39 that

$$\gamma = \sqrt{2}\int_{\wp(1)}^{\wp(2)} \sqrt{\left(\sum_{i,j} c_{ij}\frac{d\rho_i}{d\wp}\frac{d\rho_j}{d\wp}\right)\Delta\,\omega(\rho)}\,d\wp \tag{2.43}$$

To perform this integral, the density $\rho(\wp)$ along the path $\wp$ must be determined by transforming the independent variable of the differential profile equation (2.33) using the relations

$$\frac{d\rho_i}{dx} = \sqrt{\chi}\,\frac{d\rho_i}{d\wp}\quad,\quad \frac{d^2\rho_i}{dx^2} = \sqrt{\chi}\,\frac{d}{d\wp}\left(\sqrt{\chi}\,\frac{d\rho_i}{d\wp}\right) \tag{2.44}$$

The differential profile then becomes

$$\sum_j c_{ij}\sqrt{\chi}\,\frac{d}{d\wp}\left(\sqrt{\chi}\,\frac{d\rho_j}{d\wp}\right) + \frac{\chi}{2}\sum_{k,j}\frac{\partial c_{kj}}{\partial\rho_i}\frac{d\rho_k}{d\wp}\frac{d\rho_j}{d\wp} = \frac{\partial\omega}{\partial\rho_i} \tag{2.45}$$

i=1,2,...,υ-1. Equation 2.33 and 2.45 are both two-point boundary value problems. The latter, however has finite boundaries, $\wp(1)$ and $\wp(2)$, whereas the first one involves boundaries at $x = \pm\infty$. The transformed equation (Eq. 2.45) appeared to be more conveni-

ent for numerical solution (Carey at al., 1978).

When $d\wp = d\rho_1$ is chosen then the υ equations in Eq. 2.45 reduce to υ-1 equations and this choice leads automatically for a single-component fluid to the analytical solution, (2.40), of the profile equation. For the surface tension this leads to the simple formula, (2.41). If a multicomponent system is considered, similar simplification results if one chooses $G_{ij} = c_{ij}$, in which case $\Sigma_{i,j} (d\rho_i/d\wp)(d\rho_j/d\wp)=1$, $\chi=2\Delta\omega$, and

$$\gamma = \int_0^{\wp_B} \sqrt{2\,\Delta\,\omega\,(\rho(\wp))}\; d\wp \tag{2.46}$$

where $\wp_B$ is the influence parameter-scaled composition path length between phases one and two:

$$\wp_B = \int_{\substack{path \\ integral}} \sqrt{\sum_{i,j} c_{ij} \frac{d\rho_i}{d\wp} \frac{d\rho_j}{d\wp}}\; d\wp \tag{2.47}$$

In practice an iterative method must be used to determine the path length $\wp_B$ and ρ as a function of the path parameter. For example, $\wp_B$ could be guessed. With the boundary conditions $\rho(\wp=0)=\rho_1$ and $\rho(\wp_B)=\rho_2$, Eq. 2.45 can be solved for $\rho(\wp)$. A new value of $\wp_B$ could then be computed from Eq. 2.47. This process can be iterated until successive values of $\wp_B$ agreed to within some prescribed limit.

2.4 The associated perturbed anisotropic chain theory (APACT)

The APACT equation of state has its roots in the perturbed hard chain theory (PHCT) described by Beret and Prausnitz (1975) and Donohue and Prausnitz (1978). The equation of state is an extension of the ideal gas state and takes into account the difference in molecular size and shape and accounts for hydrogen bonding, polar, quadrupolar and induced polar forces. The compressibility factor Z can be expressed in the sum of contributions of the particular interactions stated above.

$$Z = 1 + Z^{assoc} + Z^{rep} + Z^{att} \tag{2.48}$$

The repulsive part (Z^{rep}) of Z is defined by the Carnahan-Starling equation of non-attractive rigid spheres (Carnahan and Starling, 1969) multiplied by the shape factor c. The attractive interactions (Z^{att}) contain three contributions, namely Lennard-Jones, induced polar and anisotropic interactions:

$$Z^{att} = Z^{LJ} + Z^{\mu ind \mu} + Z^{ani} \tag{2.49}$$

Morris et al. (1987) defined an expression for the Lennard-Jones compressibility (Z^{LJ}), while $Z^{\mu ind \mu}$ and Z^{ani}, induced-dipole and anisotropic interactions, are given by Vimalchand et al. (1985, 1986). Z^{assoc}, the hydrogen bonding part of the compressibility, is given by Ikonomou and Donohue (1986) and by Economou and Donohue (1991, 1992). Equations 2.48 and 2.49 are generalized to treat mixtures using the mixing rules which are given by Vimalchand and Donohue (1985, 1986) and by Donohue and Vimalchand (1988).
In order to describe thermodynamic properties of the pure-compounds and mixtures five molecular parameters must be determined by fitting the APACT equation of state to experimental vapor pressure and liquid density data. These molecular parameters are the enthalpy of hydrogen-bond formation, ΔH^{assoc}, the entropy of hydrogen-bond formation, ΔS^{assoc}, the characteristic temperature T^*, the characteristic volume v^* and the shape parameter c, which is one-third of the external density-independent degrees of freedom.
A full description of the APACT equation of state together with several mixing rules are extensively described in Appendix A.

3. Programming section

In calculating the interfacial tension of a fluid interface, the density profiles of all the components must be obtained.
These profiles are obtained with use of Eq. 2.1, and the rearrangement of Eq. 2.1, Eq. 2.33. The differential equations of a planar system with N components becomes

$$\frac{\partial \omega}{\partial \rho_1} = \sum_j^N \frac{d}{dx}\left(c_{1j}\frac{d\rho_j}{dx}\right) - \frac{1}{2}\sum_{k,j}^N \frac{dc_{kj}}{d\rho_1}\frac{d\rho_k}{dx}\frac{d\rho_j}{dx} \tag{3.1}$$

$$\frac{\partial \omega}{\partial \rho_2} = \sum_j^N \frac{d}{dx}\left(c_{2j}\frac{d\rho_j}{dx}\right) - \frac{1}{2}\sum_{k,j}^N \frac{dc_{kj}}{d\rho_2}\frac{d\rho_k}{dx}\frac{d\rho_j}{dx} \tag{3.2}$$

$$\vdots$$

$$\frac{\partial \omega}{\partial \rho_N} = \sum_j^N \frac{d}{dx}\left(c_{Nj}\frac{d\rho_j}{dx}\right) - \frac{1}{2}\sum_{k,j}^N \frac{dc_{kj}}{d\rho_N}\frac{d\rho_k}{dx}\frac{d\rho_j}{dx} \tag{3.3}$$

These equations cannot be solved analytically and must be solved by using a computer program, where a numerical algorithm is used for the calculation of the density profiles. The main structure of the program is represented in Figure 3.1. For detailed information one is referred to Cornelisse (1991).
The input of the program consist of the temperature T, the liquid mole fraction x, estimates of the pressure and vapor mole fraction and the APACT molecular parameters.
Before computing the interfacial tension, bubble point calculations are carried out. The system is at equilibrium when the pressure and chemical potential of component i of both phases are equal. For three phase (LLV) calculations, the equilibrium is reached when the pressure and chemical potential of component i of the liquid 1, liquid 2 and vapor are equal. The equilibrium calculations are followed by the estimation of the path length, $\wp_B$.
From the estimation the density profiles are calculated followed by a recalculation of the path length. This iterative process continues until the difference between the estimate and calculated path length lies is smaller than a given criterium. At the end the interfacial tension can be determined.

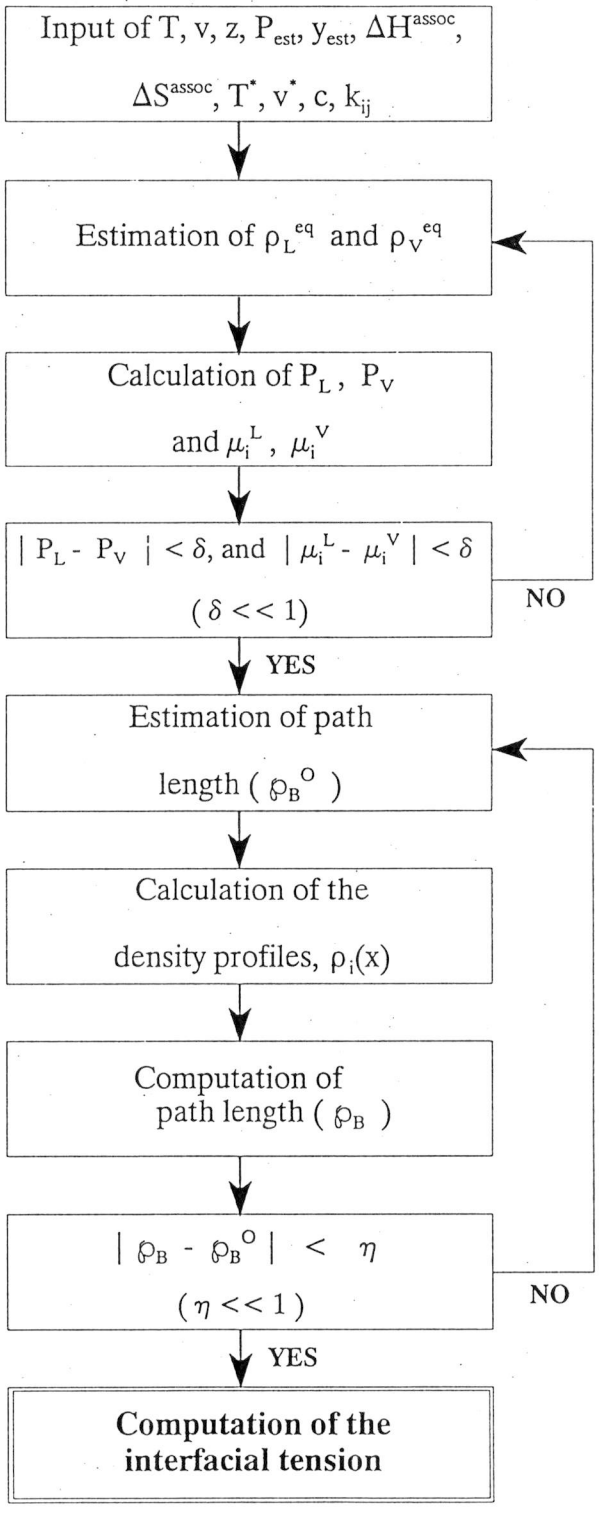

Figure 3.1 Schematic representation of the used computer program.

4. Results and discussion

4.1 Determination of the APACT equation of state parameters

As already was mentioned in paragraph 2.4, the thermodynamic properties of the pure-compounds must be determined by fitting the APACT equation of state to experimental vapor pressure and liquid density data. One of the difficulties in doing this is that several sets of model parameters are obtained for one compound. When each of these sets of model parameters is used for the calculation of phase equilibria a low absolute average deviation (AAD) is obtained.

$$\%\,AAD = \frac{100}{K}\sum_{i=1}^{K}\frac{|\,M_i^{calc} - M_i^{exp}\,|}{M_i^{exp}} \qquad (4.1)$$

where M is a thermodynamic quantity such as pressure or volume. K is the number of experimental data points.
An example where several sets of APACT-parameters were obtained is given for methanol in Table 4.1. The remaining problem is which set of parameters are chosen for the calculation of phase equilibria. The choice of the right model parameters is done by a simple procedure. It is assumed that the c-parameter or the characteristic volume, v^* of, for example, methanol has approximately the same c-value (or v^*) than ethane, because both molecules have about the same chain length. The c-values of alkanes are known in literature. The above assumption is also true for the volume, but not the characteristic temperature T^*. This parameter is not only a function of the chain length but a function of the kind of atoms in the molecule as well.

Table 4.1 Different sets of APACT-parameters for methanol.

Set	ΔH^{assoc} (kJ/mol)	$\Delta S^{assoc}/R$	T^* (K)	v^* (lit/mol) $*10^{-2}$	c [-]	%AAD density PVT	%AAD pressure PVT	%AAD P^{sat}
1	-16.736	-11.469	309.4	3.312	2.0540	0.85	1.37	0.49
2	-18.828	-11.384	311.0	3.358	1.8100	0.71	0.49	0.38
3	-20.920	-11.322	308.0	3.379	1.5884	0.65	0.70	0.31
4	-23.012	-11.424	305.4	3.401	1.3784	0.61	0.27	0.25
5	-25.104	-11.600	303.4	3.433	1.1663	0.56	0.37	0.18
6	-27.196	-11.805	300.8	3.481	0.9490	0.49	0.18	0.11
7	-29.288	-12.015	296.2	3.555	0.405	0.18	0.18	0.04

The association enthalpy of methanol which corresponds to the c-parameter of methane and the ΔH^{assoc} that corresponds with $c_{propane}$ is averaged and used to refit the right model parameters. In Table 4.2 up to 4.5, the APACT-parameters are given for n-alkanes, water, benzene, carbon-dioxide and n-alcohols.
The above procedure for determining the model parameters can be circumvented if the enthalpy of hydrogen-bond formation, ΔH^{assoc} is known. Literature values for alcohols are reported by Pimentel and Mcclellan (1960), but they range from 14.6 to 25 kJ/mol and are not very reliable. Values of ΔS^{assoc} are rarely reported and are also not very reliable (Ikonomou and Donohue, 1986).
It was shown for water by Smits et al. (1994) that the obtained APACT pure component parameters, which were determined by fitting sub-critical experimental data, can be used for calculations in the supercritical region up to very high pressures.

Table 4.2 APACT parameters for alkanes and % AAD in liquid molar volume and vapor pressure.

					% AAD		Temperature range (K)		Data points	
Compound	T^* (K)	v^* (dm^3/mol)	c	ε/k	v^{liq}	p^{sat}	v^{liq}	p^{sat}	v^{liq}	p^{sat}
n-ethane[b]	225.1	0.03195	1.1636	105	0.8	1.6	95-600	105-305	29	6
n-propane[a]	260.7	0.04295	1.3250	105	0.226	0.375			53	8
n-butane[a]	287.3	0.05332	1.5040	105	0.864	0.331			12	10
n-pentane[b]	311.4	0.06295	1.6501	105	0.3	2.1	193-473	223-453	17	5
n-hexane[a]	326.5	0.07384	1.8170	105	0.276	0.155			23	25
n-heptane[b]	337.3	0.08293	2.0243	105	1.8	1.6	233-623	298-540	17	8
n-octane[a]	347.1	0.09552	2.1860	105	0.372	0.195			13	7
n-nonane[b]	351.5	0.01058	2.4382	105	1.5	1.6	303-393	280-586	15	5
n-decane[a]	362.1	0.11806	2.5420	105	0.939	0.216			12	12

Table 4.3 APACT parameters for several compounds.

Compound	ΔH^{assoc} (kJ/mol)	$\Delta S^{assoc}/R$	T^* (K)	v^* (dm^3/mol)	c	ε/k (K)	μ^d (D)	Q (esu) $*10^{26}$	α ($Å^3$)
water[a] (2-site)	-20.10	-10.28	219.3	0.01173	1.00	350	1.75		1.59
water[a] (3-site)	-20.10	-10.97	183.8	0.01164	1.00	350	1.75		1.59
CO_2[c]			192.77	0.02227	1.1788	120		4.30	
Benzene[c]			379.94	0.05635	1.3362	127		10.00	

[a] Parameters were taken from Economou and Donohue (1992)
[b] Parameters were taken from Morris et al. (1987)
[c] Parameters were taken from Vimalchand and Donohue (1985)

Table 4.4 Model parameter for n-alcohols for the two-site APACT.

Compound	ΔH^{assoc} (kJ/mol)	ΔS^{assoc}	T^* (K)	v^* (dm^3/mol)	c	ε/k^a (K)	μ^d	α
Methanol	-19.623	-10.377	280.3	0.02422	1.2038	161	1.70	3.29
Ethanol	-23.681	-11.483	300.0	0.03432	1.3033	161	1.73	5.11
1-Propanol	-25.815	-11.994	320.3	0.04378	1.4529	161	1.68	6.74
1-Butanol	-26.317	-12.336	340.0	0.05422	1.6532	161	1.81	8.88
1-Pentanol	-26.568	-12.301	352.9	0.06399	1.8423	161	1.64	10.38
1-Hexanol	-27.029	-12.662	369.1	0.07429	1.9893	161	1.65	12.156
1-Heptanol	-26.568	-12.490	373.3	0.08365	2.2074	161	1.73	13.932
1-Octanol	-25.146	-11.866	376.3	0.09293	2.3958	161	1.73	15.708
1-Nonanol	-23.221	-11.000	377.9	0.10166	2.5704	161	1.70	17.484
1-Decanol	-19.665	-9.900	378.4	0.10921	2.7926	161	1.74	19.260

[a] Parameters were taken from Ikonomou and Donohue (1986)

Table 4.5 % AAD in liquid molar volume and vapor pressure for n-alcohols and water.

Compound	% AAD		Temperature range (K)		Data Points	
	v^{liq}	P^{sat}	v^{liq}	P^{sat}	v^{liq}	P^{sat}
Water (2-site)	0.966	0.570			60	8
Water (3-site)	1.040	0.425			60	8
Methanol	0.505	0.269	295-474	295-357	25	29
Ethanol	0.598	0.231	295-479	307-367	24	28
1-Propanol	0.675	0.143	297-500	321-378	25	34
1-Butanol	0.576	0.242	304-523	322-399	27	34
1-Pentanol	0.5834	0.129	319-549	357-514	29	33
1-hexanol	0.766	0.465	332-569	334-430	33	22
1-Heptanol	0.921	0.809	351-595	349-426	32	20
1-Octanol	1.427	1.115	364-617	358-554	31	50
1-Nonanol	1.833	2.639	375-629	375-495	32	23
1-Decanol	2.876	2.626	388-656	400-504	32	38

The APACT molecular parameters were determined with experimental data obtained from Boublik et al. (1984) and Smith et al. (1986). The dipole moments for alcohols were taken from McClellan (1989). Polarizabilities up to 1-butanol were obtained from the CRC Handbook Of Chemistry and Physics (1995). The polarizability of alcohols above 1-butanol were calculated using Landolt's rule (Moelwyn-Hughes, 1961).

The dependence of ΔH^{assoc}, ΔS^{assoc}, T^*, v^* and c as a function of the carbon number of n-alcohols is drawn in Figure 4.1 to Figure 4.5.

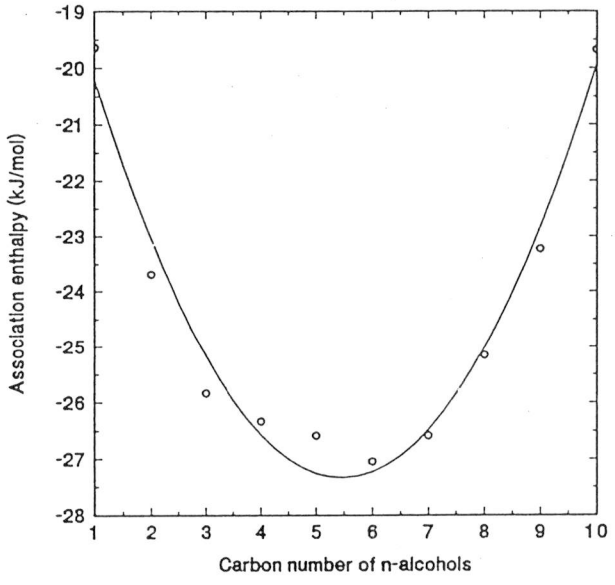

Figure 4.1 Association enthalpy for normal alcohols as a function of carbon number.

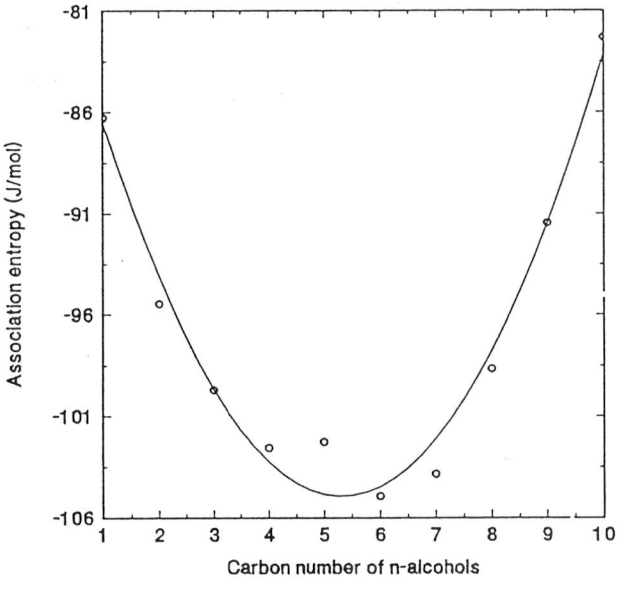

Figure 4.2 Association entropy for normal alcohols as a function of carbon number.

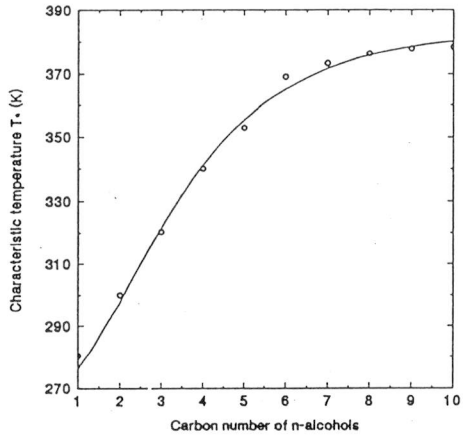

Figure 4.3 Characteristic temperature, T^* for normal alcohols as a function carbon number.

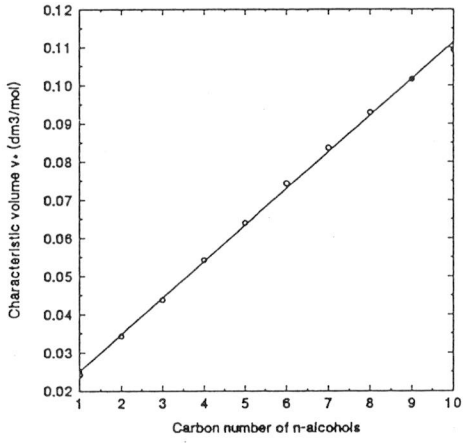

Figure 4.4 Characteristic volume, v^* for normal alcohols as a function of carbon number.

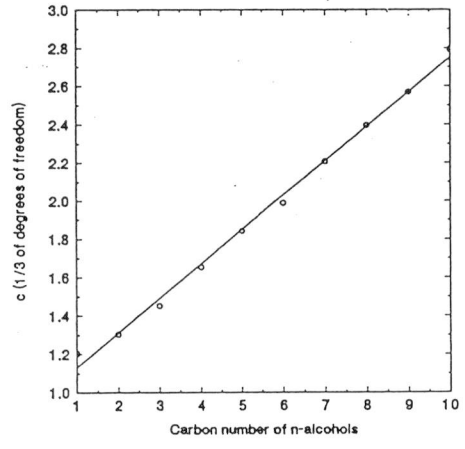

Figure 4.5 Shape parameter, c for normal alcohols as a function of carbon number.

The plot of v^* and c versus carbon number are virtually linear indicating that each $-CH_2-$ segment will contribute an equal amount to the characteristic volume, v^* or the shape parameter, c. The characteristic temperature versus carbon number shows a decreasing curve, meaning that each $-CH_2-$ segment adds less energy than the previous one. Examining the ΔH^{assoc} and $\Delta S^{assoc}/R$ against carbon number, a minimum is observed between 5 and 6. It is difficult to say, wether the parabolic shape of ΔH^{assoc} or ΔS^{assoc} versus carbon is a correct description of these parameters versus n. A possible explanation is that the degree of hydrogen-bonding, resulting in a higher association enthalpy, increases when the size of the normal alcohol increases with a $-CH_2-$ segment. The extremum in Figure 4.4 is caused by the effect that the lipophilic (fat loving) tail of the normal alcohol also increases with increasing molecular size, preventing hydrogen-bond formation.

The dependence of T^*, v^* and c versus the carbon number of alkanes is given in Figure 4.6 to show the similarity of T^* ,v^* and c between n-alcohols and n-alkanes.

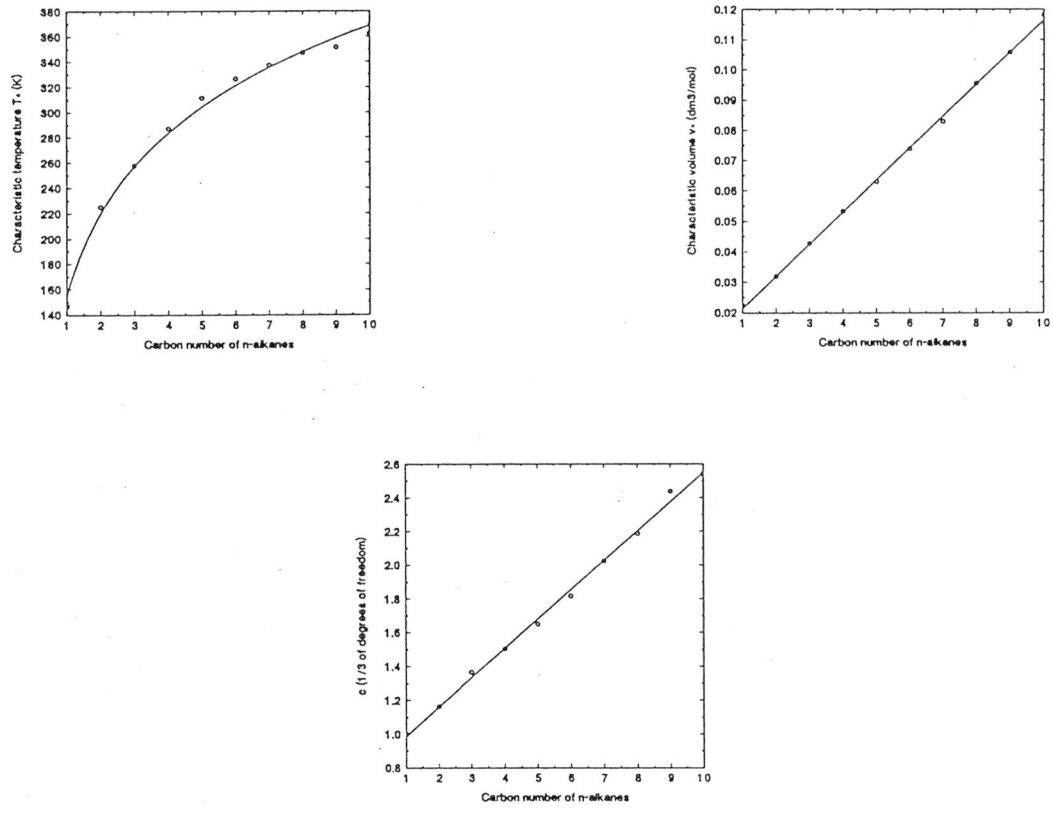

Figure 4.6 APACT parameters of normal alkanes as a function of carbon number.

4.2 Determination of the pure component influence parameters, c_{ii} and interfacial tension

Two important inputs of gradient theory are the Helmholtz free energy obtained from the equation of state and the influence parameters, c_{ij}. The influence parameters are rigorously related to the direct correlation function as was shown in Eq. 2.35. One of the problems involved here is that the direct correlation function, C_O^{ij} is not known. This correlation function was related to the two-body correlation function, g_O^{ij} given by Ornstein and Zernike (1914). The obtained integral equations is, however, cumbersome and can only be solved analytically for hard-spheres. A different approach is, therefore, preferred. Cornelisse et al. (1993) showed that good results can be obtained when the influence parameter c_{ii} of the pure component is fitted to experimental interfacial tension data. However, in this report a different approach is used.

If the influence parameter of water, fitted for each interfacial tension data point at a certain temperature, is plotted as a function of temperature then Figure 4.7 is obtained. As a comparison the influence parameter of water for the Peng-Robinson equation of state is also given.

In Figure 4.7, the c_{water} versus temperature curve for APACT can be divided into two parts, the part that increases on increasing temperature and the second one that decreases on increasing temperature. It is assumed that the second part is a physically incorrect description for c_{water} as a function of temperature. The explanation lies in the fact that the influence parameter has a increasing linear dependence of the temperature. This can be seen in Eq. 2.35, where we assume that the part right from the integral is approximately constant far away of the critical point. It can also be seen that the Peng-Robinson curve in Figure 4.7 gives a physically better description of c_{water} in the region of the critical temperature than APACT.

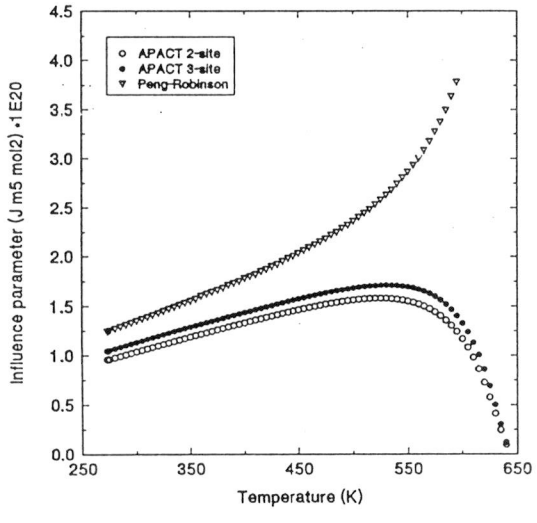

Figure 4.7 The influence parameter of water as a function of the temperature for the APACT and Peng-Robinson equation of state.

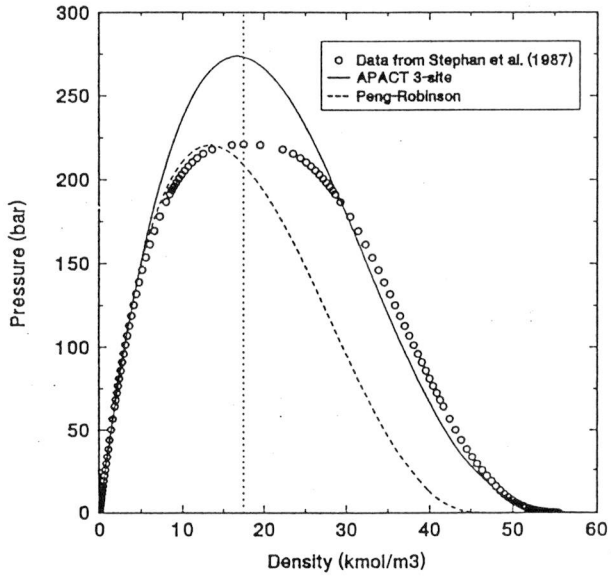

Figure 4.8 Experimental coexistence curve along with the predicted APACT and Peng-Robinson coexistence curves.

The remaining question is why APACT predicts a decreasing influence parameter as a function of temperature. The explanation is given through examining Figure 4.8, the coexistence curve of water. It can be seen that APACT overpredicts the critical pressure as well as the critical temperature (T_c(real) = 647.13 K ; T_c(APACT) = 674 K).
Figure 4.8 shows that APACT predicts a larger density difference than the experimental one in the region of the critical point. According to Eq. 2.39 (where the subscript i and j are equal) the influence parameter, c_{water} must compensate for the increasing density gradient, because the interfacial tension goes to zero. The compensation is done by a decreasing c_{water} as function of the temperature when the critical point is reached.
To summarize, the decreasing part of the APACT curve in Figure 4.7 is caused by the overprediction of the critical temperature and pressure by the APACT equation of state.
It can also be seen in Figure 4.8 that Peng-Robinson predicts the right critical pressure and critical temperature, but is very poor in predicting liquid densities. At low and moderate temperatures (T < 500 K) this causes the density gradients to be smaller than the ones predicted by APACT. The predicted influence parameters of water by Peng-Robinson are, therefore larger than the predicted influence parameters obtained by APACT.
The influence parameter as a function of temperature is determined by using a straight line given by Eq. 4.2 to fit the first, "increasing" part of Figure 4.7. The regression coefficients of water and other compounds are given in Table 4.6.

$$c_{ii} = a + b \cdot T \tag{4.2}$$

Table 4.6 Regression parameters for various compounds.

Compound	a $(J \cdot m^5 \cdot mol^2) * 10^{20}$	b $(J \cdot m^5 \cdot mol^2/K) * 10^{23}$
Water (2-site)	2.52492	2.66084
Water (3-site)	3.10659	2.77750
Methanol	0.44136	4.65671
Ethanol	2.06310	9.78824
1-Propanol	3.45936	30.54339
1-Butanol	6.04324	29.47856
1-Pentanol	13.76259	30.23951
1-Hexanol	13.69093	56.05417
1-Heptanol	20.76504*	65.69758*
1-Octanol	28.34269	80.13767
1-Nonanol	29.61897	121.39412
1-Decanol	29.45897	169.65648
Benzene	20.88989	10.24379
CO_2	2.64183	
n-Butane	17.28740	
n-Pentane	25.36499	
n-Hexane	37.20256	
n-Heptane	50.35482	
n-Octane	66.29582	
n-Decane	107.63649	

*Since there was no interfacial tension data available for 1-heptanol, the parameters a and b were fitted.

The experimental and the predicted interfacial tension of water are given in Figure 4.9. It can be seen that the two- and three-site APACT follow the experimental data very well until approximately 100 K before the critical temperature. From 550 K until the critical temperature, APACT overpredicts the interfacial tension, because the calculated influence parameter from Eq. 4.2 is larger than the values shown in Figure 4.7. It is possible to fit a polynomial function through the APACT curves in Figure 4.7, resulting in the correct prediction of the interfacial tension until the critical point. This procedure was not followed because the predicted phase behaviour by APACT would be still incorrect in the vicinity of the critical point. Accurate predictions can be obtained by incorporating scaling behaviour in the APACT equation of state.

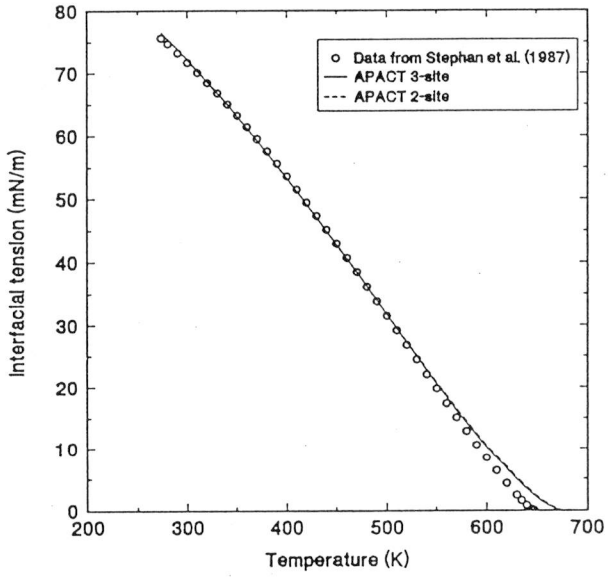

Figure 4.9 Experimental and predicted interfacial tension of water.

In Figure 4.10 it is shown why the influence parameter is taken as a function of the temperature. This figure shows three predicted interfacial tension for the three-site APACT with a constant influence parameter, obtained at one temperature. It can be seen that all the predicted curves cover only a small range in the experimental interfacial tension and fail to describe the whole region from the triple point up to the critical point of water.

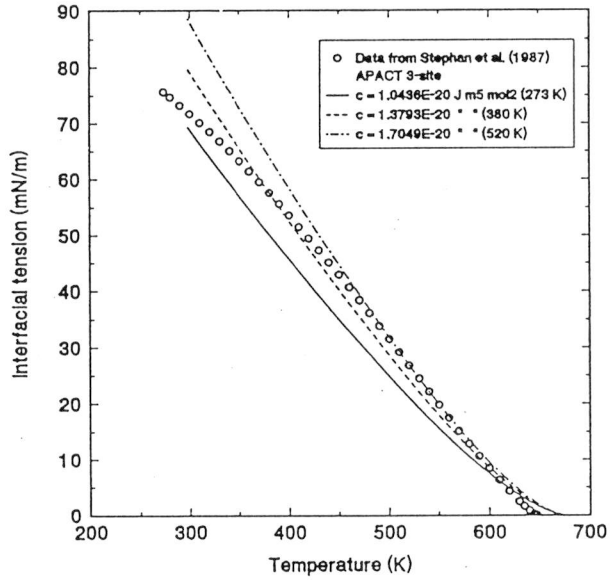

Figure 4.10 Experimental and predicted interfacial tension of water for the three-site APACT with constant influence parameters.

It can be seen in Figure 4.9, that the differences between interfacial tension predictions with the two- and three-site APACT are small.
In the Figures 4.11 up to 4.19, the influence parameter as a function of the temperature, the coexistence curve, and the experimental and predicted interfacial tension are given for ethanol, benzene and hexane.

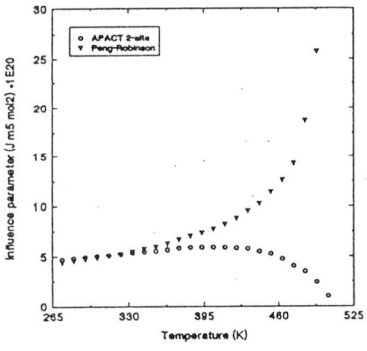

Figure 4.11 Influence parameter of ethanol as a function of the temperature.

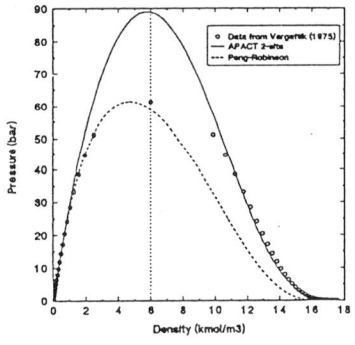

Figure 4.12 Coexistence curve of ethanol.

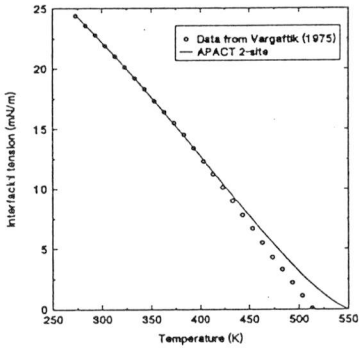

Figure 4.13 Experimental and predicted interfacial tension for ethanol.

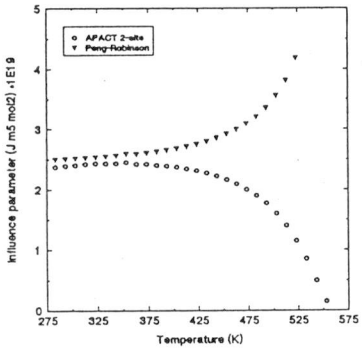

Figure 4.14 Influence parameter of benzene as a function of the temperature.

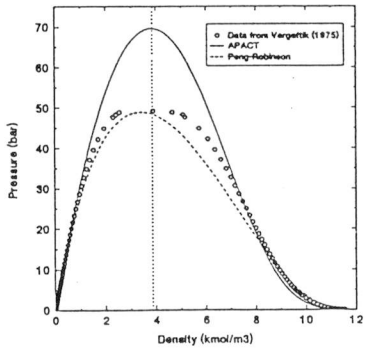

Figure 4.15 Coexistence curve of benzene.

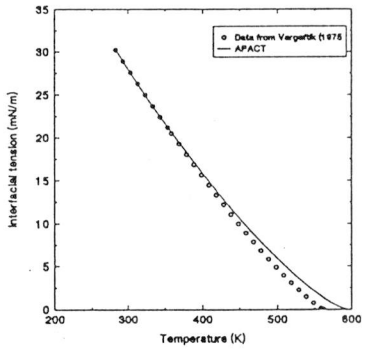

Figure 4.16 Experimental and predicted interfacial tension for benzene.

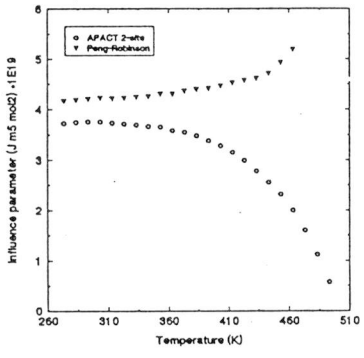

Figure 4.17 Influence parameter of hexane as a function of the temperature.

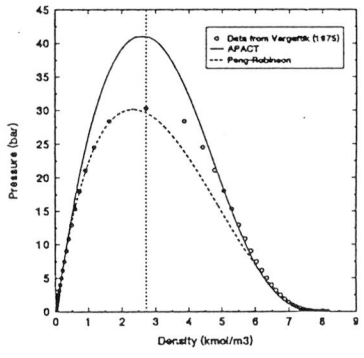

Figure 4.18 Coexistence curve of hexane.

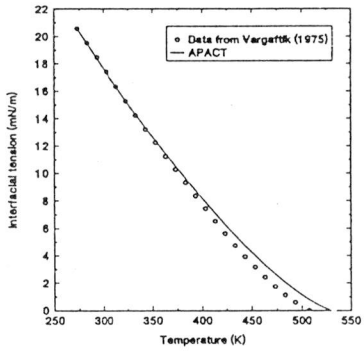

Figure 4.19 Experimental and predicted interfacial tension for hexane.

In the next section, the experimental and predicted interfacial tension are given for the pure components: methanol, 1-propanol, 1-butanol, 1-pentanol, 1-hexanol, 1-heptanol, 1-octanol, 1-nonanol, n-butane, n-pentane, n-heptane, n-octane, n-decane and carbon-dioxide. The influence parameters, c_{ii} of the normal alcohols were taken as a function of temperature, where the influence parameters for n-alkanes and carbon dioxide were taken as a constant (see Table 4.6).

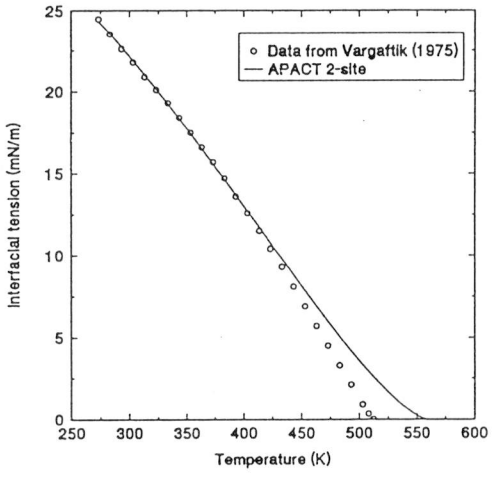

Figure 4.20 Predicted and experimental interfacial tension of methanol.

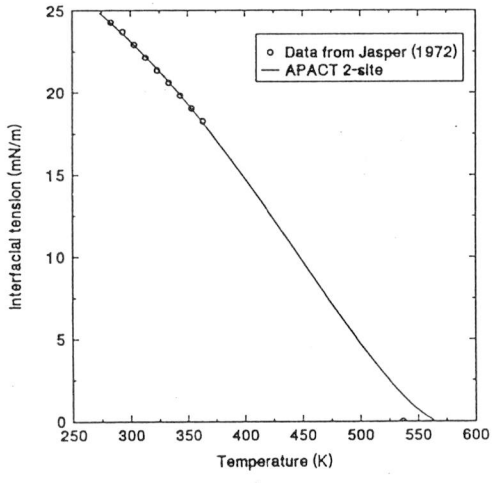

Figure 4.21 Predicted and experimental interfacial tension of 1-propanol.

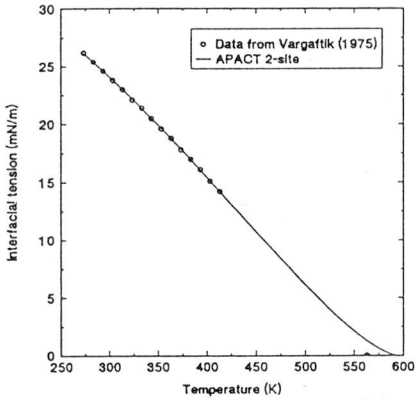

Figure 4.22 Predicted and experimental interfacial tension of 1-butanol.

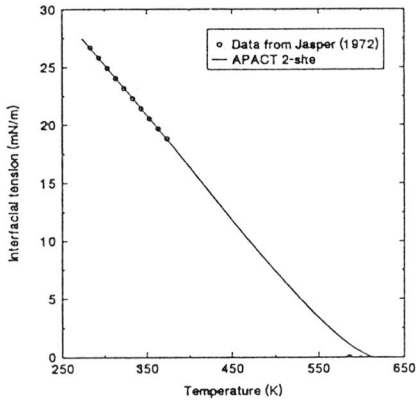

Figure 4.23 Predicted and experimental interfacial tension of 1-pentanol.

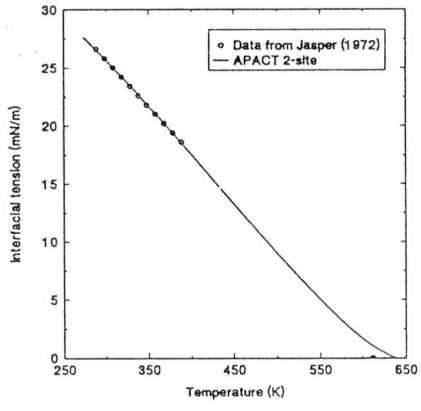

Figure 4.24 Predicted and experimental interfacial tension of 1-hexanol.

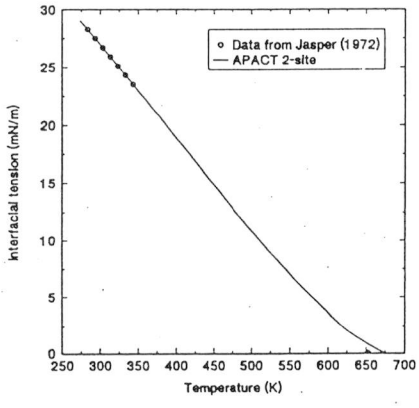

Figure 4.25 Predicted and experimental interfacial tension of 1-octanol.

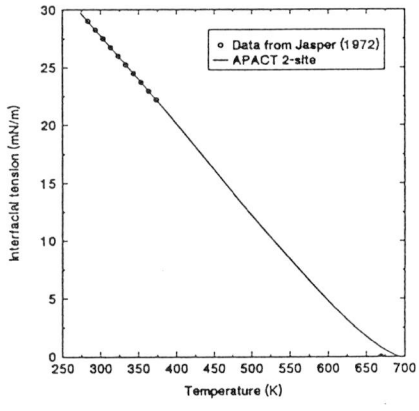

Figure 4.26 Predicted and experimental interfacial tension of 1-nonanol.

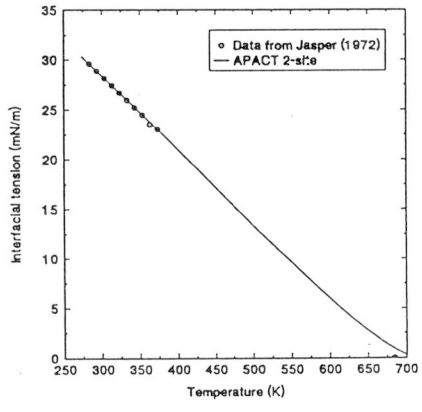

Figure 4.27 Predicted and experimental interfacial tension of 1-decanol.

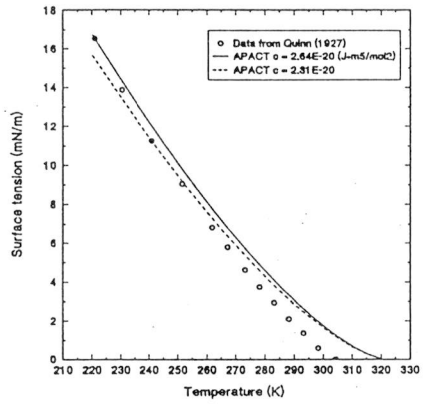

Figure 4.28 Predicted and experimental interfacial tension of carbon-dioxide.

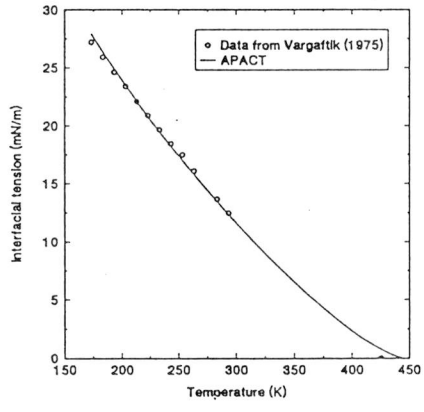

Figure 4.29 Predicted and experimental interfacial tension of n-butane.

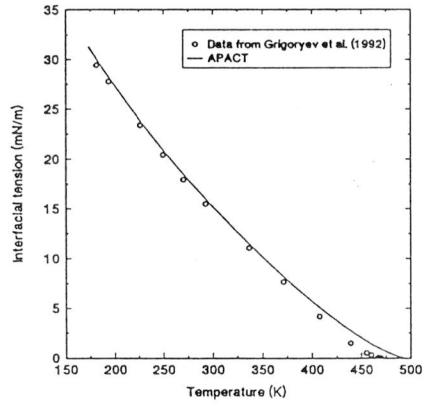

Figure 4.30 Predicted and experimental interfacial tension of n-pentane.

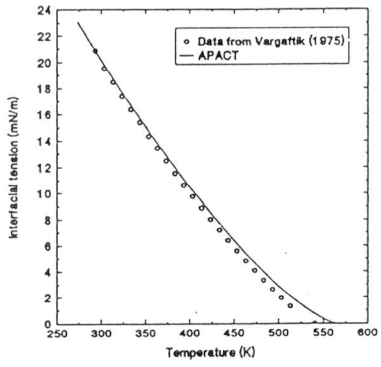

Figure 4.31 Predicted and experimental interfacial tension of n-heptane.

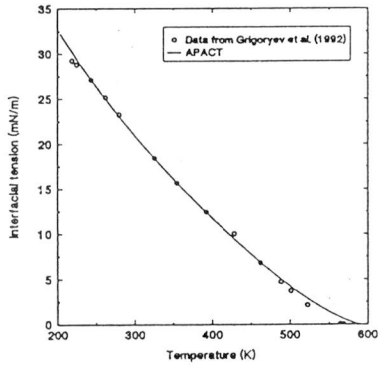

Figure 4.32 Predicted and experimental interfacial tension of n-octane.

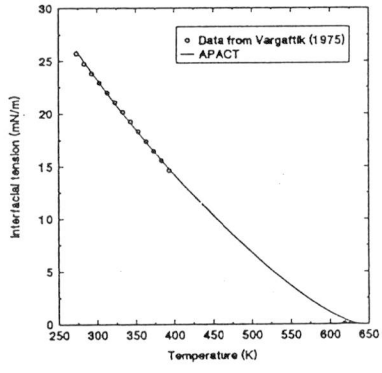

Figure 4.33 Predicted and experimental interfacial tension of n-decane.

It can be seen that the interfacial tension of compounds other than water, ethanol, benzene and hexane can be accurately described using the linear dependence of the influence parameter. Predictions are, however, less accurate in the critical region.

4.3 Multicomponent systems

The pure component influence parameters, c_{ii} in multicomponent systems, were taken as a function of temperature (see Table 4.6). The cross influence parameters, c_{ij} are determined by

$$c_{ij} = (1 - \beta_{ij}) \sqrt{c_{ii} c_{jj}} \qquad (4.3)$$

where β_{ij} is an adjustable parameter. In this report, the value of β_{ij} was set equal to zero. This has the advantage that Eq. 2.33 reduces to the following set of non-linear equations

$$\sqrt{c_{11}} [\mu_i(\rho) - \mu_i] = \sqrt{c_{ii}} [\mu_1(\rho) - \mu_1] \qquad (4.4)$$

These equations are much easier to solve than the second-order differential equations given by Eq. 2.33.

4.3.1 Binary systems

Water/n-Alcohols

In Figure 4.34 up to 4.37, the mixtures water(1)/methanol(2) and water(1)/ethanol(2) are given. It can be seen from these figures that an accurate prediction of the interfacial tension require a accurate prediction of the phase equilibria. It can also be seen that predictions of phase behaviour and interfacial tension, with a binary interaction parameter, k_{ij} of zero, are better for water/ethanol than water/methanol. A non-zero value of the k_{ij} parameter for water/methanol will improve the phase behaviour (Ikonomou and Donohue, 1988) and probably the interfacial tension as well. The binary interaction parameter, k_{ij} corrects the Lennard-Jones attractive part in APACT.

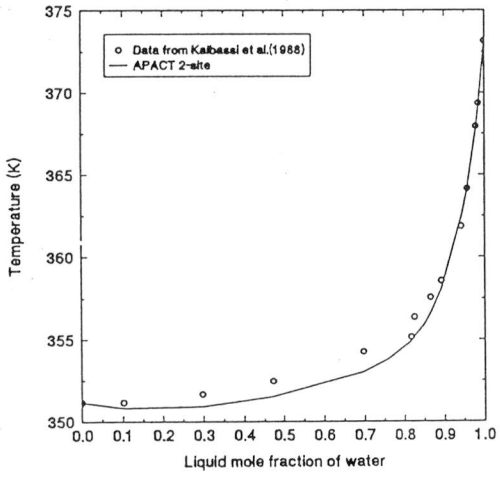

Figure 4.34 T-x diagram for water(1)/ethanol(2) at 1 atm.

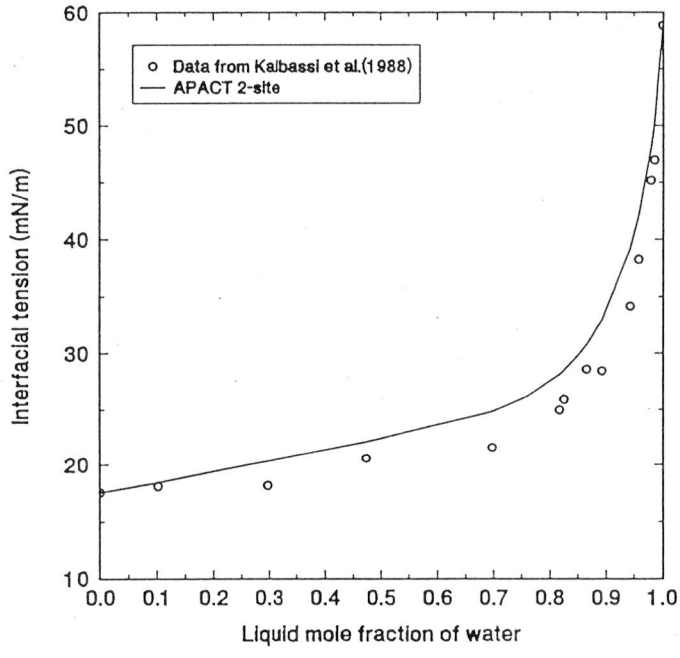

Figure 4.35 Predicted and experimental interfacial tension of water(1)/ethanol(2) at 1 atm.

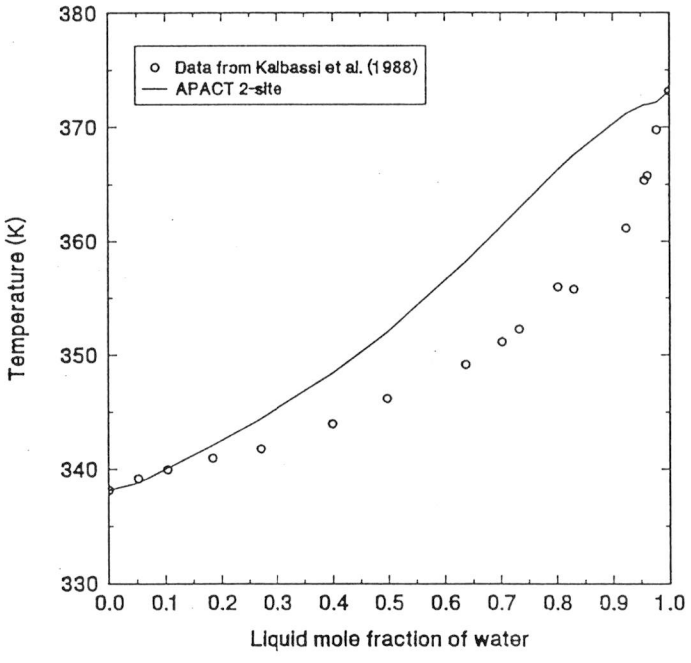

Figure 4.36 T-x diagram for water(1)/methanol(2) at 1 atm.

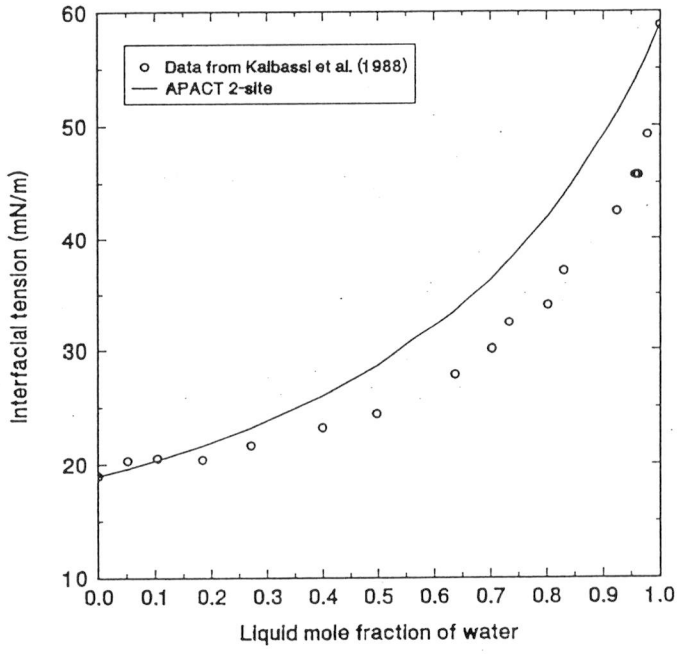

Figure 4.37 Predicted and experimental interfacial tension of water(1)/methanol(2) at 1 atm.

Figure 4.38 gives the density profiles of the liquid-vapor interfaces of water/methanol and water/ethanol at 1 atm. The density profiles of the alcohols show a maximum. The Helmholtz free energy of both nonuniform systems is minimized when the alcohol is absorbed in the interface.

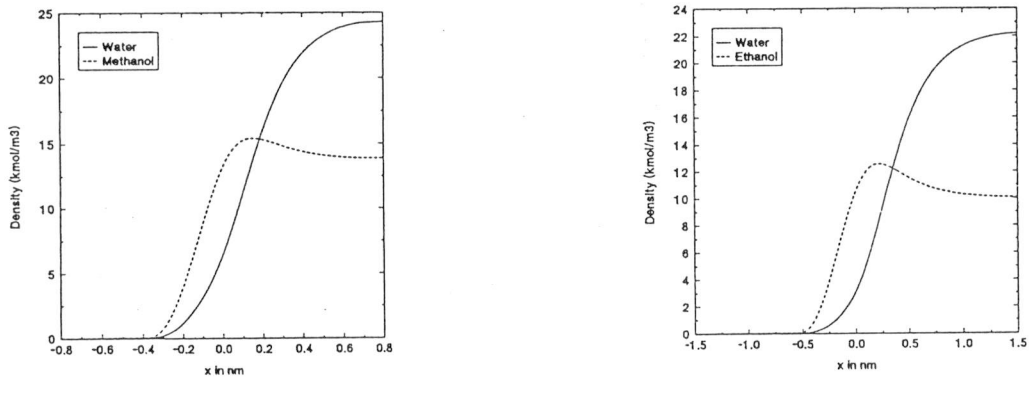

Figure 4.38 Density profiles of the systems water/methanol (x_{water} = 0.637) and water/ethanol (x_{water} = 0.697) at 1 atm.

Figure 4.39 shows the interfacial tension predictions of three phase (LLV) water/n-alcohols systems at 20 °C. L1 is indicated as the n-alcohol rich-phase and L2 as the water-rich phase. Predictions are good for the L1-V and the L1-L2 interfaces but less accurate for the L2-V interface. The binary interaction parameter, k_{ij} for water/n-alcohols are given in Table 4.7

Table 4.7 Binary interaction parameters for the systems water/n-alcohols at 20°C.

System	k_{ij}
water/1-pentanol	-0.05
water/1-hexanol	-0.07
water/1-heptanol	-0.10
water/1-nonanol	-0.14

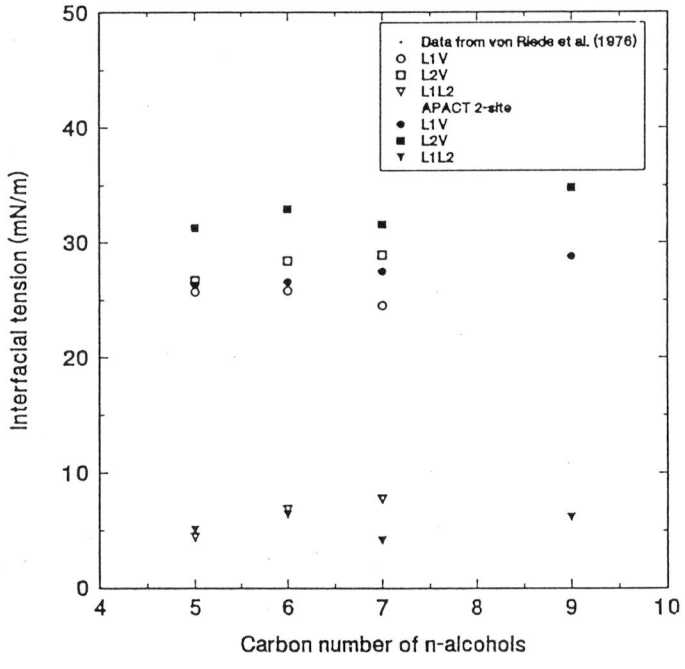

Figure 4.39 Predicted and experimental interfacial tension of the three phase systems water(1)/n-alcohols(2) at 20°C.

n-alcohols/n-alcohols

Five n-alcohol/n-alcohol systems were investigated. Figure 4.40 up to 4.45 shows the predictions of interfacial tension of methanol/1-propanol, ethanol/1-decanol, 1-propanol/1-decanol, 1-butanol/1-decanol and 1-hexanol/1-decanol. Predictions turn out to be good with zero k_{ij}-values. When the system 1-hexanol/1-decanol is examined, it can be seen that the calculated data near almost pure 1-hexanol do not predict the pure interfacial tension of 1-hexanol. This is explained by the fact that the influence parameter of 1-hexanol was fitted to the data of Jasper (1972), where Figure 4.45 show the data of Benson et al. (1972). Differences in reported values of the interfacial tension of pure compounds are commonly observed.

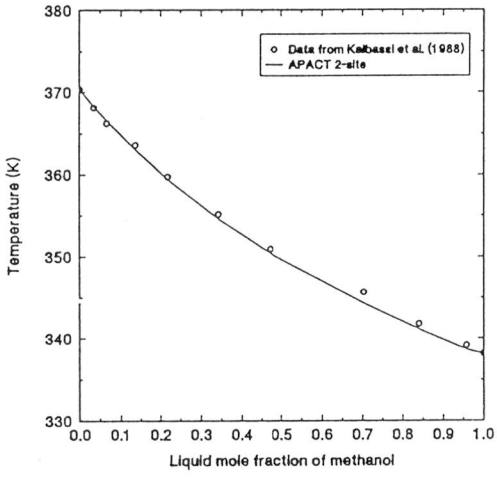

Figure 4.40 T-x diagram of methanol(1)/1-propanol(2) at 1 atm.

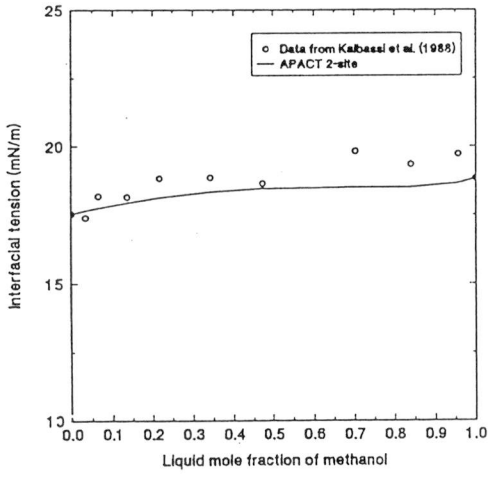

Figure 4.41 Predicted and experimental interfacial tension of methanol(1)/1-propanol(2) at 1 atm.

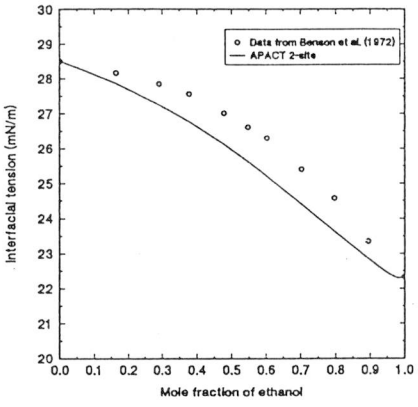

Figure 4.42 Predicted and experimental interfacial tension of ethanol(1)/1-decanol(2) at 20 °C.

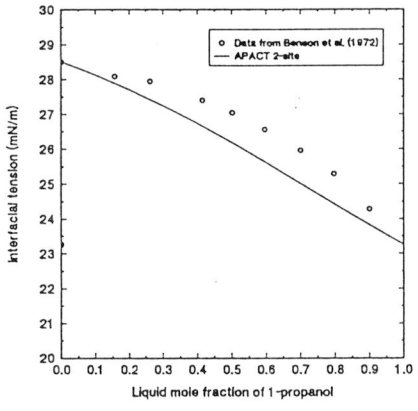

Figure 4.43 Predicted and experimental interfacial tension of 1-propanol(1)/1-decanol(2) at 20 °C.

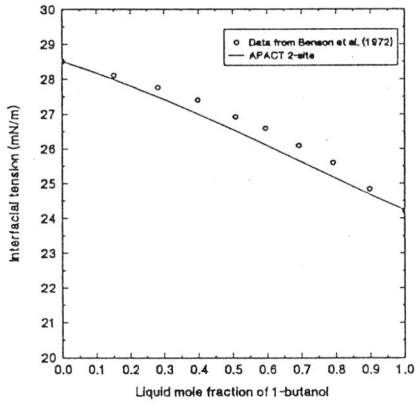

Figure 4.44 Predicted and experimental interfacial tension of 1-butanol(1)/1-decanol(2) at 20 °C.

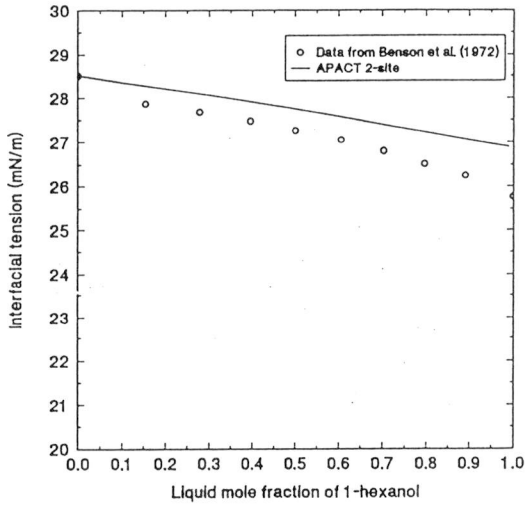

Figure 4.45 Predicted and experimental interfacial tension of 1-hexanol(1)/1-decanol(2) at 20 °C.

n-alcohols/n-alkanes

In Figure 4.46 up to 4.49, systems containing n-alcohols/n-alkanes are given. These systems are ethanol/n-hexane, ethanol/n-heptane, 1-propanol/n-hexane and 1-propanol/n-heptane. In the systems ethanol/n-hexane and ethanol/n-heptane non-zero k_{ij}-values were necessarily used, otherwise APACT would predict heteroazeotropy instead of azeotropy. For 1-propanol/n-hexane and 1-propanol/n-heptane k_{ij} values of zero were taken.

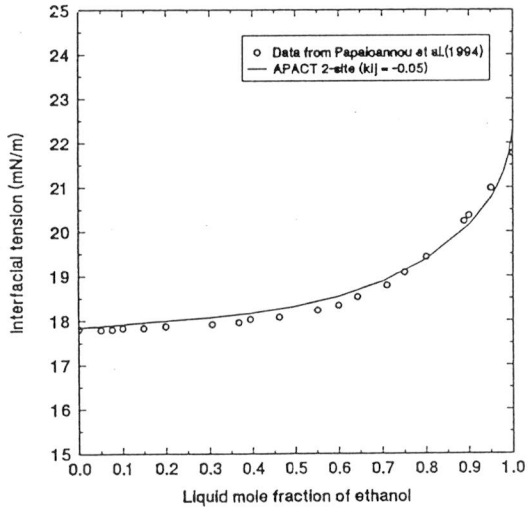

Figure 4.46 Predicted and experimental interfacial tension of ethanol(1)/n-hexane(2) at 25 °C.

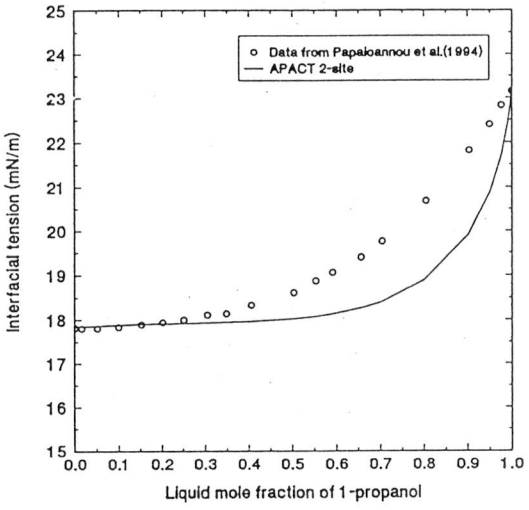

Figure 4.47 Predicted and experimental interfacial tension of 1-propanol(1)/n-hexane(2) at 25 °C.

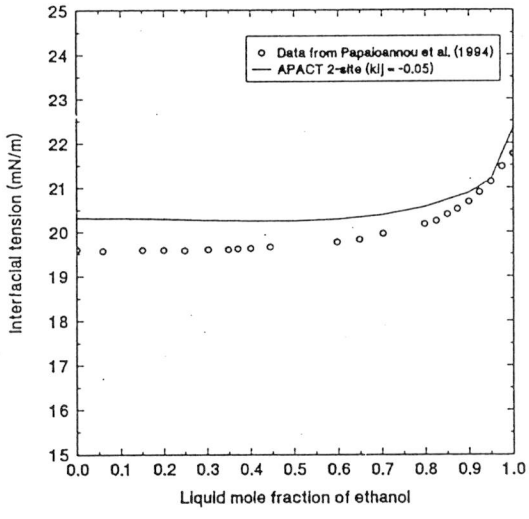

Figure 4.48 Predicted and experimental interfacial tension of ethanol(1)/n-heptane(2) at 25 °C.

When the density profiles of the mixture 1-propanol/n-heptane at 60 °C are studied, a remarkable effect is observed. It is shown in Figure 4.50 that an increasing 1-propanol density at a certain distance, x in the interface causes an decrease in the density of n-heptane. It is possible that the 1-propanol molecules are orientated, by means of hydrogen-bonding, is such a way that they do not allow other molecules in their neighbourhoods that could disturb this orientation. This results in a decrease of the larger and non-polar molecules.

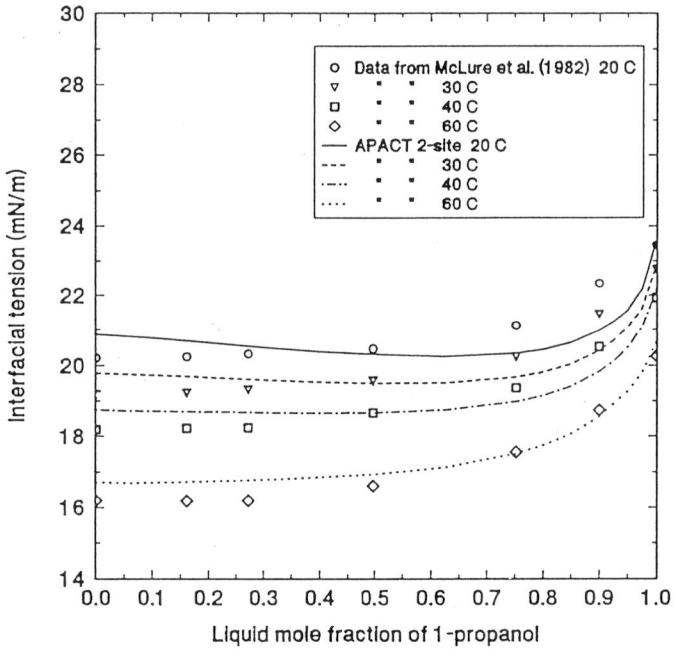

Figure 4.49 Predicted and experimental interfacial tension of 1-propanol(1)/n-heptane(2) at several temperatures.

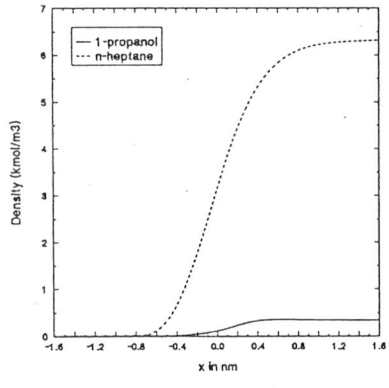

$x_{1\text{-propanol}} = 0.05$

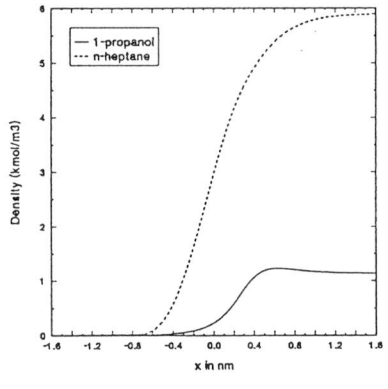

$x_{1\text{-propanol}} = 0.161$

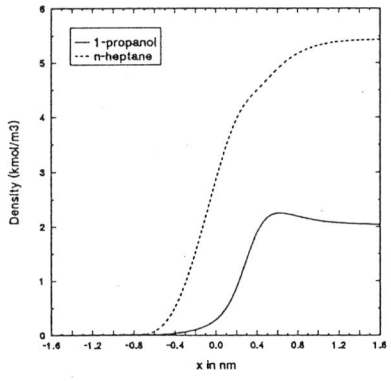

$x_{1\text{-propanol}} = 0.272$

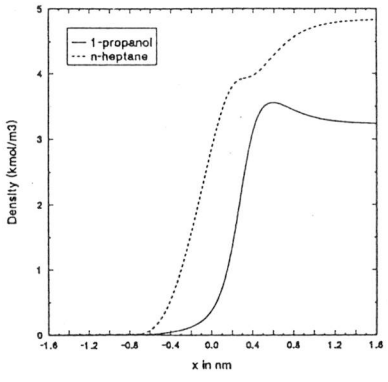

$x_{1\text{-propanol}} = 0.4$

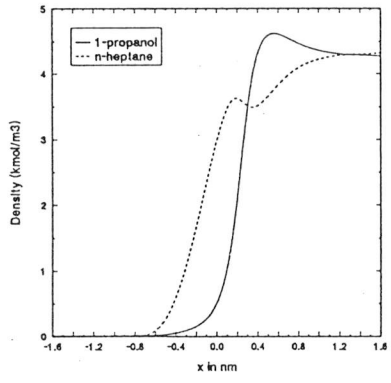

$x_{1\text{-propanol}} = 0.497$

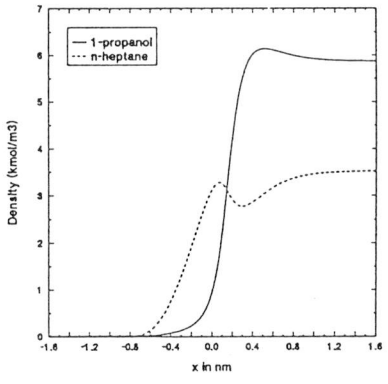

$x_{1\text{-propanol}} = 0.625$

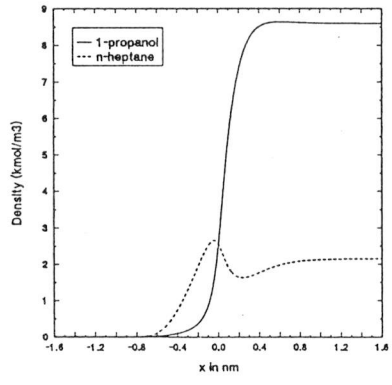

$x_{1\text{-propanol}} = 0.8$

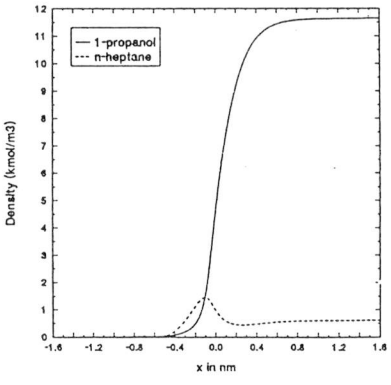

$x_{1\text{-propanol}} = 0.95$

Figure 4.50 Density profiles of 1-propanol/n-heptane at 60 °C at increasing 1-propanol composition.

In Figure 4.50 up to 4.52, the transverse pressure, the degree of association, the several contributions of the Helmholtz free energy, and the total Helmholtz free energy in the interface is given for 1-propanol/n-heptane. The transverse pressure as a function of the distance, x in the interface was calculated using Eq. 2.20. It must be noted that the transverse pressure a function of the distance is still an approximation. The extent of hydrogen-bonding in the interface is given in the expression of n_T/n_O, where the latter is calculated as a function of the distance, x.

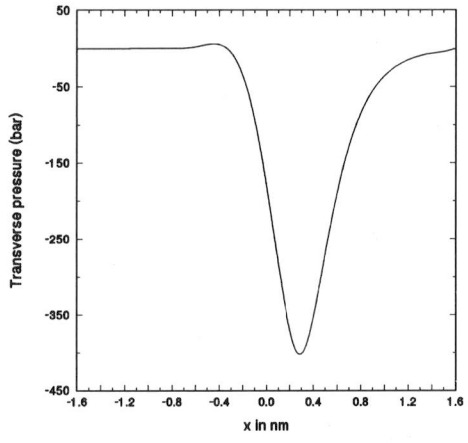

Figure 4.50 1-Propanol/n-heptane. Transverse pressure as a function of x. T = 60 °C and $x_{1\text{-propanol}} = 0.497$.

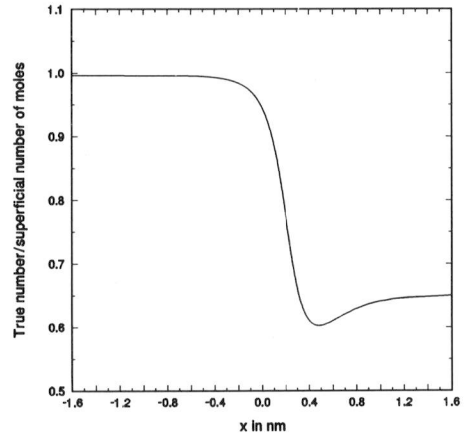

Figure 4.51 1-Propanol/n-heptane. Degree of association as a function of x. T= 60 °C and $x_{1\text{-propanol}} = 0.497$.

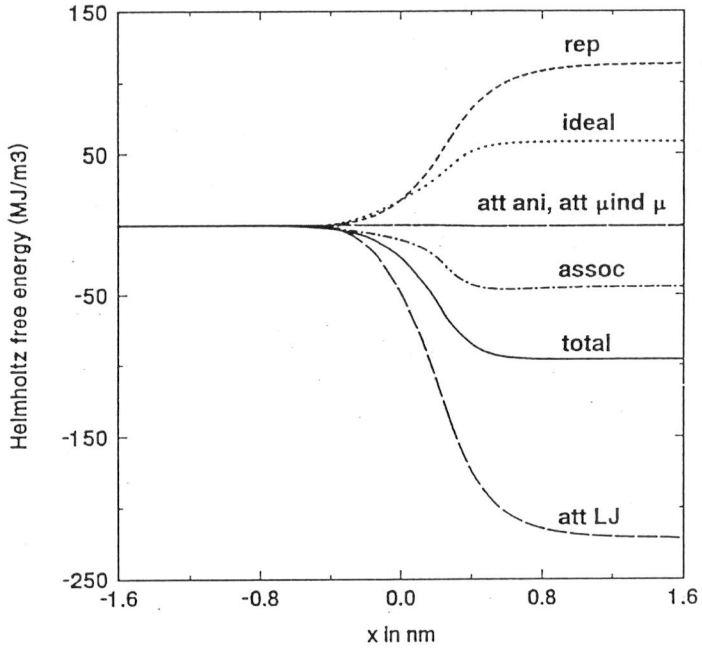

Figure 4.52 1-Propanol/n-heptane. Helmholtz free energy density as a function of x. T = 60 °C and $x_{1\text{-propanol}} = 0.497$.

Although Eq. 2.20 is an incorrect description for the transverse pressure as a function of the distance, it can still be valuable to give an insight how the forces in the interface are represented. The largest absolute value of P_T is approximately 375 bar. This huge tension, is considerably higher than the bulk pressure, P_N or p_0 (approximately 0.3 bar).
The extent of hydrogen-bond formation is shown in Figure 4.51. It can be seen that higher densities yield a low value of n_T/n_0 and, therefore, a greater extent of hydrogen-bonds. It can also be seen that a minimum is observed caused by the fact that at that distance, the density of 1-propanol has a maximum value. Figure 4.52 shows the different contributions to the Helmholtz energy as well as the total Helmholtz free energy. All functions increase or decrease monotically in the interface

n-alcohols/benzene

In Figure 4.53 and 4.54 the systems ethanol/benzene and 1-octanol/benzene at 25 °C are given. It can be seen that the experimental data at near pure n-alcohol do not predict the pure component interfacial tension of the n-alcohols. A possible explanation for these deviations are impurities in the system. The experimental data was obtained from Shastri et al. (1993) and they reported that the used chemicals were 99% pure. A small impurity does not cause a considerable effect on the phase behaviour but can largely effect the interfacial tension data, because the impurity might accumulate in the interfacial zone of the system.

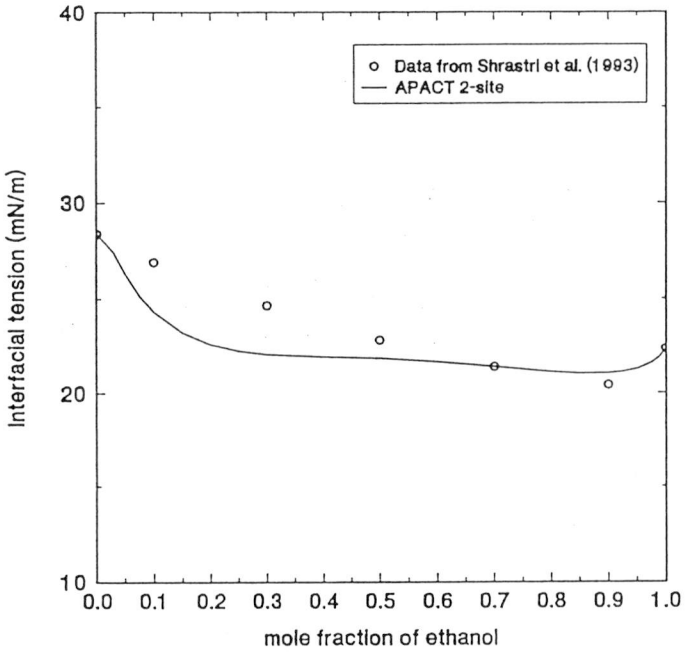

Figure 4.53 Predicted and experimental interfacial tension of ethanol(1)/benzene(2) at 25 °C.

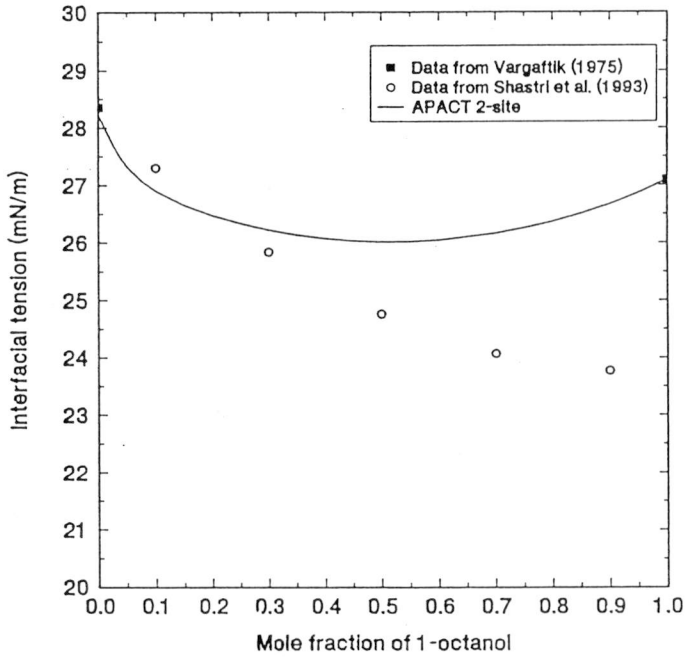

Figure 4.54 Predicted and experimental interfacial tension of 1-octanol(1)/benzene(2) at 25 °C.

water/n-alkanes

In Figure 4.55 up to 4.57 three phase (LLV) systems of water/n-alkanes are investigated. For unknown reasons, the model was not able to calculate the density profiles, and therefore the interfacial tension, of the water-rich liquid-vapor (L1V) interface and the liquid-liquid (L1L2) interface. It can be seen that the prediction are accurate without the use of a binary interaction parameter, k_{ij}.

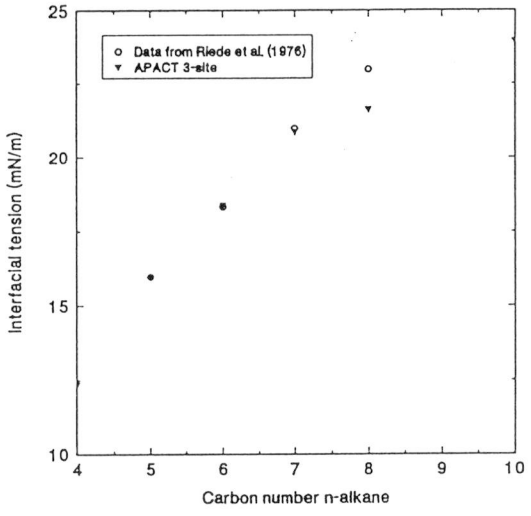

Figure 4.55 Predicted and experimental interfacial tension data of the L2V (organic-vapor) interface for water(1)/n-alkanes(2) at 20 °C.

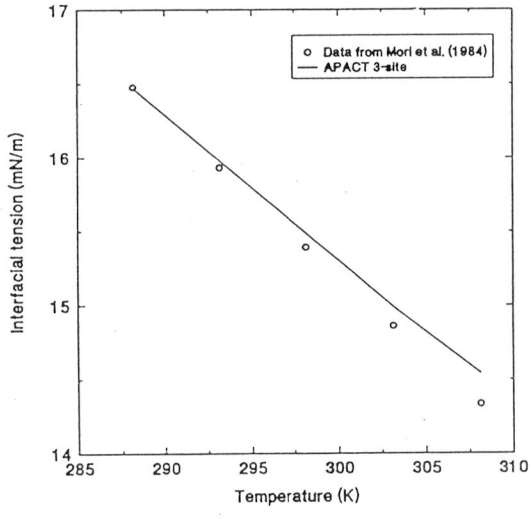

Figure 4.56 Predicted and experimental interfacial tension data of the L2V (organic-vapor) interface for water(1)/n-pentane(2) at several temperatures.

CO_2/water

Figure 4.57 and 4.58 show to different water/carbon-dioxide systems. Predictions of interfacial tension are reasonably well for 1 bar and are poor for the isotherm (T = 71 °C). The two systems were calculated using a zero value of the binary interaction parameter, k_{ij}.

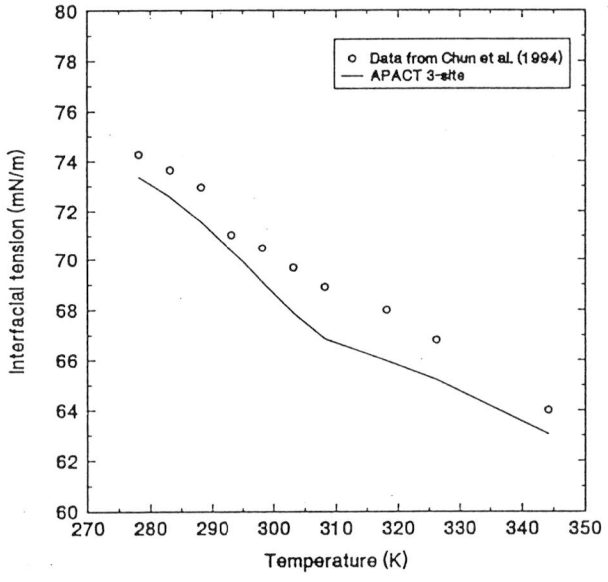

Figure 4.57 Predicted and experimental interfacial tension of water(1) /carbon-dioxide(2) at 1 bar.

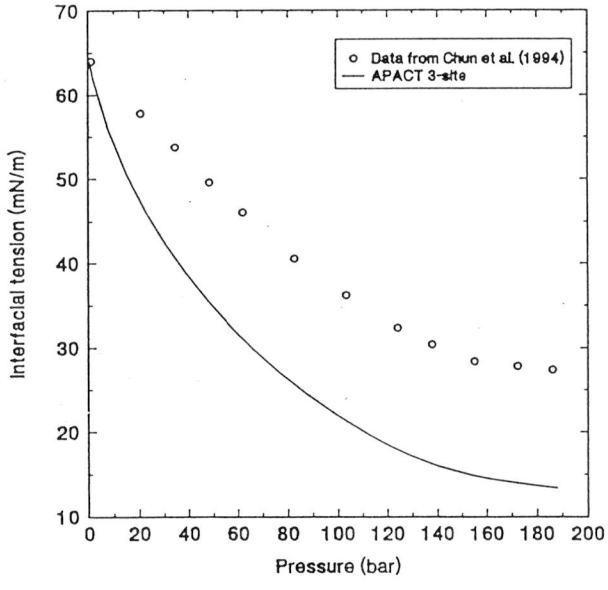

Figure 4.58 Predicted and experimental interfacial tension of water(1)/carbon-dioxide(2) at 71 °C.

To investigate the prediction of phase equilibria and interfacial tension of system without hydrogen-bonding species, binary mixtures such as benzene/n-hexane and carbon-dioxide/benzene were examined. In Figure 4.59 the mixture benzene/n-hexane is given. Without the use of a k_{ij}-parameter, predictions turn out to be good.

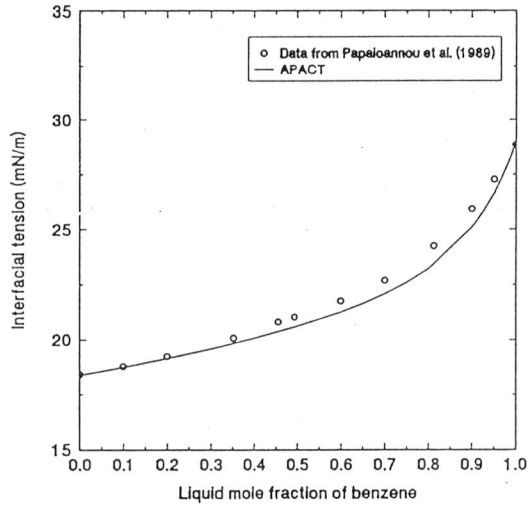

Figure 4.59 Predicted and experimental interfacial tension of benzene(1)/n-hexane(2) at 20 °C.

In Figure 4.60 up to 4.63 the phase equilibria and the interfacial tension is given for carbon-dioxide/benzene at 344.3 K.

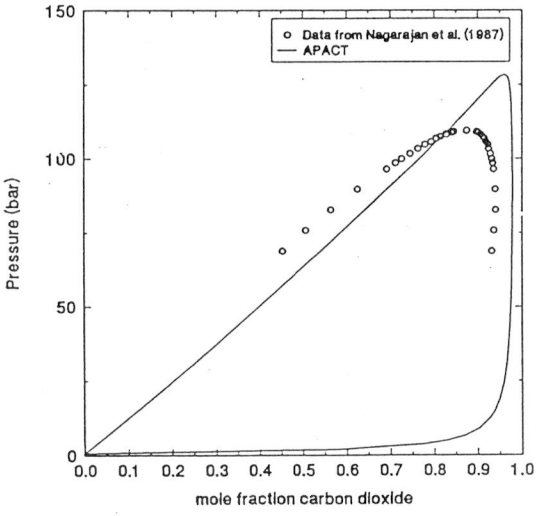

Figure 4.60 P-xy curve for carbon-dioxide(1)/benzene(2) at 344.3 K.

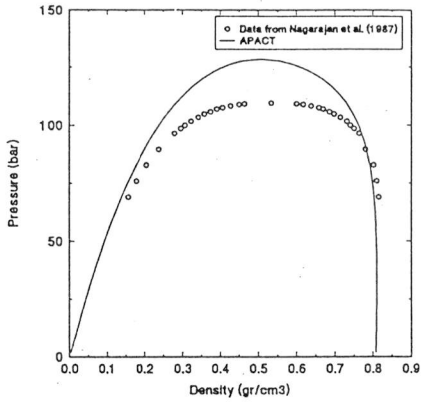

Figure 4.61 Coexistence curve of carbon-dioxide(1)/benzene(2) at 344.3 K.

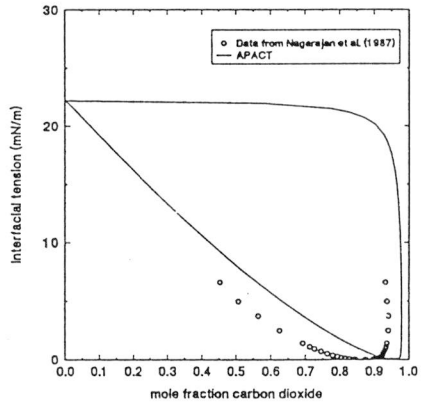

Figure 4.62 Predicted and experimental interfacial tension versus mole fraction CO_2 of carbon-dioxide(1)/benzene(2) at 344.3 K.

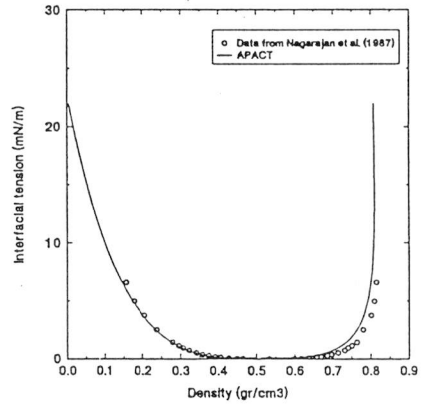

Figure 4.63 Predicted and experimental interfacial tension versus density of carbon-dioxide(1)/benzene(2) at 344.3 K.

It can be seen that the critical pressure of the CO_2/benzene mixture is overpredicted caused by the APACT equation of state. It can also be seen that the critical composition of carbon-dioxide is shifted to the right compared with the experimental value. This effect is explained as follows. The calculated critical density is shifted to the left, compared to the experimental one, and, therefore the mole fraction of the lighter component, CO_2 must be higher.
In the Figures 4.63 up to 4.64 the density profiles for several CO_2-composition are plotted. These figures are shown to observe the increasing width of the interfacial zone when the critical point of this system at 344.3 K is reached.

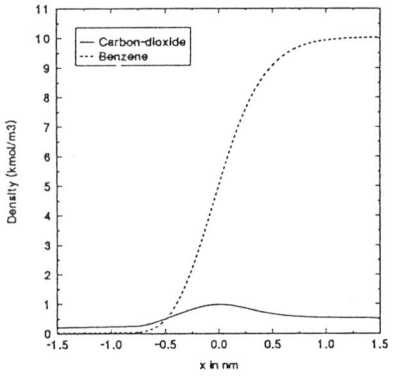

x_{CO2} = 0.05

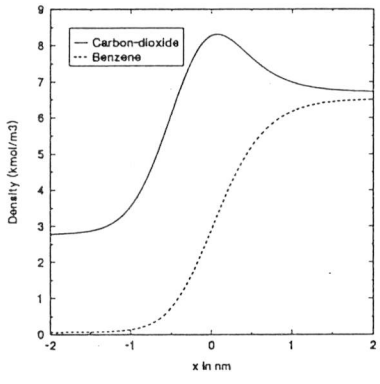

x_{CO2} = 0.507

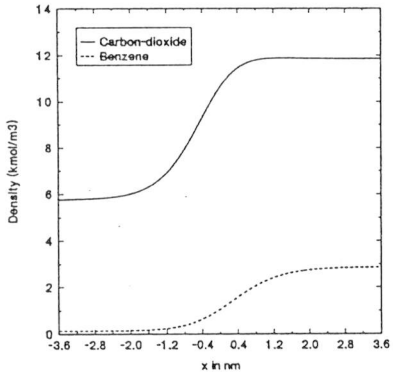

x_{CO2} = 0.805

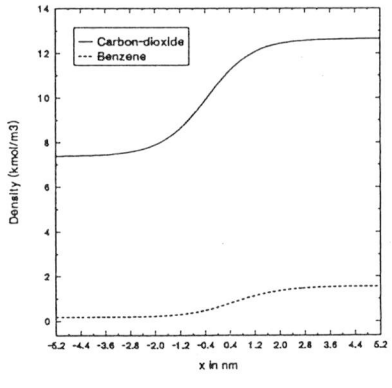

x_{CO2} = 0.89

Figure 4.63 Density profiles of carbon-dioxide(1)/benzene(2) at 344.3 K for several CO_2-compositions.

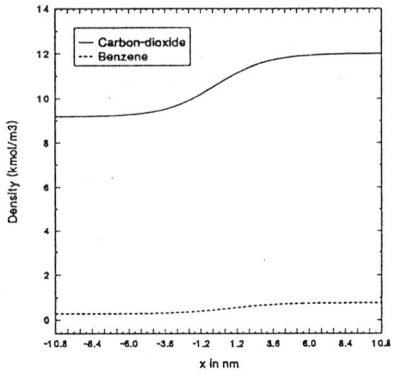

$x_{CO2} = 0.94$

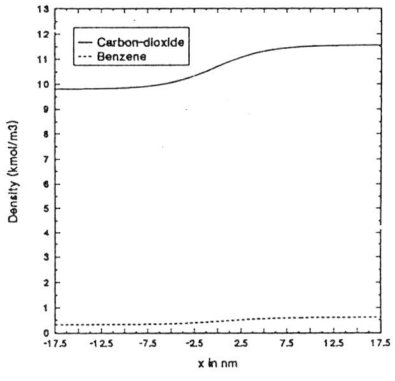

$x_{CO2} = 0.95$

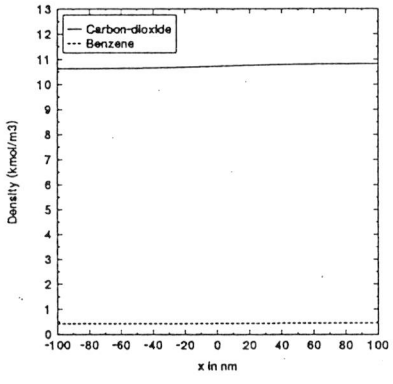

$x_{CO2} = 0.96$

Figure 4.64 Density profiles of carbon-dioxide(1)/benzene(2) at 344.3 K for several CO_2-compositions.

4.3.2 Ternary systems

Two ternary systems were investigated. The first one is the system water/methanol/1-propanol and the second carbon-dioxide/n-butane/n-decane. The predicted and experimental interfacial tension of water/methanol/1-propanol system are given in Table 4.8.

Table 4.8 Predicted and experimental interfacial tension of water(1)/methanol(2)/1-propanol(3) at 1 atm (data from Kalbassi et al. 1988).

Data point	x_{water}	$x_{methanol}$	T (K) (experimental)	γ (mN/m) (experimental)	T (K) (predicted)	γ (mN/m) (predicted)
1	0.1489	0.8458	341.15	19.77	341.3	20.91
2	0.14	0.788	342.15	19.50	342.7	20.00
3	0.1684	0.7044	345.15	19.06	344.8	19.95
4	0.0205	0.178	362.15	17.40	360.3	18.22
5	0.3457	0.111	360.85	19.07	356.0	20.40
6	0.2583	0.3972	351.05	19.99	351.6	20.00
7	0.2288	0.4689	340.95	18.57	350.2	19.91
8	0.1934	0.5544	347.45	19.61	348.3	19.81
9	0.955	0.0298	363.65	37.32	361.7	32.85
10	0.6126	0.369	362.15	34.55	354.9	27.04
11	0.8476	0.1395	357.15	34.50	354.9	32.07
12	0.7209	0.2691	360.50	30.56	359.4	31.11
13	0.6194	0.3727	346.35	28.45	356.3	29.56

Predictions of temperature and interfacial tension turn out to be good except for the data points 9 and 10.
In Figure 4.65 and 4.66, the density profiles of water/methanol/1-propanol at 1 atm for x_{water} = 0.1684 and $x_{methanol}$ = 0.7044 is given. It is shown that 1-propanol also has a decrease in the density as was shown for the binary mixture 1-propanol/n-heptane.

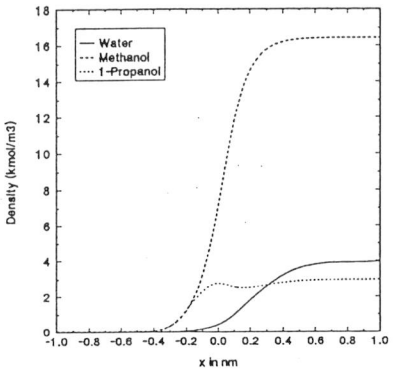

Figure 4.65 Density profile for water(1)/ methanol(2)/1-propanol(3) at 1 atm for x_1, x_2, x_3 is 0.1684, 0.7044, 0.1272.

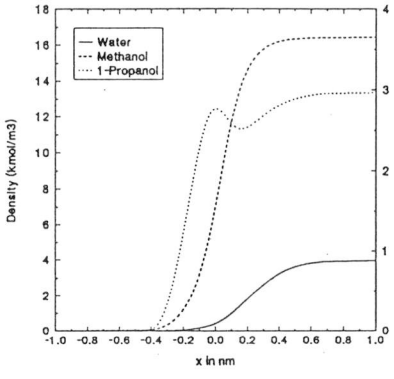

Figure 4.66 Same plot only the 1-propanol density is plotted on the right Y-axis.

In the Figures 4.67 up to 4.72 the phase equilibria and the interfacial tension are given for carbon-dioxide/n-butane/n-decane at 344.3 K. The critical pressure of this ternary mixture is overpredicted caused by the APACT equation of state. The critical composition of CO_2 is shifted to the right where the critical composition of n-butane is slightly shifted to the left. The shift of CO_2 is explained in the same as was done at the system CO_2/benzene.

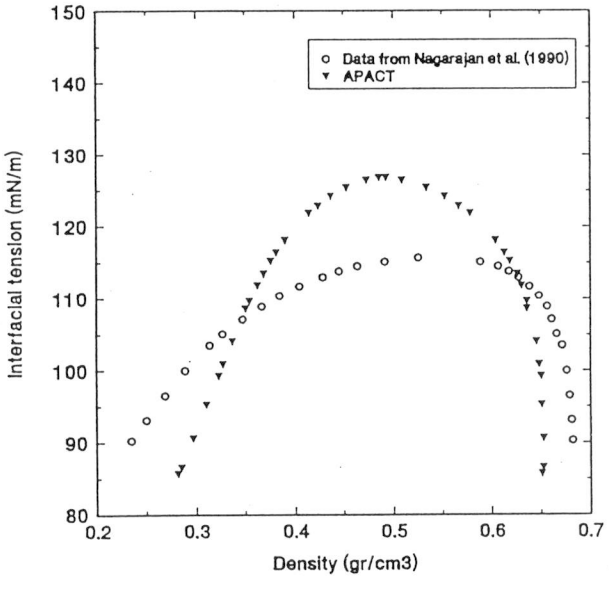

Figure 4.67 Coexistence curve for carbon-dioxide(1)/n-butane(2)/n-decane(3) at 344.3 K.

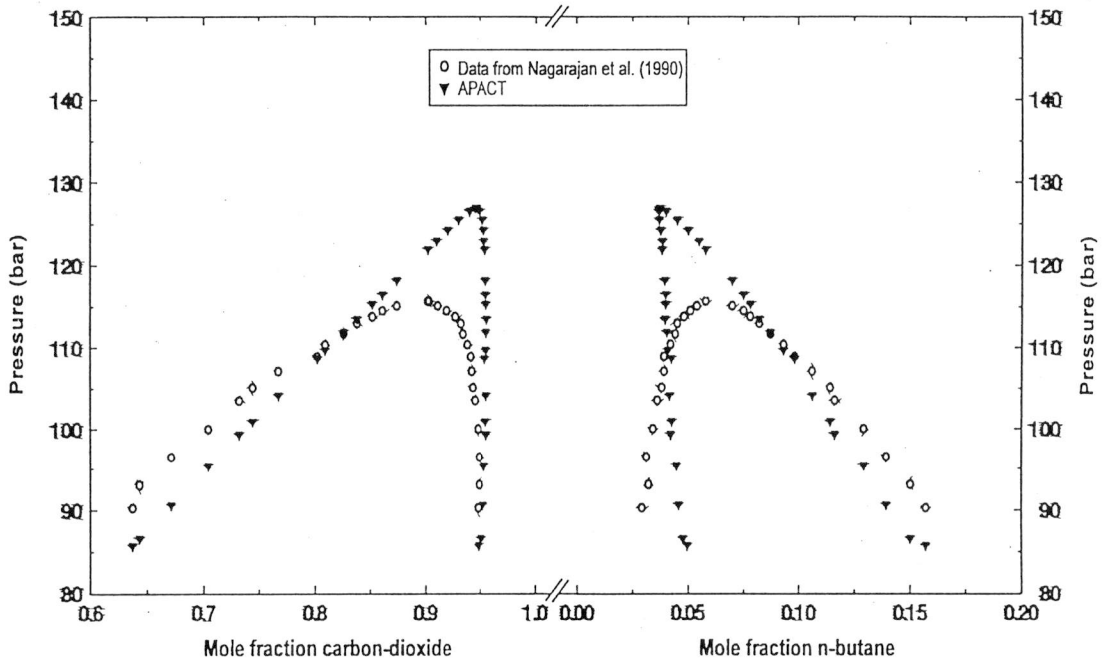

Figure 4.68 P-x diagram for carbon-dioxide(1)/n-butane(2)/n-decane(3) at 344.3 K.

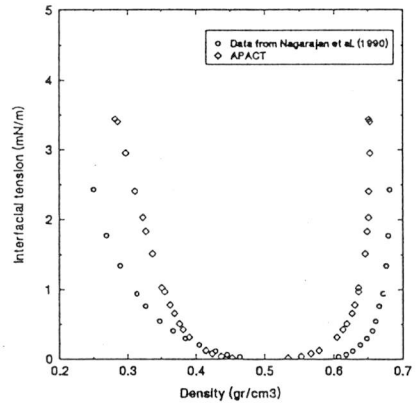

Figure 4.69 γ-ρ plot for carbon-dioxide(1)/n-butane(2)/n-decane(3) at 344.3 K.

The P-x and γ-x projections of the CO_2/n-butane/n-decane system is given in Figures 4.68 and 4.69. They are to be interpretated as follows. At a certain pressure or interfacial tension, one can find, by drawing a horizontal line, two liquid and two gas mole fractions of carbon-dioxide and n-butane. These are the equilibrium values at that certain pressure or interfacial tension.

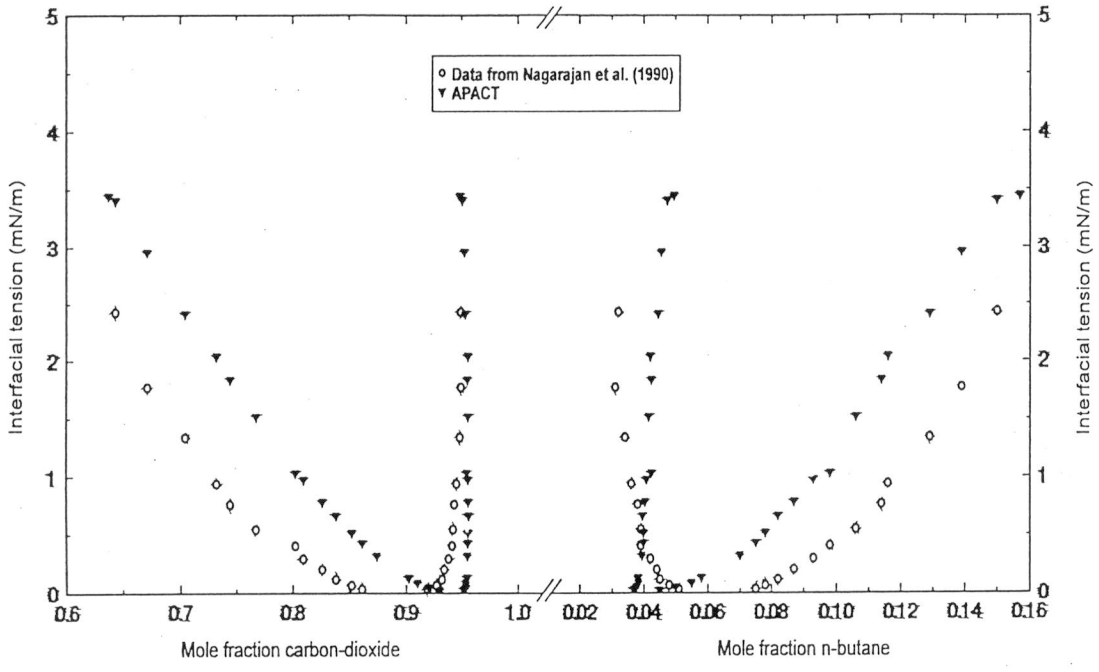

Figure 4.70 Predicted and experimental interfacial tension versus x of the system carbon-dioxide(1)/n-butane(2)/n-decane(3) at 344.3 K.

This chapter is ended by including some remarks.
The remarkable density profiles obtained from the binary mixture 1-propanol/n-heptane are not unique for this particular systems. Profiles which are shown in Figure 4.50 were also obtained from the following mixtures: ethanol/n-hexane, ethanol/n-heptane, ethanol/benzene, 1-octanol/benzene, methanol/1-propanol, methanol/1-decanol, ethanol/1-decanol, 1-propanol/1-decanol, 1-butanol/1-decanol, 1-hexanol/1-decanol and water/methanol/1-propanol. The decreasing density effect was not observed in systems like water/n-alcohols, water/n-alkanes, carbon-dioxide/n-alkanes, carbon-dioxide/water and benzene/n-hexane. Although we can only guess what happens in the interface, a possible explanation for this decrease in the larger component is that the alcohol molecules are oriented in the interface in such a way that the component, with the larger molecular size, is being displaced.

The prediction of interfacial tension of several systems can even be approved when non-zero values of the binary interaction parameter, k_{ij} are used. It is promising that zero values of the k_{ij}-parameter were used, but is not a proof for the validity of the equation of state.

Most of the systems were examined at room temperatures. The need for testing the model at elevated temperatures and pressures indicates that the interfacial tension data base must be enlarged.

5. Conclusions and closing remarks

It can be concluded that the gradient theory in conjunction with the APACT equation of state provides a successful tool for predicting interfacial tension of pure compounds and mixtures. Although it is known that empirical correlations in some cases are able to accurately describe interfacial tensions, they cannot provide a detailed molecular structure of the interface. This information, of course is provided by the gradient theory, because in order to calculate interfacial tension, the density profiles of all components in the interfacial region must be obtained.

By fitting the five pure component parameters of APACT (the enthalpy of hydrogen-bond formation, the entropy of hydrogen-bond formation, the characteristic temperature, the characteristic volume and the shape parameter) to experimental pressure-volume-temperature data, it was observed that several sets of molecular parameter for one compound can be obtained, as was shown for methanol. One of the five molecular parameters must be chosen. It was chosen to obtain the shape parameter, c from the shape parameters of alkanes given by Morris et all. (1987) and Economou and Donohue (1992).
It was also shown that APACT overpredicts the critical pressure as well as the critical temperature for hydrogen-bonding, polar and non-polar fluids, for both pure compounds as well as mixtures. This behaviour is typical for all classical equations of state and APACT, which is also classical, forms no exception.

Predictions of the interfacial tensions for pure compounds obtained with a influence parameter, c_{ii} that is a linear function of the temperature are more accurate than calculations using a constant influence parameter. Although the empirical approach for determining c_{ii} limits the predictive value of the model, it can still be valuable for the investigation of microstructures between fluid phases.
Predictions are, however, less accurate in the vicinity of the critical point, caused by fact that the linear dependence of the influence parameter as a function of the temperature is incorrect. It was not chosen to give a better description of c_{ii} near the critical point. A better description results in an accurate calculation of the interfacial tension near the critical temperature, but still gives poor predictions of the phase behaviour, especially the coexistence densities. This problem, however, can be solved by incorporating scaling behaviour in the APACT equation of state, which was not tried is this report.
It is known that gradient theory has some shortcomings (Telo da Gama and Evans, 1979 ; Rawlinson and Widom, 1989). The gradient theory in conjunction with a classical equation of state does not correctly describe the interfacial tension in the critical region and its applications far away from the critical point causes deviations, because of the limiting validity of the gradient expansion. Fitting the influence parameter to experimental interfacial tension data corrects for these deviations .

For binary and ternary mixtures gradient theory in conjunction with APACT predicts reasonably well their phase behaviour as well as the interfacial tension for liquid-vapor and liquid-liquid-vapor interfaces. There are some exceptions, such as carbon-dioxide water and n-alcohol-benzene. Predictions were not very accurate, however, a remark should be made here. If predictions and experimental data show considerable deviations, a critical look at the experimental data is advisable, before concluding that the model has its shortcomings. For example, when the experimental data of the mixture benzene-ethanol or benzene-1-octanol is examined, it can be seen that for measurements at the composition $x_{alcohol}$ close to one, the measured interfacial tension does not come close to the pure component interfacial tension. A small impurity does not cause a considerable change in the phase behaviour, but can largely effect the interfacial tension, because the impurity might accumulate in the interface.

More accurate predictions can be obtained with the use of the binary interaction parameter k_{ij}, which corrects for the attractive part of APACT, or the adjustable parameter $ß_{ij}$. If predictions were poor, it was tried to obtain better results with only the binary interaction parameter, k_{ij}. This parameter affects not only the phase behaviour but the calculation of the interfacial tension as well. The adjustable parameter, $ß_{ij}$ only effects the calculation of tension, and its value was set to zero. In some systems where azeotropy occurred, such as the systems hexane-ethanol, heptane-ethanol, non-zero k_{ij} values were necessarily needed, otherwise APACT would predict heteroazeotropy, resulting in an incorrect calculation of the interfacial tensions.

Finally a remarkable effect was observed firstly in the density profile of the mixture 1-propanol/n-heptane at 60 °C. The increasing 1-propanol concentration causes a decrease in the density of n-heptane, at a certain distance in the interface. This effect was also observed in the systems ethanol/n-hexane, ethanol/n-heptane, ethanol/benzene, 1-octanol /benzene, methanol/1-propanol, methanol/1-decanol, ethanol/1-decanol, 1-propanol/1-decanol, 1-butanol/1-decanol, 1-hexanol/1-decanol and water/methanol/1-propanol. It was not observed at systems like water/methanol, water/ethanol, water/n-alkanes, carbon-dioxide/n-alkanes, carbon-dioxide /water and benzene/n-hexane.
This decrease in density of the second component only appears in systems with linear alcohols and when there was a differences in molecular size between both components. A possible explanation for the effect is that the smallest component, the alcohol, which density increases along the interfacial zone, is oriented (through hydrogen-bonding) in such a way that is does not allow other molecules in its neighbourhood, resulting in a decrease in the density of the second component.

6. Literature

Barker, J.A., and Henderson, D.J., 1967. Journal of Physical Chemistry, 47, 474.

Benson, G.C., and Lam, V.T., 1971. Surface Tension of Binary Systems II. Mixtures of Alcohols. Journal of Colloid and Interface Science, 38, 295-301.

Beret, S, and Prausnitz, J.M., 1975. Perturbed Hard-Chain Theory: An Equation of State for Fluids Containing Small or Large Molecules. AIChE Journal, 21, 1123-1131.

Bongiorno , V., and Scriven, L.E., 1975. Modified Van Der Waals theory of fluid interfaces. Physical Review A, 12, 2213-2224.

Bongiorno , V., and Scriven, L.E., 1976. Molecular Theory of Fluid Interfaces. Journal of Colloid and Interface Science, 57, 463-475.

Boublík, T., Fried, V., and Hála, E., 1984. The Vapour Pressures of Pure Substances. Physical Science Data 17, Elsevier Amsterdam.

Cahn, J.W., and Hilliard, J.E., 1958. Free Energy of a Nonuniform System. I. Interfacial Free Energy. Journal of Chemical Physics, 28, 258-267.

Carey, B.S., and Scriven, L.E., 1978. On gradient theories of fluid interfacial stress and structure. Journal of Chemical Physics, 69, 5040-5049.

Carey, B.S., Scriven, L.E., and Davis, H.T., 1980. Semiemperical Theory od Surface Tension of Binary Systems. AIChE Journal, 26, 705-711.

Carnahan, N.F., and Starling, K.E., 1969. Equation of State for Nonattracting Rigid Spheres. Journal of Chemical Physics, 51, 635-636.

Chun, B-S., and Wilkinson, G.T., 1994. Interfacial Tension in High Pressure Carbon Dioxide Mixtures, Paper presented to 3rd International Symposium on Supercritical Fluids, Strassbourg (France).

Cornelisse, P.M.W., Peters, C.J., and de Swaan Arons, J., 1993. Application of the Peng-Robinson Equation of State to Calculate Interfacial Tensions and Profiles at Vapour-Liquid Interfaces. Fluid Phase Equilibria, 82, 199-129.

Cornelisse, P.M.W., Peters, C.J., and de Swaan Arons, J., 1993. Simultaneous prediction of phase equilibria, interfacial tension and concentration profiles. Molecular physics, 80, 941-955.

Cornelisse, P.M.W., 1991. Gradient Theory: Tension and Structure in liquid-Vapor nterfaces, Masters Thesis, TU Delft.

Cotterman, R.L., Schwarz, B.J., and Prausnitz, J.M., 1986. Molecular Thermodynamics for Fluids at Low and High densities. AIChe Journal, 32, 1787-1798.

CRC Handbook of Chemistry and Physics, 75th edition, 1994-1995.

Davis, H.T., and Scriven, L.E., 1982. Stress and Structure in Fluid Interfaces. Advances in Chemical Physics, 49, 357.

Donohue, M.D., and Prausnitz, J.M., 1978. Perturbed Hard Chain Theory for Fluid Mixtures: Thermodynamic Properties for Mixtures in natural Gas and Petroleum technology. AIChE Journal, 24, 849-860.

Donohue, M.D., and Vimalchand, P., 1988. The Perturbed-Hard-Chain Theory. Extensions and Applications. Fluid Phase Equilibria, 40, 185-211.

Economou, I.G., and Donohue, M.D., 1991. Chemical, Quasi-Chemical and Perturbation Theories for Associating Fluids. AIChE Journal, 37, 1875-1893.

Economou, I.G., and Donohue, M.D., 1992. Equation of State with Multiple Associating Sites for Water and Water-Hydrocarbon Mixtures. Industrial and Engineering Chemistry Research, 31, 2388-2394.

Grigoryev, B.A., Nemzer, B.V., Kuromov, D.S., and Sengers, J.V., 1992. Surface Tension of Normal Pentane, Hexane, Heptane, and Octane. International Journal of Thermophysics, 13, 453.

Grootendorst, A.W. en Meulenberg, B. 1987."Analyse", Delftse Uitgevers Maatschappij, Delft.

Gubbins, K.E., and Twu, G.H., 1978. Chemical Engineering Science, 33, 863.

Heideman, R.A., and Prausnitz, J.M., 1976. Proc. Natl. Sci. U.S.A., 73, 1773.

Huang, S.H., and Radosz, M., 1990. Ind. Eng. Chem. Fundam., 15, 59.

Ikonomou, G.D., and Donohue, M.D., 1986. Thermodynamics of Hydrogen-Bonded Molecules: The Associated Perturbed Anisotropic Chain Theory. AIChE Journal, 32, 1716-1725.

Ikonomou, G.D., and Donohue, M.D., 1988. Extension of the Associated Perturbed Anisotropic Chain Theory to Mixtures with More Than One Associating Component. Fluid Phase Equilibria, 39, 129-159.

Jasper, J.J., 1972. The Surface Tension of Pure Liquid Compounds. Journal of Physical Chemistry Reference Data, 5, 841-1009.

Kalbassi, M.A., and Biddulph, M.W., 1988. Surface Tensions of Mixtures at Their Boiling Points. Journal of Chemical and Engineering Data, 33, 473-476.

Lord Rayleigh, 1892. Phil. Mag., 33:208.

Mc Clellan, A.L., 1989. Tables of Experimental Dipole Moments, vol. 3, Rahara Enterprises, El Cerrito.

McLure, I.A., Sipowska, J.T., and Pegg, I.L., 1982. Surface tensions of (an alkohol + an alkane). 1. Propan-1-ol + heptane. Journal of Chemical Thermodynamics, 14, 733-741.

Moelwyn-Hughes, E.A., 1961. Physical Chemistry, Oxford.

Mori, Y.H., Tsul, N, and Kiyomiya, M., 1984. Surface and Interfacial Tensions and Their Combined Properties in Seven Binary, Immiscible Liquid-Liquid-Vapor Systems. Journal of Chemical Engineering Data, 29, 407-412.

Morris, W.O., Vimalchand, P., and Donohue, M.D., 1987. The Perturbed-Soft-Chain Theory: An Equation of State based on the Lennard-Jones Potential. Fluid Phase Equilibria, 32, 103-115.

Nagarajan, N., and Robinson, Jr., R.L., 1987. Equilibrium Phase Compositions, Phase Densities, and Interfacial Tensions for CO_2 + Hydrocarbon Systems. 3. CO_2 + Cyclohexane. 4. CO_2 + Benzene. Journal of Chemical and Engineering Data, 32, 369-371.

Nagarajan, N., and Robinson, Jr., R.L., 1990. Equilibrium Phase Compositions, Phase Densities, and Interfacial Tensions for CO_2 + Hydrocarbon Systems. 6. CO_2 + n-Butane + n-Decane. Journal of Chemical and Engineering Data, 35, 228-231.

Ornstein, L.S., and Zernike, F., 1914, Proc. Acad. Sci. Amsterdam, 17, 793.

Papaioannou, D., and Panayiotou, C.G., 1989. Surface Tension of Binary Liquid Mixtures. Journal of Colloid and Interface Science, 130, 433-438.

Papaioannou, D., and Panayiotou, C.G., 1994. Surface Tensions and relative Adsorptions in Hydrogen-Bonded Systems. Journal of Chemical Engineering Data, 39, 457-462.

Percus, J.K., and Yevick, G.J., 1958, Physical Review, 110, 1.

Pimental, G.C., and McClellan, A.L., 1960. The Hydrogen Bond, San Francisco.

Quinn, E.L., 1927. Surface Tension of Liquid Carbon Dioxide, Journal of the American Chemical Society, 49, 2704.

Rowlinson, J.S., and Widom, B., 1989. Molecular Theory of Capillarity (Oxford:Clarendon).

Sahimi, M., and Taylor, B.N., 1991. Surface tension of binary liquid-vapor mixtures: A comparison of mean-field and scaling theories. Journal of Chemical Physics, 95, 6749-6760.

Srinivas Shastri, S., Mukherjee, A.K., and Das, T.R., 1993. Surface Tension of Some Binary Organic Solutions of Alkylbenzenes and 1-Alkohols. Journal of Chemical Engineering Data, 38, 399-400.

Smith, B.D., and Srivastava, R., 1986. Thermodynamic Data for Pure Compounds. Physical Science Data 25, Elsevier Amsterdam.

Smits, P.J., Economou, I.G., Peters, C.J., and de Swaan Arons, J., 1994. Equation of State Description of Thermodynamic Properties of Near-Critical and Supercritical Water. Journal of Physical Chemistry, 98, 12080-12985.

Stephan, K., and Hildwein, H., 1987. Recommended data of selected compounds and binary mixtures, Chemistry Data Series, vol. IV, parts 1+2, Dechema, Frankfurt.

Telo Da Gama, M.M., and Evans, R., 1979. The density profile and surface tension of a Lennard-Jones fluid from a generalized van der Waals theory. Molecular Physics, 38, 367-375.

Van der Waals, J.D., 1979. The Thermodynamic Theory of Capillarity Under the Hypothesis of a Continuous Variation of Density. Journal of Statistical Physics, 20, 197-.

Vargaftik, N.B., 1975. Tables on the Thermophysical Properties of Liquids and Gases, Hemisphere Publishing Corporation, John Wiley & Sons, Inc, New York.

Vimalchand, P, Celmins, I, and Donohue, M.D., 1986. Thermodynamics of Multipolar Molecules. The Perturbed-Anisotropic-Chain Theory. American Chemical Society Symposium Series No. 300, 297-313.

Vimalchand, P, Celmins, I, and Donohue, M.D., 1986. VLE Calculations for Mixtures Containing Multipolar Compounds Using the Perturbed Anisotropic Chain Theory. AIChE Journal, 32, 1735-1737.

Vimalchand, and Donohue, M.D., 1985. Thermodynamics of Quadrupolar Molecules: The Perturbed-Anisotropic-Chain Theory, Ind. Eng. Chem. Fundam., 24, 246-257.

Von Riede, H., Vohland, S, und Schuberth, H., 1976. Ober- und Grenzflächenspannungen binärer heterogener flüssiger Systeme mit Wasser bzw. Äthylenglykol als einer der beiden Komponenten, Z. Phys. Chemie, 257, 529-538.

Yang, A.J.M., Fleming, P.D., and Gibbs, J.H., 1976. Molecular theory of Surface tension. Journal of Chemical Physics, 64, 3732-3745.

7. List of symbols

a	:	Fit parameter for the pure component influence parameter, c_{ii}.
b	:	Fit parameter for the pure component influence parameter, c_{ii}.
A	:	Helmholtz free energy (density).
c	:	Shape parameter.
c_{ij}	:	Influence parameter.
d_3r	:	Volume element.
C_O^{ij}	:	Direct correlation function.
F	:	Helmholtz free energy density.
f	:	Helmholtz free energy density distribution.
F_I	:	Force of transducer in the interface.
F_B	:	Force of transducer in the bulk phase.
g_O	:	Pair correlation function.
ΔH^{assoc}	:	Enthalpy of hydrogen-bong formation.
k	:	Boltzmann constant.
k_{ij}	:	Binary interaction parameter of APACT.
$k_{ij}^{(1)}$	:	Components used in gradient theory.
$k_{ij}^{(2)}$	:	Components used in gradient theory.
k_1	:	First contribution of the influence parameter.
k_2	:	Second contribution of the influence parameter.
L_i	:	Components used in gradient theory.
L	:	Length of the interfacial zone.
N	:	Number of components.
p_o	:	Pressure at equilibrium.
P	:	Pressure Tensor.
P	:	Pressure.
r	:	Distance.
s	:	Distance.
ΔS^{assoc}	:	Entropy of hydrogen-bong formation.
T	:	Temperature.
V	:	Total volume.
T^*	:	Characteristic temperature.
v^*	:	Characteristic volume.
w	:	Width of the interfacial zone.
x	:	Distance in the interface.
z	:	Distance in the interface perpendicular to x.
Z	:	Compressibility

GREEK

α	:	Phase α.
β	:	Phase β.
μ	:	Chemical potential.
ρ	:	Density or density distributions.
γ	:	Surface/Interfacial tension.
ω	:	Thermodynamic potential.
$\Delta\omega$	:	Thermodynamic potential difference.
χ	:	Function of the path parameter, $\wp$

SUBSCRIPT

T	:	Transverse
N	:	Normal
O	:	Homogeneous property.

SUPERSCRIPT

Assoc	:	Hydrogen-bonding part.
rep	:	Carnahan-Starling repulsive part.
att	:	Attractive part.
LJ	:	Lennard-Jones attractive part.
ani	:	Anisotropic attractive part.
μindμ	:	Isotropic Dipole induced-dipole attractive part.

OTHER

$\wp$	:	Path.
$\wp_B$	:	Path length.

APPENDIX A

Associated perturbed anisotropic chain theory (APACT)

The APACT equation of state, as was mentioned in paragraph 2.4, was originally introduced by Ikonomou and Donohue (1986) and can be described in terms of the compressibility factor Z:

$$Z = 1 + Z^{assoc} + Z^{rep} + Z^{att} \tag{A.1}$$

The APACT Helmholzt free energy and chemical potential of component i can described in the same as the compressibility factor Z, namely

$$A = A^{ig} + A^{assoc} + A^{rep} + A^{att} \tag{A.2}$$

$$\mu_i = \mu_i^{ig} + \mu_i^{assoc} + \mu_i^{rep} + \mu_i^{att} \tag{A.3}$$

where

$$M^{att} = M^{LJ} + M^{\mu ind \mu} + M^{ani} \tag{A.4}$$

M^{att} stands for the compressibility Z^{att}, the Helmholtz free energy A^{att} or the chemical potential of component i μ_i^{att}.
Separate terms in APACT will be described below.

The ideal gas Helmholtz free energy (A^{ig}) and chemical potential ($_i\mu^{ig}$) are calculated from the ideal gas law:

$$A^{ig} = RT - RT \sum_{i=1}^{N} z_i \ln\left(\frac{V}{z_i}\right) \tag{A.5}$$

$$\mu_i^{ig} = RT - RT\ln\left(\frac{V}{z_i}\right) \tag{A.6}$$

The hard sphere terms in APACT given by Z^{rep}, A^{rep}, μ_i^{rep} are given by the Carnahan-Starling equation of state for hard spheres (Carnahan and Starling, 1969). These repulsions are:

$$Z^{rep} = <c> \frac{4\left(\frac{\tau}{\tilde{v}_d}\right) - 2\left(\frac{\tau}{\tilde{v}_d}\right)^2}{\left(1 - \frac{\tau}{\tilde{v}_d}\right)^3} \tag{A.7}$$

$$\frac{A^{rep}}{RT} = <c> \frac{4\left(\frac{\tau}{\tilde{v}_d}\right) - 3\left(\frac{\tau}{\tilde{v}_d}\right)^2}{\left(1 - \frac{\tau}{\tilde{v}_d}\right)^2} \tag{A.8}$$

$$\frac{\mu_i^{rep}}{RT} = c_i \frac{4\left(\frac{\tau}{\tilde{v}_d}\right) - 3\left(\frac{\tau}{\tilde{v}_d}\right)^2}{\left(1 - \frac{\tau}{\tilde{v}_d}\right)^2} - <c> \frac{\tau \frac{v_{d,i}^*}{v}\left(4 - 2\frac{\tau}{\tilde{v}_d}\right)}{\left(1 - \frac{\tau}{\tilde{v}_d}\right)^3} \tag{A.9}$$

$$where\ \tau = \frac{\pi}{6}\sqrt{2}\ ;\ <c> = \sum_i^N z_i c_i \tag{A.10}$$

$$\tilde{v}_d = \frac{v}{<v_d^*>_L}\ ;\ <v_d^*>_L = \sum_{i=1}^N z_i \frac{N_A r_i \sigma_{ii}^3}{\sqrt{2}}\left(\frac{d_{ii}}{\sigma_{ii}}\right)^3 \tag{A.11}$$

The ratio of the segmental soft- and hardcore diameter is given by Cotterman et al. (1986)

$$\frac{d_{ii}}{\sigma_{ii}} = \frac{1 + 0.2977\tilde{T}}{1 + 0.33163\tilde{T} + 0.0010477\tilde{T}^2}\ ,where\ \tilde{T} = \frac{T}{T_{ii}^*} \tag{A.12}$$

$$\frac{d_{ij}}{\sigma_{ij}} = \frac{1}{2}\left(\frac{d_{ii}}{\sigma_{ii}} + \frac{d_{jj}}{\sigma_{jj}}\right) \tag{A.13}$$

$$\varepsilon_{ij} = \sqrt{\varepsilon_{ii}\,\varepsilon_{jj}}(1 - k_{ij}) \tag{A.14}$$

The Lennard-Jones attractions Z^{LJ}, A^{LJ}, μ_i^{LJ} are obtained from the perturbed soft chain theory (PSCT) described by Morris et al. (1987). These attractive terms are calculated by extending the perturbation expansion of Barker and Henderson (1967) for spherical molecules to chainlike molecules. The terms are given below.

$$Z^{LJ} = \frac{Z_1^{LJ} + Z_2^{LJ} - 2 Z_1^{LJ} \dfrac{A_2^{LJ}}{A_1^{LJ}}}{\left(1 - \dfrac{A_2^{LJ}}{A_1^{LJ}}\right)^2} \tag{A.15}$$

$$A^{LJ} = \frac{A_1^{LJ}}{\left(1 - \dfrac{A_2^{LJ}}{A_1^{LJ}}\right)} \tag{A.16}$$

$$\mu_i^{LJ} = \frac{\mu_{i,1}^{LJ} + \mu_{i,2}^{LJ} - 2 \mu_{i,1}^{LJ} \dfrac{\mu_{i,2}^{LJ}}{\mu_{i,1}^{LJ}}}{\left(1 - \dfrac{\mu_{i,2}^{LJ}}{\mu_{i,1}^{LJ}}\right)^2} \tag{A.17}$$

where the first and second order terms, described by the superscript 1 en 2, are

$$Z_1^{LJ} = \frac{1}{T} \sum_{m=1}^{6} \frac{m A_{1m} < cT^{*1} > < v_d^{*} >^m}{v^m} \tag{A.18}$$

$$Z_2^{LJ} = \frac{1}{T^2} \sum_{m=1}^{4} \left[\frac{m C_{1m} < cT^{*2} > < v_d^{*} >^m}{2 v^m} + \frac{(m+1) C_{2m} < cT^{*1} > < T^{*} >_L < v_d^{*} >^{m+1}}{v^{m+1}} \right.$$

$$\left. + \frac{(m+2) C_{3m} < cT^{*} > < T^{*} >^2 < v_d^{*} >^{m+2}}{2 v^{m+2}} \right] \tag{A.19}$$

$$\frac{A_2^{LJ}}{RT} = \frac{1}{T^2}\sum_{m=1}^{4}\left[\frac{C_{1m}<cT^{*2}><v_d^*>^m}{2v^m} + \frac{C_{2m}<cT^{*1}><T^*>_L<v_d^*>^{m+1}}{v^{m+1}}\right. \tag{A.20}$$

$$\left. + \frac{C_{3m}<cT^*><T^*>^2<v_d^*>^{m+2}}{2v^{m+2}}\right] \tag{A.21}$$

$$\frac{\mu_{i,1}^{LJ}}{RT} = \frac{1}{T}\sum_{m=1}^{6}\frac{A_{1m}<cT^{*1}><v_d^*>^m(1 + <cT^*>_i^D + m<v^*>_i^D)}{2v^m} \tag{A.22}$$

$$\frac{\mu_{i,2}^{LJ}}{RT} = \frac{1}{T^2}\sum_{m=1}^{4}\left[\frac{C_{1m}<cT^{*2}><v_d^*>^m(1 + <cT^{*2}>_i^D + m<v_d^*>_i^D)}{2v^m}\right.$$

$$+ \frac{C_{2m}<cT^{*1}><T^*>_L<v_d^*>^{m+1}(1 + <cT^*q>_i^D + m<v_d^*>_i^D)}{v^{m+1}}$$

$$\left. + \frac{C_{3m}<cT^{*1}><T^*>^2<v_d^*>^{m+2}(1 + <cT^*>_i^D + <T^*>_i^D + (m+2)<v_d^*>_i^D)}{2v^{m+2}}\right] \tag{A.23}$$

d/σ in the mixing terms of the second-order Lennard-Jones compressibility Z_2^{LJ}, Helmholtz free energy A_2^{LJ} and chemical potential $\mu_{i,2}^{LJ}$ are evaluated with a reduced temperature (T tilde) of one.

The mixing rules for the Lennard-Jones attractive compressibility, Helmholzt free energy, and chemical potential are given by Donohue and Prausnitz (1978).

$$<v_d^*> = \sum_{i=1}^{N}\sum_{j=1}^{N} z_i z_j \frac{N_A r_i d_{ij}^3}{\sqrt{2}} \qquad ; \qquad d_{ij} = \sigma_{ij}\left(\frac{d_{ij}}{\sigma_{ij}}\right)^3 \tag{A.24}$$

$$<cT^{*n}> = \frac{\sum_{i=1}^{N}\sum_{j=1}^{N} z_i z_j c_i \left(\frac{\varepsilon_{ij} q_i}{k c_i}\right)^n \frac{N_A r_j d_{ji}^3}{\sqrt{2}}}{\sum_{i=1}^{N}\sum_{j=1}^{N} z_i z_j \frac{N_A r_i d_{ij}^3}{\sqrt{2}}} \tag{A.25}$$

$$<T^*>_L = \frac{\sum_{i=1}^{N} z_i q_i \frac{\varepsilon_{ij} q_i}{k c_i}}{\sum_{i=1}^{N} z_i q_i} \tag{A.26}$$

$$<T^*>^2 = \frac{\sum_{i=1}^{N}\sum_{j=1}^{N} z_i z_j \frac{\varepsilon_{ij} q_i}{k c_i} q_i \frac{N_A r_j d_{ji}^3}{\sqrt{2}}}{\sum_{i=1}^{N}\sum_{j=1}^{N} z_i z_j q_i \frac{N_A r_j d_{ij}^3}{\sqrt{2}}} \tag{A.27}$$

$$<v_d^*>_i^D = \frac{\sum_{j=1}^{N} z_j \frac{N_A (r_i d_{ij}^3 + r_j d_{ji}^3)}{\sqrt{2}}}{\sum_{k=1}^{N}\sum_{l=1}^{N} z_k z_l \frac{N_A r_k d_{lk}^3}{\sqrt{2}}} - 1 \tag{A.28}$$

$$<T^*>_i^D = \frac{\sum_{j=1}^{N} z_j \left[q_i \frac{\varepsilon_{ij} q_i}{k c_i} \frac{N_A r_j d_{ji}^3}{\sqrt{2}} + q_j \frac{\varepsilon_{ji} q_j}{k c_j} \frac{N_A r_i d_{ij}^3}{\sqrt{2}} \right]}{\sum_{m=1}^{N} \sum_{n=1}^{N} z_m z_n q_m \frac{\varepsilon_{mn} q_m}{k c_m} \frac{N_A r_n d_{nm}^3}{\sqrt{2}}}$$

$$- \frac{\sum_{j=1}^{N} \left[q_i \frac{N_A r_j d_{ji}^3}{\sqrt{2}} + q_j \frac{N_A r_i d_{ij}^3}{\sqrt{2}} \right]}{\sum_{m-1}^{N} \sum_{n=1}^{N} z_m z_n q_m \frac{N_A r_n d_{nm}^3}{\sqrt{2}}} \qquad \text{(A.29)}$$

$$<cT^{*n}>_i^D = \frac{\sum_{j=1}^{N} z_j \left[c_i \left(\frac{\varepsilon_{ij} q_i}{k c_i} \right)^n \frac{N_A r_j d_{ji}^3}{\sqrt{2}} + c_j \left(\frac{\varepsilon_{ji} q_j}{k c_j} \right)^n \frac{N_A r_i d_{ij}^3}{\sqrt{2}} \right]}{\sum_{l=1}^{N} \sum_{m=1}^{N} z_l z_m c_l \left(\frac{\varepsilon_{lm} q_l}{k c_l} \right)^n \frac{N_A r_m d_{ml}^3}{\sqrt{2}}}$$

$$- \frac{\sum_{j=1}^{N} z_j \frac{N_A (r_i d_{ij}^3 + r_j d_{ji}^3)}{\sqrt{2}}}{\sum_{l=1}^{N} \sum_{m=1}^{N} z_l z_m \frac{N_A r_l d_{ml}^3}{\sqrt{2}}} \qquad \text{(A.30)}$$

$$<cT^* q>_i^D = <cT^{*1}>_i^D + \frac{q_i \frac{\varepsilon_{ii} q_i}{k c_i}}{\sum_{i=1}^{N} z_i q_i \frac{\varepsilon_{ii} q_i}{k c_i}} - \frac{q_i}{\sum_{i=1}^{N} z_i q_i} \qquad \text{(A.31)}$$

The segmental radius σ_{ii}, the number of segments per molecule r_i and the surface area of a molecule relative to a spherical segment q_i are

$$\sigma_{ii} = \sqrt[3]{\frac{v_{ii}^{*}\sqrt{2}}{r_i}} \tag{A.32}$$

$$r_i = \frac{v_{ii}^{*}}{8.667 \cdot 10^{-2}} \tag{A.33}$$

$$q_i = \frac{T_{ii}^{*} c_i k}{\varepsilon} \tag{A.34}$$

where $8.667*10^{-2}$ is the volume (lit./mol) of a CH_2-segment.

The universal constants for molecules interactng with Lennard-Jones potential have the following values

A_{11} = -8.538022
A_{12} = -5.276135
A_{13} = 3.730389
A_{14} = -7.539783
A_{15} = 23.306949
A_{16} = -11.197068

C_{11} = -3.9381909	C_{21} = 11.70262	C_{31} = -37.01896
C_{12} = -3.1926783	C_{22} = -3.0915196	C_{32} = 26.927112
C_{13} = -4.9299963	C_{23} = 4.0092149	C_{33} = 26.672754
C_{14} = 10.0296636	C_{24} = -20.025379	C_{34} = 0.0

The anisotropic attractions (Z^{ani}, A^{ani} and μ_i^{ani}) as well as the isotropic dipole-induced dipole interactions ($Z^{\mu ind\mu}$, $A^{\mu ind\mu}$, $\mu_i^{\mu ind\mu}$) are obtained from the perturbed anisotropic chain theory (PACT) described by Vimalchand and Donohue (1985) and Vimalchand et al. (1986). The anisotropic interactions are calculated using the perturbation expansion of Gubbins and Twu (1978).
The isotropic dipole-induced dipole interactions are

$$Z^{\mu ind\mu} = -2\sqrt{2}\,\pi \frac{<c(\tilde{\alpha}_j T^*_{\mu_i} + \tilde{\alpha}_i T^*_{\mu_j})\, v^*>}{vT} J^{(6)} \left[1 + \tilde{\rho} \frac{\partial \ln (J^{(6)})}{\partial \tilde{\rho}} \right] \tag{A.35}$$

$$\frac{A^{\mu ind\mu}}{RT} = -2\sqrt{2}\,\pi \frac{<c(\tilde{\alpha}_j T^*_{\mu_i} + \tilde{\alpha}_i T^*_{\mu_j})\, v^*>}{vT} J^{(6)} \tag{A.36}$$

$$\frac{\mu_i^{\mu ind\mu}}{RT} = -2\sqrt{2}\,\pi \frac{<\mu\, did>_i}{vT} J^{(6)} \tag{A.37}$$

The anisotropic contribution to the compressibility, Helmholtz free energy and chemical potential are calculated by means of three types of molecular interactions, namely dipole-dipole ($\mu\mu$), quadrupole-quadrupole (QQ), and dipole-quadrupole (μQ) interactions:

$$Z^{ani} = \frac{Z_2^{ani} + Z_3^{ani} - 2Z_2^{ani} \dfrac{A_3^{ani}}{A_2^{ani}}}{\left(1 - \dfrac{A_3^{ani}}{A_2^{ani}} \right)^2} \tag{A.38}$$

$$A^{ani} = \frac{A_2^{ani}}{\left(1 - \dfrac{A_3^{ani}}{A_2^{ani}} \right)} \tag{A.39}$$

$$\mu_i^{ani} = \frac{\mu_{i,2}^{ani} + \mu_{i,3}^{ani} - 2\mu_{i,2}^{ani} \dfrac{A_3^{ani}}{A_2^{ani}}}{\left(1 - \dfrac{A_3^{ani}}{A_2^{ani}} \right)^2} \tag{A.40}$$

where

$$Z_2^{ani} = Z_2^{\mu\mu} + Z_2^{QQ} + Z_2^{\mu Q} \tag{A.41}$$

$$Z_3^{ani} = Z_{3B}^{\mu\mu\mu} + Z_{3A}^{QQQ} + Z_{3B}^{QQQ} + 3Z_{3B}^{\mu\mu Q} + 3Z_{3B}^{\mu QQ} \tag{A.42}$$

The subscripts two and three denote the two and three body interactions, respectively. These interactions are described below.

Dipolar interactions:

$$Z_2^{\mu\mu} = -\frac{2\sqrt{2}\,\pi}{3}\frac{<c\,T_\mu^{*2}\,\nu^*>}{\nu\,T^2}\,J^{(6)}\left[1 + \tilde{\rho}\,\frac{\partial \ln(J^{(6)})}{\partial \tilde{\rho}}\right] \tag{A.43}$$

$$Z_{3B}^{\mu\mu\mu} = \frac{32\,\pi^3}{135}\sqrt{\frac{14\,\pi}{5}}\,\frac{2<c\,T_\mu^{*(3)}\,\nu^{*(2)}>}{\nu^2\,T^3}\,K_{\mu\mu\mu}\left[2 + \tilde{\rho}\,\frac{\partial \ln(K_{\mu\mu\mu})}{\partial \tilde{\rho}}\right] \tag{A.44}$$

$$\frac{A_2^{\mu\mu}}{RT} = -\frac{2\sqrt{2}\,\pi}{3}\frac{<c\,T_\mu^{*2}\,\nu^*>}{\nu\,T^2}\,J^{(6)} \tag{A.45}$$

$$\frac{A_{3B}^{\mu\mu\mu}}{RT} = \frac{32\,\pi^3}{135}\sqrt{\frac{14\,\pi}{5}}\,\frac{2<c\,T_\mu^{*(3)}\,\nu^{*(2)}>}{\nu^2\,T^3}\,K_{\mu\mu\mu} \tag{A.46}$$

$$\frac{\mu_{i,2}^{\mu\mu}}{RT} = -\frac{2\sqrt{2}\,\pi}{3}\frac{<\mu\,d2>_i}{\nu\,T^2}\,J^{(6)} \tag{A.47}$$

$$\frac{\mu_{i,3B}^{\mu\mu\mu}}{RT} = \frac{32\,\pi^3}{135}\sqrt{\frac{14\,\pi}{5}}\,\frac{2<\mu\,d3>_i}{\nu^2\,T^3}\,K_{\mu\mu\mu} \tag{A.48}$$

Quadrupolar interactions:

$$Z_2^{QQ} = -\frac{14\sqrt{2}\,\pi}{5}\,\frac{<c\,T_Q^{*2}\,v^{*}>}{v\,T^2}\,J^{(10)}\left[1 + \tilde{\rho}\,\frac{\partial \ln J^{(10)}}{\partial \tilde{\rho}}\right] \tag{A.49}$$

$$Z_{3A}^{QQ} = -\frac{144\,\pi\sqrt{2}}{245}\,\frac{<c\,T_Q^{*3}\,v^{*}>}{v\,T^3}\,J^{(15)}\left[1 + \tilde{\rho}\,\frac{\partial \ln J^{(15)}}{\partial \tilde{\rho}}\right] \tag{A.50}$$

$$Z_{3B}^{QQQ} = -\frac{32\,\pi^3}{2025}\,\sqrt{2002\,\pi}\,\frac{2<c\,T_Q^{*3}\,v^{*2}>}{v^2\,T^3}\,K_{QQQ}\left[1 + \tilde{\rho}\,\frac{\partial \ln K_{QQQ}}{\partial \tilde{\rho}}\right] \tag{A.51}$$

$$A_2^{QQ} = -\frac{14\sqrt{2}\,\pi}{5}\,\frac{<c\,T_Q^{*2}\,v^{*}>}{v\,T^2}\,J^{(10)} \tag{A.52}$$

$$\frac{A_{3A}^{QQ}}{R\,T} = -\frac{144\,\pi\sqrt{2}}{245}\,\frac{<c\,T_Q^{*3}\,v^{*}>}{v\,T^3}\,J^{(15)} \tag{A.53}$$

$$\frac{A_{3B}^{QQQ}}{R\,T} = -\frac{32\,\pi^3}{2025}\,\sqrt{2002\,\pi}\,\frac{2<c\,T_Q^{*3}\,v^{*2}>}{v^2\,T^3}\,K_{QQQ} \tag{A.54}$$

$$\frac{\mu_{i,2}^{QQ}}{R\,T} = -\frac{14\sqrt{2}\,\pi}{5}\,\frac{<\mu\,Q2>_i}{v\,T^2}\,J^{(10)} \tag{A.55}$$

$$\frac{\mu_{i,3A}^{QQ}}{RT} = -\frac{144\pi\sqrt{2}}{245}\frac{<\mu Q3A>_i}{\nu T^3}J^{(15)} \tag{A.56}$$

$$\frac{\mu_{i,3B}^{QQQ}}{RT} = -\frac{32\pi^3}{2025}\sqrt{2002\,\pi}\frac{<\mu Q3B>_i}{\nu T^3}K_{QQQ} \tag{A.57}$$

Dipolar-Quadrupolar interactions:

$$Z_2^{\mu Q} = -\sqrt{2}\pi\frac{<c(T_{\mu Q}^{*2} + T_{Q\mu}^{*2})\nu^*>}{\nu T^2}J^{(8)}\left[1 + \tilde{\rho}\frac{\partial \ln J^{(8)}}{\partial \tilde{\rho}}\right] \tag{A.58}$$

$$Z_{3B}^{\mu\mu Q} = 19.34\frac{<cT_{\mu\mu Q}^{*(3)}\nu^{*(2)}>}{\nu^2 T^3}K_{\mu\mu Q}\left[1 + \tilde{\rho}\frac{\partial \ln K_{\mu\mu Q}}{\partial \tilde{\rho}}\right] \tag{A.59}$$

$$Z_{3B}^{\mu QQ} = -23.094\frac{2<cT_{\mu QQ}^{*(3)}\nu^{*(2)}>}{\nu^2 T^3}K_{\mu QQ}\left[1 + \tilde{\rho}\frac{\partial \ln K_{\mu QQ}}{\partial \tilde{\rho}}\right] \tag{A.60}$$

$$\frac{A_2^{\mu Q}}{RT} = -\sqrt{2}\pi\frac{<c(T_{\mu Q}^{*2} + T_{Q\mu}^{*2})\nu^*>}{\nu T^2}J^{(8)} \tag{A.61}$$

$$\frac{A_{3B}^{\mu\mu Q}}{RT} = 19.34\frac{<cT_{\mu\mu Q}^{*(3)}\nu^{*(2)}>}{\nu^2 T^3}K_{\mu\mu Q} \tag{A.62}$$

$$\frac{A_{3B}^{\mu QQ}}{RT} = -23.094 \frac{2 < c T_{\mu QQ}^{*(3)} v^{*(2)} >}{v^2 T^3} K_{\mu QQ} \tag{A.63}$$

$$\frac{\mu_{i,2}^{\mu Q}}{RT} = -\sqrt{2}\pi \frac{< \mu dQ >_i}{v T^2} J^{(8)} \tag{A.64}$$

$$\frac{\mu_{i,3B}^{\mu\mu Q}}{RT} = 19.34 \frac{< \mu d2Q >_i}{v^2 T^3} K_{\mu\mu Q} \tag{A.65}$$

$$\mu_{i,3B}^{\mu QQ} = -23.094 \frac{2 < \mu dQ2 >_i}{v^2 T^3} K_{\mu QQ} \tag{A.66}$$

The mixing rules for PACT are given by Vimalchand and Donohue (1985):

$$< c T_{\mu}^{*2} v^{*} > = \sum_{i=1}^{N} \sum_{j=1}^{N} z_i z_j T_{\mu,i}^{*} T_{\mu,j}^{*} \frac{q_i c_j}{q_j} \frac{N_A r_j \sigma_{ji}^3}{\sqrt{2}} (1 - k_{\mu_{ij}})^2 \tag{A.67}$$

$$< c T_{\mu}^{*(3)} v^{*(2)} > = \sum_{i=1}^{N} \sum_{j=1}^{N} \sum_{k=1}^{N} z_i z_j z_k T_{i,\mu}^{*} T_{j,\mu}^{*} T_{k,\mu}^{*} \frac{q_i c_j}{q_j} \frac{N_A r_j \sigma_{ji}^3}{\sqrt{2}} \frac{N_A r_k \sigma_{kj}^3}{\sqrt{2}} (1 - k_{\mu ij})^2 \tag{A.68}$$

$$< c T_{Q}^{*2} v^{*} > = \sum_{i=1}^{N} \sum_{j=1}^{N} z_i z_j T_{Q,i}^{*} T_{Q,j}^{*} \frac{q_i c_j}{q_j} \frac{N_A r_j \sigma_{ji}^3}{\sqrt{2}} \tag{A.69}$$

$$< c T_{Q}^{3*} v^{*} > = \sum_{i=1}^{N} \sum_{j=1}^{N} z_i z_j c_i T_{i,Q}^{*3/2} T_{j,Q}^{*3/2} \left(\frac{q_i c_j}{q_j c_i} \right)^{\frac{3}{2}} \frac{N_A r_j \sigma_{ji}^3}{\sqrt{2}} \tag{A.70}$$

$$<c\,T_Q^{*(3)}\,\nu^{*(2)}> \;=\; \sum_{i=1}^{N}\sum_{j=1}^{N}\sum_{k=1}^{N} z_i z_j z_k\, T_{i,Q}^{*}\, T_{j,Q}^{*}\, T_{k,Q}^{*}\, \frac{q_i c_j}{q_j}\, \frac{N_A r_j \sigma_{ji}^3}{\sqrt{2}}\, \frac{N_A r_k \sigma_{kj}^3}{\sqrt{2}} \tag{A.71}$$

$$<c(T_{\mu Q}^{*2} + T_{Q\mu}^{*2})\nu^{*}> \;=\; \sum_{i=1}^{N}\sum_{i=1}^{N} z_i z_j (T_{i,\mu}^{*} T_{j,Q}^{*} + T_{i,Q}^{*} T_{j,\mu}^{*})\, \frac{q_i c_j}{q_j}\, \frac{N_A r_j \sigma_{ji}^3}{\sqrt{2}} \tag{A.72}$$

$$<c\,T_{\mu\mu Q}^{*(3)}\,\nu^{*(2)}> \;=\; \sum_{i=1}^{N}\sum_{j=1}^{N}\sum_{k=1}^{N} z_i z_j z_k c_i\, T_{i,\mu}^{*}\, T_{j,\mu}^{*}\, T_{k,Q}^{*}\, \frac{N_A r_j \sigma_{ji}^3}{\sqrt{2}}\, \frac{N_A r_k \sigma_{kj}^3}{\sqrt{2}}\,(1 - k_{\mu ij})^2 \tag{A.73}$$

$$<c\,T_{\mu QQ}^{*(3)}\,\nu^{*(2)}> \;=\; \sum_{i=1}^{N}\sum_{j=1}^{N}\sum_{k=1}^{N} z_i z_j z_k c_i\, T_{i,\mu}^{*}\, T_{j,Q}^{*}\, T_{k,Q}^{*}\, \frac{N_A r_j \sigma_{ji}^3}{\sqrt{2}}\, \frac{N_A r_k \sigma_{kj}^3}{\sqrt{2}}\,(1 - k_{\mu ij})^2 \tag{A.74}$$

$$<c(\tilde{\alpha}_j T_{i,\mu}^{*} + \tilde{\alpha}_i T_{j,\mu}^{*})\nu^{*}> \;=\; \sum_{i=1}^{N}\sum_{j=1}^{N} z_i z_j c_i \left[\tilde{\alpha}_i T_{j,\mu}^{*}\, \frac{\sigma_{ii}^3}{\sigma_{ij}^3} + \tilde{\alpha}_j T_{i,\mu}^{*}\, \frac{\sigma_{jj}^3}{\sigma_{ji}^3}\right] \frac{N_A r_j \sigma_{ji}^3}{\sqrt{2}} \tag{A.75}$$

$$<\mu\, d2>_i \;=\; \sum_{j=1}^{N} z_j \left[\frac{q_i c_j}{q_j}\, T_{i,\mu}^{*}\, T_{j,\mu}^{*}\, \frac{N_A r_j \sigma_{ji}^3}{\sqrt{2}} + \frac{q_j c_i}{q_i T_{i,\mu}^{*} T_{j,\mu}^{*}}\, \frac{N_A r_i \sigma_{ij}^3}{\sqrt{2}}\right](1 - k_{\mu ij})^2$$

$$+ \sum_{l=1}^{N}\sum_{m=1}^{N} z_l z_m\, \frac{q_l c_m}{q_m}\, T_{l,\mu}^{*}\, T_{m,\mu}^{*}\, \frac{N_A r_m \sigma_{ml}^3}{\sqrt{2}}\,(1 - k_{\mu lm})^2 \;*$$

$$\left[\left(\tilde{\rho}\, \frac{\partial \ln J^{(6)}}{\partial \tilde{\rho}}\right) <\nu^{*}>_i^{D} - \left(\tilde{T}\, \frac{\partial \ln J^{(6)}}{\partial \tilde{T}}\right) <T^{*}>_i^{Q}\right] \tag{A.76}$$

with

$$<T^*>_i^Q = \frac{\sum_{l=1}^{N}\sum_{m=1}^{N} z_l z_m \frac{\varepsilon_{lm} q_l}{k c_l}}{\sum_{j=1}^{N} z_j \left(\frac{\varepsilon_{ij} q_i}{k c_i} + \frac{\varepsilon_{ji} q_j}{k c_j} \right)} - 2 \qquad \text{(A.77)}$$

$$<v^*>_i^D = \frac{\sum_{j=1}^{N} z_j \frac{N_A (r_i \sigma_{ij}^3 + r_j \sigma_{ji}^3)}{\sqrt{2}}}{\sum_{k=1}^{N}\sum_{l=1}^{N} z_k z_l \frac{N_A r_k \sigma_{lk}^3}{\sqrt{2}}} - 1 \qquad \text{(A.78)}$$

$<\mu d3> =$

$$\sum_{j=1}^{N}\sum_{k=1}^{N} z_j z_k T_{i,\mu}^* T_{j,\mu}^* T_{k,\mu}^* \left(c_i \frac{N_A r_j \sigma_{ji}^3}{\sqrt{2}} \frac{N_A r_k \sigma_{kj}^3}{\sqrt{2}} + c_j \frac{N_A r_k \sigma_{kj}^3}{\sqrt{2}} \frac{N_A r_i \sigma_{ik}^3}{\sqrt{2}} + c_k \frac{N_A r_i \sigma_{ik}^3}{\sqrt{2}} \frac{N_A r_j \sigma_{ji}^3}{\sqrt{2}} \right)$$

$$+ \sum_{l=1}^{N}\sum_{m=1}^{N}\sum_{n=1}^{N} z_l z_m z_n c_l T_{l,\mu}^* T_{m,\mu}^* T_{n,\mu}^* \frac{N_A r_m \sigma_{ml}^3}{\sqrt{2}} \frac{N_A r_n \sigma_{nm}^3}{\sqrt{2}} *$$

$$\left[\tilde{\rho} \frac{\partial \ln K_{\mu\mu\mu}}{\partial \tilde{\rho}} <V^*>_i^D - \tilde{T} \frac{\partial \ln K_{\mu\mu\mu}}{\partial \tilde{T}} <T^*>_i^Q \right] \qquad \text{(A.79)}$$

$<\mu Q2> =$

$$\sum_{j=1}^{N} z_j \left(\frac{q_i c_j}{q_j} T_{i,Q}^* T_{j,Q}^* \frac{N_A r_i \sigma_{ij}^3}{\sqrt{2}} + \frac{q_j c_i}{q_i} T_{i,Q}^* T_{j,Q}^* \frac{N_A r_i \sigma_{ij}^3}{\sqrt{2}} \right) +$$

$$\sum_{l=1}^{N}\sum_{m=1}^{N} z_l z_m T_{l,Q}^* T_{m,Q}^* \frac{q_l c_m}{q_m} \frac{N_A r_m \sigma_{ml}^3}{\sqrt{2}} \left(\tilde{\rho} \frac{\partial \ln J^{(10)}}{\partial \tilde{\rho}} <v^*>_i^D - \tilde{T} \frac{\partial \ln J^{(10)}}{\partial \tilde{T}} <T^*>_i^Q \right) \qquad \text{(A.80)}$$

$$<\mu Q3A> =$$

$$\sum_{j=1}^{N} z_j \left[\left(\frac{q_i c_j}{q_j c_i} \right)^{\frac{3}{2}} c_i T_{i,Q}^{*\,3/2} T_{j,Q}^{*\,3/2} \frac{N_A r_j \sigma_{ji}^3}{\sqrt{2}} + \left(\frac{q_j c_i}{q_i c_j} \right)^{\frac{3}{2}} c_j T_{i,Q}^{*\,3/2} T_{j,Q}^{*\,3/2} \frac{N_A r_i \sigma_{ij}^3}{\sqrt{2}} \right] +$$

$$\sum_{l=1}^{N} \sum_{m=1}^{N} c_l \left(\frac{q_l c_m}{q_m c_l} \right)^{\frac{3}{2}} T_{l,Q}^{*\,3/2} T_{m,Q}^{*\,3/2} \frac{N_A r_m \sigma_{ml}}{\sqrt{2}} \left[\tilde{\rho} \frac{\partial \ln J^{(15)}}{\partial \tilde{\rho}} <\nu^*>_i^D - \tilde{T} \frac{\partial \ln J^{(15)}}{\partial \tilde{T}} <T^*>_i^Q \right] \qquad \text{(A.81)}$$

$$<\mu Q3B> =$$

$$\sum_{j=1}^{N} \sum_{k=1}^{N} z_j z_k T_{i,Q}^* T_{j,Q}^* T_{k,Q}^* \left(c_i \frac{N_A r_j \sigma_{ji}^3}{\sqrt{2}} \frac{N_A r_k \sigma_{kj}^3}{\sqrt{2}} + c_j \frac{N_A r_k \sigma_{kj}^3}{\sqrt{2}} \frac{N_A r_i \sigma_{ik}^3}{\sqrt{2}} + c_k \frac{N_A r_i \sigma_{ik}^3}{\sqrt{2}} \frac{N_A r_j \sigma_{ji}^3}{\sqrt{2}} \right)$$

$$+ \sum_{l=1}^{N} \sum_{m=1}^{N} \sum_{n=1}^{N} z_l z_m z_n c_l T_{l,Q}^* T_{m,Q}^* T_{n,Q}^* \frac{N_A r_m \sigma_{ml}^3}{\sqrt{2}} \frac{N_A r_n \sigma_{nm}^3}{\sqrt{2}} *$$

$$\left[\tilde{\rho} \frac{\partial \ln K_{QQQ}}{\partial \tilde{\rho}} <V^*>_i^D - \tilde{T} \frac{\partial \ln K_{QQQ}}{\partial \tilde{T}} <T^*>_i^Q \right] \qquad \text{(A.82)}$$

$$<\mu dQ2> = \sum_{j=1}^{N} z_j \left(T_{i,\mu}^* T_{j,Q}^* + T_{i,Q}^* T_{j,\mu}^* \right) \cdot \left(\frac{q_i c_j}{q_j} \frac{N_A r_j \sigma_{ji}^3}{\sqrt{2}} + \frac{q_j c_i}{q_i} \frac{N_A r_i \sigma_{ij}^3}{\sqrt{2}} \right)$$

$$+ \sum_{l=1}^{N} \sum_{m=1}^{N} \left(T_{l,\mu}^* T_{m,Q}^* + T_{l,Q}^* T_{m,\mu}^* \right) \frac{q_l c_m}{q_m} \frac{N_A r_m \sigma_{ml}^3}{\sqrt{2}} *$$

$$\left[\tilde{\rho} \frac{\partial \ln J^{(8)}}{\partial \tilde{\rho}} <\nu^*>_i^D - \tilde{T} \frac{\partial \ln J^{(8)}}{\partial \tilde{T}} <T^*>_i^Q \right] \qquad \text{(A.83)}$$

$$<\mu\, dQ3A> = \sum_{j=1}^{N}\sum_{k=1}^{N} K_{\mu\mu Q}\left(T^*_{i,\mu}\, T^*_{j,\mu}\, T^*_{l,Q}\, c_i \frac{N_A r_j \sigma^3_{ji}}{\sqrt{2}} \frac{N_A r_k \sigma^3_{kj}}{\sqrt{2}} + \right.$$

$$\left. T^*_{i,Q} T^*_{j,\mu}\, T^*_{k,\mu}\, c_j \frac{N_A r_k \sigma^3_{kj}}{\sqrt{2}} \frac{N_A r_i \sigma^3_{ik}}{\sqrt{2}} + T^*_{i,\mu}\, T^*_{j,Q}\, T^*_{k,\mu}\, c_k \frac{N_A r_i \sigma^3_{ik}}{\sqrt{2}} \frac{N_A r_j \sigma^3_{ji}}{\sqrt{2}} \right) +$$

$$\sum_{l=1}^{N}\sum_{m=1}^{N}\sum_{n=1}^{N} c_l\, T^*_{l,\mu}\, T^*_{m,\mu}\, T^*_{n,Q} \frac{N_a r_m \sigma^3_{ml}}{\sqrt{2}} \frac{N_a r_n \sigma^3_{nm}}{\sqrt{2}} (1 - k_{\mu lm}) *$$

$$\left[\tilde{\rho} \frac{\partial \ln K_{\mu\mu Q}}{\partial \tilde{\rho}} <v^*>^D_i - \tilde{T} \frac{\partial \ln K_{\mu\mu Q}}{\partial \tilde{T}} <T^*>^Q_i \right] \qquad \text{(A.84)}$$

$$<\mu\, dQ3A> = \sum_{j=1}^{N}\sum_{k=1}^{N} K_{\mu QQ}\left(T^*_{i,\mu}\, T^*_{j,Q}\, T^*_{l,Q}\, c_i \frac{N_A r_j \sigma^3_{ji}}{\sqrt{2}} \frac{N_A r_k \sigma^3_{kj}}{\sqrt{2}} + \right.$$

$$\left. T^*_{i,Q} T^*_{j,\mu}\, T^*_{k,Q}\, c_j \frac{N_A r_k \sigma^3_{kj}}{\sqrt{2}} \frac{N_A r_i \sigma^3_{ik}}{\sqrt{2}} + T^*_{i,Q}\, T^*_{j,Q}\, T^*_{k,\mu}\, c_k \frac{N_A r_i \sigma^3_{ik}}{\sqrt{2}} \frac{N_A r_j \sigma^3_{ji}}{\sqrt{2}} \right) +$$

$$\sum_{l=1}^{N}\sum_{m=1}^{N}\sum_{n=1}^{N} c_l\, T^*_{l,\mu}\, T^*_{m,Q}\, T^*_{n,Q} \frac{N_a r_m \sigma^3_{ml}}{\sqrt{2}} \frac{N_a r_n \sigma^3_{nm}}{\sqrt{2}} (1 - k_{\mu lm}) *$$

$$\left[\tilde{\rho} \frac{\partial \ln K_{\mu QQ}}{\partial \tilde{\rho}} <v^*>^D_i - \tilde{T} \frac{\partial \ln K_{\mu QQ}}{\partial \tilde{T}} <V^*>^Q_i \right] \qquad \text{(A.85)}$$

$$<\mu\, did> = \sum_{j=1}^{N} z_j \left(\tilde{\alpha}_i \frac{\sigma_{ii}^3}{\sigma_{ij}^3} T_{i,\mu}^* + \tilde{\alpha}_j \frac{\sigma_{jj}^3}{\sigma_{ji}^3} T_{j,\mu}^* \right) \cdot \left(c_i \frac{N_A r_j \sigma_{ji}^3}{\sqrt{2}} + c_j \frac{N_A r_i \sigma_{ij}^3}{\sqrt{2}} \right) +$$

$$\sum_{l=1}^{N} \sum_{m=1}^{N} z_l z_m c_l \left(\tilde{\alpha}_m \frac{\sigma_{mm}^3}{\sigma_{ml}^3} T_{l,\mu}^* + \tilde{\alpha}_l \frac{\sigma_{ll}\hat{}3}{\sigma_{lm}^3} T_{m,\mu}^* \right) \frac{N_a r_m \sigma_{ml}^3}{\sqrt{2}} *$$

$$\left[\tilde{\rho} \frac{\partial \ln J^{(6)}}{\partial \tilde{\rho}} <v^*>_i^D - \tilde{T} \frac{\partial \ln J^{(6)}}{\partial \tilde{T}} <T^*>_i^Q \right] \qquad \text{(A.86)}$$

The characteristic dipole temperature $T_{i,\mu}$, quadrupole temperature $T_{i,Q}$ and the reduced polarizability α tilde can be evaluated by using the following epressions for $T_{i,\mu}$, $T_{i,Q}$ and α tilde:

$$T_{i,\mu}^* = \frac{3.08482\ \mu_i^d}{c_i\ v_i^*} = \frac{\varepsilon_{i,\mu}\, q_i}{c_i\, k} \qquad \text{(A.87)}$$

$$T_{i,Q}^* = \frac{1.7464 \cdot 10^{-2}\, Q_i^2}{c_i\, (v_i^*)^{2/3}} = \frac{\varepsilon_{i,Q}\, q_i}{c_i\, k} \qquad \text{(A.88)}$$

$$\tilde{\alpha}_i = \frac{4.2589 \cdot 10^{-4}\ \alpha_i}{v_i^*} \qquad \text{(A.89)}$$

where μ_i^d, q_i and α tilde are the dipole moment of component i, the quadrupole moment of component i and the average polarizability of component i, respectively. These values can be taken from literature.
The J and K integrals in the anisotropic expressions are calculated by:

$$\ln J^{(n)} = A_n (\sqrt{2}\,\tilde{\rho})^2 \ln \tilde{T} + B_n (\sqrt{2}\,\tilde{\rho})^2 + C_n (\sqrt{2}\,\tilde{\rho}) \ln \tilde{T} + D_n (\sqrt{2}\,\tilde{\rho}) + E_n \ln \tilde{T} + F_n \qquad \text{(A.90)}$$

$$\ln K_{xxx} = A_{xxx} (\sqrt{2}\,\tilde{\rho})^2 \ln \tilde{T} + B_{xxx} (\sqrt{2}\,\tilde{\rho})^2 + C_{xxx} (\sqrt{2}\,\tilde{\rho}) \ln \tilde{T} + D_{xxx} (\sqrt{2}\,\tilde{\rho}) + E_{xxx} \ln \tilde{T} + F_{xxx} \qquad \text{(A.91)}$$

$$\frac{\tilde{\rho}\ \partial \ln J^{(n)}}{\partial \tilde{\rho}} = A_n 4\,\tilde{\rho}^2 \ln \tilde{T} + B_n 4\,\tilde{\rho}^2 + C_n \sqrt{2}\,\tilde{\rho} \ln \tilde{T} + D_n \sqrt{2}\,\tilde{\rho} \tag{A.92}$$

$$\tilde{T}\ \frac{\partial \ln J^{(n)}}{\partial \tilde{T}} = A_n\left(\sqrt{2}\,\tilde{\rho}\right) + C_n\left(\sqrt{2}\,\tilde{\rho}\right) + E_n \tag{A.93}$$

where

$$\tilde{\rho} = \frac{<v^*>}{v} \quad ; \quad <v^*> = \sum_{i=1}^{N}\sum_{j=1}^{N} z_i z_j \frac{N_A r_i \sigma_{ij}^3}{\sqrt{2}} \tag{A.94}$$

$$\tilde{T} = \frac{T}{<T^*>} \quad ; \quad <T^*> = \sum_{i=1}^{N}\sum_{j=1}^{N} z_i z_j \frac{\varepsilon_{ij} q_i}{k\, c_i} \tag{A.95}$$

The partial derivatives of K_{xxx} with respect to ρ and T tilde have simular expressions in Eq. A.92 and A.93.

The constants A_n, A_{xxx}, F_n and F_{xxx} are given by Gubbins and Twu (1978):

A_6 = -0.488498	:	$A_{\mu\mu\mu}$ = -1.050534
B_6 = 0.863195	:	$B_{\mu\mu\mu}$ = 1.747476
C_6 = 0.761344	:	$C_{\mu\mu\mu}$ = 1.749366
D_6 = -0.750086	:	$D_{\mu\mu\mu}$ = -1.999227
E_6 = -0.218562	:	$E_{\mu\mu\mu}$ = -0.661046
F_6 = -0.538463	:	$F_{\mu\mu\mu}$ = -3.028720
A_{10} = -0.698790	:	A_{15} = -0.856655
B_{10} = 1.278054	:	B_{15} = 1.587957
C_{10} = 1.020604	:	C_{15} = 1.169885
D_{10} = -0.880027	:	D_{15} = -0.928269
E_{10} = -0.140749	:	E_{15} = -0.074849
F_{10} = -1.222733	:	F_{15} = -1.698853

A_{QQQ} = -1.616385
B_{QQQ} = 2.881007
C_{QQQ} = 2.577600
D_{QQQ} = -2.484990
E_{QQQ} = -0.828596
F_{QQQ} = -4.175589

A_8 = -0.611295 : $A_{\mu\mu Q}$ = -1.130955
B_8 = 1.103390 : $B_{\mu\mu Q}$ = 2.249120
C_8 = 0.921359 : $C_{\mu\mu Q}$ = 2.135877
D_8 = -0.838804 : $D_{\mu\mu Q}$ = -2.278530
E_8 = -0.197999 : $E_{\mu\mu Q}$ = -0.773166
F_8 = -0.940714 : $F_{\mu\mu Q}$ = -3.704690

$A_{\mu QQ}$ = -1.490116
$B_{\mu QQ}$ = 2.619997
$C_{\mu QQ}$ = 2.404319
$D_{\mu QQ}$ = -2.420706
$E_{\mu QQ}$ = -0.829466
$F_{\mu QQ}$ = -3.930928

A_6,..,F_6 = constants for the two body interaction between two dipoles.
$A_{\mu\mu\mu}$,..,$F_{\mu\mu\mu}$ = constants for the three body interactions between three dipoles.
A_{10},..,F_{10} = constants for the two body interaction between two quadrupoles.
A_{15},..,F_{15} = constants for the three body interaction between three quadrupoles (part 1).
A_{QQQ},..,F_{QQQ} = constants for the three body interaction between three quadrupoles (part 2).
A_8,..,F_8 = constants for the two body interaction between a dipole and a quadrupole.
$A_{\mu\mu Q}$,..,$F_{\mu\mu Q}$ = constants for the three body interaction between two dipoles and a quadrupole.
$A_{\mu QQ}$,..,$F_{\mu QQ}$ = constants for the three body interaction between two quadrupoles and a dipole.

Pure substances and mixtures are considered to form n-mers caused by hydrogen bonding. The extent of hydrogen bonding is given in the form of the ratio of the total number of moles of all chemical species, n_T divided by the superfial number of moles, n_O (no hydrogen bonding). If no hydrogen bonding is present this ratio should be equal to unity. On the other hand when a substance has a strong tendency to form hydrogen bonds, the ratio should approach zero. The ratio n_T/n_O is temperature, pressure and volume dependent and also influenced by the equilibrium constant, K for hydrogen bond formation. Several models were developed to derive equations for the ratio n_T/n_O. Only three models will be discussed here. The models are: the infinite equilibria model (Ikonomou and Donohue, 1986), also referred as the two-site model, the three site model (Economou and Donohue, 1992) and the mixed two-site model (Ikonomou and Donohue, 1988).

Before discussing these model, the association compressibility (Z^{assoc}), Helmholtz free energy (A^{assoc}) and chemical potential (μ_i^{assoc}) are given

$$Z^{assoc} = \frac{n_T}{n_O} - 1 \qquad \text{(A.96)}$$

$$A^{assoc} = RT\left[\sum_{i=1}^{N} z_i \ln\left(\frac{n_{1i}}{n_{i0}}\right) - \frac{n_T}{n_O}\right] \qquad \text{(A.97)}$$

$$\mu_i^{assoc} = RT \ln\left(\frac{n_{1i}}{n_{i0}}\right) \qquad \text{(A.98)}$$

$$\mu_j^{assoc}\Big|_{j\neq i} = 0 \qquad \text{(A.99)}$$

where component 1 denotes the associating species. $n_{1i}\backslash n_{iT}$ equals unity for a non-associating component.

The two-site model is useful in describing hydrogen bonding of molecules that form lineair associating products. The name two-site indicates two hydrogen bonding sites per molecule and the model is therefore applicable to mixtures of diluents (non-associating species) and aliphatic alcohols or water. It was developed using an approach similar of Heidemann and Prausnitz (1976).

The equilibruim constant K and the expressions for n_T/n_O are

$$K_1 = e^{-\frac{\Delta H_1^{assoc}}{RT} + \frac{\Delta S_1^{assoc}}{R}} \tag{A.100}$$

$$S_1 = \frac{z_1 K_1 R_g T}{v} \tag{A.101}$$

$$\frac{n_{11}}{n_{10}} = \left(\frac{2}{1 + \sqrt{1 + 4S_1}} \right)^2 \tag{A.102}$$

$$\frac{n_T}{n_0} = 1 - \frac{n_{11}}{n_{10}} z_1 S_1 = 1 - \frac{4 z_1^2 K_1 R_g T}{v \left(1 + \sqrt{1 + \frac{4 z_1 K_1 R_g T}{v}} \right)^2} \tag{A.103}$$

where n_{11}/n_{10} is the total number of monomer of the associating species devided by the superficial number of moles of monomer. R_g is the gas-constant R devided by 1.01325 bar.

A model which is based on three hydrogen bonding sites per molecule is the so-called three-site model and is usefull for water diluent or ammonia diluent mixtures.
This model was extracted from the statistial associating fluid theory (SAFT) equation of state given by Huang and Radosz (1990). The expressions voor n_T/n_O and n_{11}/n_{10} are:

$$\frac{n_{11}}{n_{10}} = \frac{2}{1 + 4S_1 - S_1^2 + (1 + S_1)\sqrt{1 + 6S_1 + S_1^2}} \tag{A.104}$$

$$\frac{n_T}{n_0} = \frac{2 z_1}{1 + S_1 + \sqrt{1 + 6S_1 + S_1^2}} + 1 - z_1 \tag{A.105}$$

where S_1 is given by Eq. A.101.

Finally, the mixed two-site model (Ikonomou and Donohue, 1988) is an extension of the two-site model to treat two or more associating species and one or more diluents. The expression for n_T/n_O is

$$K_i = e^{-\frac{\Delta H_i^{assoc}}{RT} + \frac{\Delta S_i^{assoc}}{R}} \tag{A.106}$$

$$S_i = \frac{z_i K_i R_g T}{v} \tag{A.107}$$

$$\frac{n_{1i}}{n_{i0}} = \left(\frac{2}{1 + \sqrt{1 + 4 S_i}} \right)^2 \tag{A.108}$$

$$\frac{n_T}{n_0} = \sum_{i=1}^{m} \frac{2 z_i}{1 + \sqrt{1 + 4 S_i}} + \sum_{j=m+1}^{m+n} z_j \tag{A.109}$$

where m is the number of associating species and n the number of diluents.